SWINGING WAKE MECHANISM FOR INTERFACE WAVE GENERATION AND PERMISSIBLE RANGE OF PARAMETERS FOR EXPLOSIVE WELDING

A Thesis Submitted
in Partial Fulfilment of the Requirements
for the Degree of

DOCTOR OF PHILOSOPHY

By

RAMESH CHANDRA GUPTA

to the

DEPARTMENT OF MECHANICAL ENGINEERING

INDIAN INSTITUTE OF TECHNOLOGY KANPUR

JULY, 1981

TO

MY PARENTS

WITH REGARDS

ME-1981-D-GUP-SWI

CERTIFICATE

This is to certify that this work on 'Swinging Wake Mechanism for Interface Wave Generation and Permissible Range of Parameters for Explosive Welding' has been carried out by Shri Ramesh Chandra Gupta under my supervision and it has not been submitted elsewhere for a degree.

G S Kainth 30/7/81

DR. G.S. KAINTH
Professor
Department of Mechanical Engineering
Indian Institute of Technology
Kanpur, India

July, 1981

ACKNOWLEDGEMENTS

I express my deep sense of gratitude and profound regards to Dr. G.S. Kainth for his keen interest and invaluable guidance in bringing up the present work.

I am grateful to Dr. Jagdish Lal, Principal and Dr. B.K. Gupta, Head of Mechanical Engineering Department, M.N.R. Engineering College, Allahabad for granting the study leave to carry out the research work.

I am also thankful to Professor H.C. Agrawal, Prof. G.K. Lal, Prof. A. Ghosh, Prof. B.L. Dhoopar, Prof. M.M. Oberoi, Prof. V.K. Garg, Prof. B.D. Agrawal, Prof.S.N. Bandopadhyaya, Dr. M.K. Muju and Dr. Prasanta Kumar of Mechanical Engineering Department, I.I.T. Kanpur, for their encouragements.

I thank Dr. M.S. Kalra, Mechanical Engineering Department, I.I.T. Kanpur, for his help, suggestions and discussions.

I am thankful to the District Authorities (District Magistrate, Suptd. of Police and Fire Officer) for granting and renewing the licence for explosives.

My thanks are also due to Mr. O.P. Bajaj, Mr. R.M. Jha, Mr. B.P. Viswakarma, Mr. B.P. Bhartia, Mr. H. Rahman, Mr. A.K. Gupta, Mr. S.P. Gupta, Mr. R.K. Baid, Mr.K.L.Patel,

Mr. R.C. Mahesh, Mr. D.K. Sarkar, Mr. S.C. Soni, Mr. S.N. Tewari, Mr. S.B.S. Mishra, Mr. K.N. Singh and many others for their help at various stages.

I also wish to thank Mr. B.L. Arora and Mr. S.S. Kushwaha for their assistance in preparing the figures. I am thankful to Mr. J.P. Gupta for his excellent work in typing the manuscript.

Finally, I am grateful to my wife, Veena and my daughters, Ruchi and Sonia for their patience, help and understanding during this research.

(RAMESH CHANDRA GUPTA)

CONTENTS

LIST OF FIGURES

LIST OF TABLES

NOMENCLATURE

α	Set-up angle
α_1, α_2	Inclination of direction of collision to plate-I and plate -II
β	Obliquity angle
β_1, β_2	Obliquity angle of plate-I and plate-II
β_E	Obliquity angle for jet-no-jet (weld-no-weld) condition
β_F	Obliquity angle beyond which fluidized zone in plate vanishes
β_L	Lower obliquity angle below which re-entrant jet is absent
β_O	Optimum obliquity angle for maximum amplitude
β_{OJ}	Optimum obliquity angle for maximum re-entrant jet thickness/mass
β_W	Obliquity angle for wave-no-wave boundary
γ	Angular position of stagnation point on rotating cylinder (chapter II)
δ	Small quantity $\delta \rightarrow 0$
ε	V_{FS}/V_F
η	Degree of distortion
θ	Instantaneous tilt of swinging wake (as used in chapter III), and Direction of velocity (as used in chapter IV)
θ_c	Angle between the collision direction and a

λ	Wavelength
μ	Viscosity
ν	Kinematic viscosity
ξ	Contribution to the wavelength when the wake is moving from lower density material to higher density material
ρ	Density
ρ_1, ρ_2	Densities of the two plates ($\rho_1 \leq \rho_2$)
σ_{ts}	Ultimate tensile strength
τ	= p, theoretical yield shear strength of metal
ϕ	Dynamic bend angle, potential function (chapter II)
χ	Strength of doublet (chapter II)
ψ	Loss factor (chapter V), stream function (chapter II)
Γ	Circulation (chapter II)
a	Radius of rotating cylinder (as used in chapter II)
a_1	Twice the contribution to wavelength when wake swings from bottom position towards material of lower density
a_2	Twice the contribution to wavelength when wake swings from top position towards material of higher density
c	Amplitude to wavelength ratio = (h/λ)
d	Diameter of obstacle
h	Wake height, wave amplitude (Fig. 1.4 and Fig. 1.5)
i	$= \sqrt{-1}$

k	Fraction of total wake height occupied by the metal of density ρ_1
2ℓ	Length of wake
m	Mass of the wake
p	Pressure (chapter III), theoretical strength (Chap.V)
p_o	Free stream pressure
p_1, p_2	Corresponding pressures in the two fluid regions
p_s	Specific pressure (Eulers number) $= p/(\frac{1}{2}\rho V_p^2)$
r	$= t_1^*/t_2^*$
r_r	$= t_r^*/t_2^*$
r_s	$= t_s^*/t_2^*$
r_v	$= V_S/V_F$
t	Plate thickness
t_f	Fluidized thickness of the plate
t_1, t_2	Thicknesses of two plates
t_1^*, t_2^*	Normalised thickness of plates
t_r, t_s	Thicknesses of re-entrant jet and salient jet
t_r^*, t_s^*	Corresponding thicknesses of re-entrant jet and salient jet contributed by normalised thicknesses of the two plate jets
$t_{r_1}^*, t_{r_2}^*$	Re-entrant jet contributed by normalised thicknesses of plates I and II

w	Width of fluidized zone
(x,y)	Co-ordinates in physical plane
x_1	Abscissa of obstacle centre w.r.t. stagnation point as origin.
(x_o,y_o)	Co-ordinates of intersection point of extension of stagnation streamlines w.r.t. stagnation point
z	$= x + iy$
(e/m)	Explosive loading = mass of explosive e/ accelerated mass m
A,B,C	Constants given by equations (2.23), (2.24) and (2.25)
A^*,B^*,C^*	$A^* = A$, $B^* = B$, $C^* = C$ if β_1 and β_2 are suitably interchanged in the integrals
C	Specific heat
C_b	Bulk sound speed
E_c	Collision energy
E_ℓ	Explosive loading number $= \frac{0.612\ e/m}{2 + e/m}$
E_w	Explosive welding number $= p/(\frac{1}{2}\rho V_D^2)$
G	Modulus of Rigidity
I	Moment of Inertia of Swinging wake
L, L^*	Lift force
L	Energy loss in collision (chapter V)
N_1	Frequency of swinging wake
Re	Reynolds number

S	Stagnation point
T_{mp}	Melting point temperature
U	Speeds of the free streamlines of all the jets
U_1, U_2	Speeds of two incomming jets
V_c	Collision velocity
V_D, V_{D_1}, V_{D_2}	Detonation velocity of explosive
V_F	Velocity of flyer plate jet
V_{FS}	Velocity of vortex street
V_J	Velocity of jet after impact (considering energy loss)
V_P, V_{P_1}, V_{P_2}	Plate velocity
V_s	Sonic velocity.

SYNOPSIS

A Thesis Entitled " Swinging Wake Mechanism for Interface-Wave Generation and Permissible Range of Parameters for Explosive Welding " submitted in Partial Fulfilment of the Requirements For the Degree of Doctor of Philosophy by R.C. Gupta to the Department of Mechanical Engineering, Indian Institute of Technology, Kanpur, July, 1981 under the Supervision of Professor G.S. Kainth.

Explosive welding is classified into two broad categories viz. (i) symmetric welding and (ii) asymmetric welding on the basis whether explosive is laid on both the plates or on only one plate. This classification seems to be inadequate to explain certain features of explosive welding such as distortion of interface wave. In order to study the mechanism of explosive welding for general situation, various types of asymmetries arising from differences in plate material and explosive charge are classified.

A hydrodynamic model of explosive welding for general arrangement is analysed. It is considered that there are two stagnation streamlines which seperate the main jet into corresponding salient jet and re-entrant jet. The model considers an obstacle bounded by the stagnation streamlines and that the wake behind the obstacle swings from side to side producing a wavy interface. Flow of two dissimilar fluids meeting at an angle over an obstacle is analysed and expression for the lift force acting on the wake is obtained.

Many theories have been proposed so far to explain the wave formation, however, these theories do not explain some of the observed phenomena such as distortion satisfactorily. A 'Swinging Wake Mechanism' for interface wave generation in explosive welding is proposed. Expressions for amplitude to wavelength ratio and degree of distortion are developed. The model explains the generation of interface wave in explosive welding and distortion of the wavy weld interface for the case of dissimilar metal combination. The theory predicts that (i) degree of distortion increases with increase in the difference in densities of the two materials and (ii) amplitude to wavelength ratio of interface wave for dissimilar metal combination is lower than that for similar metal combination. Theoretical predictions are in reasonable agreement with the experimental results of Onzawa and Ishii and other workers.

Following the complex velocity analysis, expression for diameter of obstacle for general arrangement of explosive welding is developed. The expression reduces to the equation given by Reid and Sherif for obstacle-diameter for ideally symmetric situation. From the analysis it is concluded that smaller waves would be produced in asymmetric situation as compared to waves in symmetric welding. Also, waves would be smaller for dissimilar metal combination as compared to waves in similar metal combination.

The limited extent of fluidized zone in explosive welding within which fluidlike behaviour can be considered has not been sufficiently emphasised in literature. Furthermore, the energy loss during collision in explosive welding is generally ignored. A model based on the limited extent of fluid zone and energy-loss is analysed for asymmetric welding. An expression is developed for the mass of the re-entrant jet which shows a reasonable agreement with Meyer's experimental results.

Earlier research work shows that nature of experimental variation of wave-amplitude with obliquity angle in asymmetric welding situation is such that wavy interface is formed above a certain angle β_L and below and angle β_W. Furthermore, there is a maxima in wave amplitude corresponding to an obliquity angle β_0. A straight bond is formed when obliquity angle is increased from β_W to β_W and no welding takes place above β_E. These angles depend upon the material properties of the flyer plate and its velocity V_p. In the present analysis it is shown that all the obliquity angles (β_L, β_0, β_W and β_E) depend upon Euler's number (specific pressure) defined by $p_s = p\ (\frac{1}{2} \rho V_p^2)$ where p is the theoretical strength of the flyer plate material and ρ is its density. Expression for these limiting angles have been developed. The importance of Euler's number in explosive welding is emphasised. Based on this model, a

selection procedure for explosive welding parameters is suggested. A weldability window for explosive welding is studied.

Explosive welding experiments on plate-cladding, variable angle experiments and tube to tube-plate welding are carried out to demonstrate the applicability of the suggested selection procedure for explosive welding parameters.

CHAPTER I

INTRODUCTION AND REVIEW OF LITERATURE

1.1 INTRODUCTION

Explosive welding is done by progressive high velocity oblique impact between two metal plates by detonating an explosive charge which is laid on the top of a flyer plate. Explosive welding has come to play an important role in many industries [1] such as chemical, atomic energy, aircraft, space, cryogenic, and power generating industries. Explosive bonding process is extensively used for flat plate cladding of dissimilar metals required for fabricating chemical equipment used in corrosive service conditions. Explosive welding is applied to large plate cladding [2-6], welding of tubes to tube-plates of heat exchangers [7-18], tube plugging [17-27], welding of pipes [28-35], production of duplex [36-39] and triplex tubing [40], and fibre reinforced materials [41-44]. Other applications include : butt welding and lap welding [45], production of mono and bimetalic array of rods [46], manufacture of multilayered foil cylinders [47-48], fabrication of honey-combed structure [49] and rib reinforced panels [7] and production of clad electrode materials [50]. Commercialization of explosive welding process is in progress [51-52].

1.2 DEVELOPMENT OF EXPLOSIVE WELDING

During the second world war it was observed that metallic fragments of bombs occasionaly stuck to metallic objects in the vicinity of targets. Also, it was known for a long time that bullets fired at metal target sometimes stuck to the target. Carl in 1944 [53] observed wavy interface between two half hard brass shims welded by using a charge of high detonation velocity. Lavrentiev, as reported by Deribas [54], recognised explosive welding in 1946. Credit for recognising explosive welding is usually given to Philipchuk [55] who in 1957 observed that metal blank sometimes got welded to metal die in explosive forming and filed a patent application [56]. It appears that during the same period Pearson [57-58] was also engaged in confidential work on explosive welding.

Birkhoff [59] in 1948, while studying the mechanism of hollow explosives with lined cavities, suggested the formation of jet (re-entrant jet) and slug (salient jet) using a wedge shaped liner. Walsh, Shreffler and Willing [60] in 1953 studied the limiting conditions for jet formation in high velocity collision. Allen et al. [61] in 1954 noted that the explosive welding occurs due to the oblique impact of a cylinder on a thin target and observed the interface waves produced by surface jetting.

Other early research workers in the field were Davenport and Duvall [62], Davenport [63], Cowan and Holtzman [64-65], Tardif [66], Holtzman and Ruderhausen [6], Boes [67], Wills and Murdie [28], Polaclyko and Williams [68], Baran and Costello [69], Reinheart and Pearson [70], Bahrani and Crossland [71] and Addison et al. [72].

Following the work of Allen et al. [61] much work has been done in the field of explosive welding in U.S.A., U.K., West Germany, East Germany, Russia, Japan, Sweden, Brazil, Poland and Czechoslovakia. Explosive welding is now recognised as a practical process and finds specific commercial applications. Some of the review articles on explosive welding appear in references [73-80].

1.3 MECHANISM OF EXPLOSIVE WELDING

Explosive welding is broadly classified into two categories viz. (a) symmetric welding and (b) asymmetric welding, on the basis whether explosive is laid on both the plates or on one plate only. Inclined arrangement is one in which plates are kept at some inclination whereas in parallel arrangement the two plates are kept parallel at some distance (stand-off) apart.

Schematic diagram of inclined arrangement of asymmetric explosive welding is shown in Fig. 1.1-a. The flyer

plate is kept inclined at an angle α to the parent plate. Explosive is laid on the flyer plate while buffer plate is kept in between to avoid damage to the flyer plate. Explosive is ignited from one end with a detonator. Figure 1.1-b describes the configuration of the flyer plate during the process of welding [73-80]. Various assumptions have been made regarding the direction of velocity of the flyer plate. Birkhoff [59] considered that the direction of flyer plate velocity bisects the angle SPC. Many workers consider that the direction of the velocity is approximately normal to the moving flyer plate. However, all the assumptions lead to similar conclusions. The following simple relationships are usually used (Figs. 1.1 and 1.2).

$$V_W = V_P/\sin\beta \qquad (1.1.a)$$

$$V_F = V_P/\tan\beta \qquad (1.1.b)$$

$$\phi = \tan^{-1}\left(\frac{V_P}{V_D}\right) \qquad (1.1.c)$$

and

$$\beta = \alpha + \phi \qquad (1.1.d)$$

where, α, ϕ and β are the set-up angle, the (dynamic) bend angle and the (dynamic) obliquity angle respectively, V_D, V_P, V_F and V_W are detonation velocity of explosive,

flyer plate velocity, stream velocity and collision velocity respectively.

Thus for parallel arrangement ($\alpha = 0$), $V_W = V_D \approx V_F$

Various formulae for plate velocity have been suggested [81-83], the equation given by Gurney et al. [81] is as follows

$$V_P = \frac{0.612\ e/m}{2 + e/m}\ V_D \qquad (1.2)$$

where, e/m is the explosive loading (ratio of explosive mass to accelerated mass).

Equation (1.2) is the simplest one among all the formulae for plate velocity in explosive welding. Hay [86] mentioned that the plate velocity given by all the formulae converge for values of explosive loading usually used for explosive welding.

Figure 1.2-a shows the collision of the flyer plate, moving at an impact velocity V_p, with the parent plate. Figure 1.2-b represents kinematically equivalent system such that the stagnation point S is considered at rest. Birkhoff [59] assumed that strength of the metal can be neglected as compared to the high pressure encountered in collision and considered classical hydrodynamics of perfect fluid. Hence, the flyer plate is considered to impinge on the parent plate

as main fluid jet which divides into (i) salient jet and (ii) re-entrant jet as shown in Fig. 1.2-c. Robinson [87] showed that strain rate in explosive welding is usually higher than the critical strain rate (10^7/sec) above which the material behaves like an inviscid fluid.

By considering conservation of mass and momentum, mass of the re-entrant jet - m_r and that of the salient jet - m_s are given by

$$m_r = m(1 - \cos \beta)/2 \qquad (1.3.a)$$

$$m_s = m(1 + \cos \beta)/2 \qquad (1.3.b)$$

The importance of re-entrant jet for explosive welding is well emphasised in literature [77, 78, 80, 88]. The re-entrant jet in fact contains not only the contaminated layer of flyer plate but also the surface layer of the parent plate. The virgin plate-surfaces come in contact under high pressure resulting in welding. Bergmann et al. [89] and others [90-91] have shown experimentally that re-entrant jet is actually formed in explosive welding and there is a loss of weight of plates after collision [91]. High speed photography by Bergmann et al. [89] and Onzawa and Ishii [90] confirmed the existence of the re-entrant jet. Condition for jetting seems to correspond to the condition for welding [88].

Walsh, Shreffler and Willing [60] showed that below a certain critical angle jetless configuration exists and re-entrant jet is absent. Limiting condition for jetting has also been reported by Allen et al. [92], Cowan and Holtzman [64].

Pearson [58] thought explosive welding occured as a result of large amount of plastic interaction between the surfaces to be welded. Davenport [63] thought that explosive welding is a form of cold pressure welding. Holtzman and Rudershausen [7] were of the opinion that the metallic jet produced by impact subsequently melts to form the bond. Boes [67] considered that the explosive welding is basically a form of friction welding. Not withstanding some early confusion regarding the mechanism of explosive welding, most of the investigators now agree that surface jetting is essential for the formation of a good bond.

1.4 WELDED INTERFACE

Depending upon welding parameters, nature of the welded interface [60] may be

(i) straight (direct) bond

(ii) wavy interface, and

(iii) uniform layer of solidified melt.

Davenport [63] pointed out the following advantages of a wavy interface : (i) the waves increase the area of contacting surfaces several folds and thus expose a great deal of fresh surface on the plates which readily bond under pressure, (ii) waves provide very high strains in the thin surface layers which greatly increase the mobility of the atoms and dislocations in these layers, and (iii) the waves provide a mechanical interlocking. Hay [86] concluded on the basis of the results of Bayce [93] that the maximum shear strength coincides with the wavy interface. In direct bond regime there are often areas of non bonding, while in the extremely turbulent regime beyond the condition of wave formation, the shear strength decreases rapidly due to the formation of continuous melt zones [60]. Contrary to common belief, sometimes a straight interface may have equally high strength as that exhibited by a wavy interface [80]. Bahrani and Crossland [94] stated that 'waves act as interlocking serrations' in shear tests but they further stated that 'the welds with smaller interfacial waves gave better results in tension tests and also in bend tests, whereas it was noted that large waves produced stress concentration and sometimes caused cracks'.

1.5 THEORIES OF INTERFACE WAVE GENERATION

It is intriguing that under such a violent condition of explosion, regular periodic waves are formed in explosive welding. The appearance of such periodic waves

are also found on eroded blades of steam turbines, pumps and other solids impacted by high velocity liquid jets and drops[95].

Many theories for interface wave formation have been proposed so far. Most of the theories fall within one of the following categories.

1.5.1 Indentation Model

According to Abrahamson's mechanism [96] the parent plate is plastically indented at the collision point and a hump is driven forward. The hump grows until at a certain instant the main jet climbs over the hump leaving it behind and the process continues. Bahrani et al. [97] proposed a mechanism similar to that of Abrahamson and gave a detailed explanation of wave formation and appearance of vortices attached to crest and trough of the waves (Fig. 1.3). They considered that the flyer plate jet indents the parent plate, and it is deflected upward modifying the shape of the hump. The stagnation point transfers to the top of the hump and starts forming a new hump while descending thereby producing successive waves. The mechanism of Bahrani et al. [97] finds support from metalographic examination of welds. The mechanism thus explains the formation of vortices attached to crest and trough of the waves and further suggests that at a greater angle of incidence the interface is straight as the main jet pushes the shallow hump ahead of it.

Watanable et al. [98] attributed the periodicity to the influence of the period of instability of re-entrant jet. Babul and Wlodarczylk [99] introduced the concept of 'bulk sound speed' based upon the bulk modulus of the material and opined that periodicity in the indentation results from a periodic oscillation of stagnation point velocity about the local sound speed.

1.5.2 Stress Wave Mechanism

Godunov et al. [100] attributed the interface wave formation to the effect of rarefaction waves produced when the compressive shock emanating from the stagnation point are reflected from the free surface of the flyer plate. Deribas et al. [101-104] studied the effect of initial parameters on wave formation. From the work of Godunov et al. [100], Deribas [105] conclude that the waves in explosive welds are caused by self-excited vibrations produced by a rigid indentor.

1.5.3 Hydrodynamic Instability Model

Hunt [106] suggested that principal features of wavy weld interface are consistent with a mechanism which arises as a result of Helmholtz instability between the re-entrant jet and parent plate-jet. Cowan and Holtzman [64] and Cowan et al. [107] showed that interface wave formation in explosive welding is analogous to (i) the formation of

vortex street in fluid flow around an obstacle and (ii) the collision of liquid streams. They explained the transition from a straight bond to a wavy bond on the basis of Reynolds number which they [107] defined as

$$R_e = \frac{\rho_F + \rho_P}{2(H_F + H_P)} V_F^2$$

where ρ_F and ρ_P are the densities of the flyer plate and parent plate material and H_F and H_P are the corresponding diamond pyramid hardnesses.

Klein [108] noticed that the general appearance of the welded interface is similar to the von Karman vortex street (Fig. 1.4). Klein's experimental investigation showed that average value of amplitude to wavelength ratio (h/λ) of welded interface is approximately 0.3 which is close to the value of stable spacing ratio of 0.281 in Karman vortex street. Keller [109] experimentally found three critical velocities in the case of explosive welding corresponding to laminar flow, the formation of periodic current and turbulent flow.

Kowalickand Hay [110-111] applied vortex shedding theory to wave formation (Fig. 1.5) in explosive welding. They considered the collision of two plates as a fluid flow problem with the re-entrant jet corresponding to an obstacle (barrier) in the flow. The flow regime behind an obstacle is

is governed by Reynolds number (Re) given by

$$Re = \frac{V_F L}{\nu} \qquad (1.4)$$

where ν is kinematic viscosity of the metal jet, V_F is the stream velocity and L is the barrier height. Transition from laminar flow to a flow containing vortex street occurs when the Reynolds number is in the range $2 < Re < 3.2$. However, the wave formation was observed upto $Re \approx 10$ [110]. Some notable work on vortex shedding and oscillations in fluid flow is found in references[112-114].

Robinson [87] suggested that the interface wave formation is due to the fact that velocity profile behind the stagnation point may have one or two inflection points. Such a velocity distribution causes shear flow region which exhibits Helmholtz instability leading to the wavy interface provided the effect of viscosity does not damp out the instability.

Reid [88] considered Birkhoff's wake oscillator model [115-116] as a possible mechanism for interface wave generation and explained fingured tip appearance of lead-steel weld interface. Gupta and Kainth [117] and Botros and Groves [118] extended the wake oscillator model with certain modifications.

Onzawa and Ishii [119], Reid [88] and Reid and Sherif [120] have used vortex shedding model to predict wavelength of interface wave. While comparing the theory of Reid and Sherif [120] with Robinson's theory [87], Reid [121] concluded that essentially the bases of the two approaches are similar as the width of the disturbance to the flow [87] is of the order of the diameter of obstacle in the flow [120].

Sobky and Blazynski [122-123] considered the flow analogy of explosive welding and showed that similar waves as that observed in explosive welding are produced if one fluid stream collides with another fluid.

1.5.4 Contradicting Nature of the Theories of Interface Wave Generation

The indentation theory appears to be reasonable for asymmetric welding situation. Hunt's mechanism [106] depends upon a particular asymmetry in the welding arrangement and presumably implies that waves will not be produced [88] in symmetric arrangement. Waves in symmetric arrangement have also been observed and as mentioned by Reid [88] 'this would lead one to suspect that Hunt's mechanism is incorrect'. Reid [88] further opines that the mechanism of Godunov et al. [100] would appear to cast doubt on the production of waves in symmetric case, since ideally the symmetry implies equal pressure distribution on either side of the interface.

The mechanism of Bahrani et al. [97] suggested that the wave formation is ahead of the stagnation point, whereas, the mechanism of Godunov et al. [100] and vortex shedding mechanism [110] imply that the wave formation is behind the stagnation point.

Deribas [105] criticised the vortex shedding theory on the basis that waves without vortices are also observed in explosive welding, whereas Crossland [80] mentioned that 'in fact such waves can also be observed in fluids'.

Sobky and Blazynski [123] conclude that 'there exists more than one mechanism, operating under different conditions and governed by the initial parameters of the welding process'.

1.6 INTERFACE WAVE CHARACTERISTICS

1.6.1 Amplitude and Wavelength of Interface Wave

Experimental investigation of Klein [108] and Kowalickand Hay [110] show that average value of amplitude to wavelength ratio $c = h/\lambda$ is about 0.3 which is close to the value of stable spacing ratio of 0.281 for Karman vortex street. The large scatter found in h/λ ratio is attributed to unknown geometry of obstacle and fluctuation of flow due to hump deformation [110].

Reid and Johnson [124] used indentation analysis and predicted the wave amplitude using Hunt's formula. However, while considering the analogy between welded interface and Karman vortex street, the amplitude of interface wave is usually taken equal to the wake height h in the fluid flow over an obstacle of diameter d and that $h = 1.25\ d$. The wavelength of the interface is thus written as $\lambda = 1.25\ d/c$. While discussing the various theories of wave formation in explosive welding, Reid [88] stated that 'the vortex shedding mechanism is therefore as good as any of the other theories proposed to date', on the basis that the theories of Hunt[106], Godunov et al. [100], Onzawa and Ishii [119] predict the relationship for asymmetric situation as $\lambda \propto t\ \beta^2$, where t is the thickness of plate and β is the obliquity angle. Later on Reid and Sherif [120] developed the relation for symmetric situation as $\lambda \propto t\ \beta$.

Experimental work of Bahrani and Crossland [94] showed that wave formation occurs only within a certain range of obliquity angles.

Reid and Langdale [125-126] studied the modulation of waves and opined that scatter in the amplitude and wavelength is not necessarily random.

1.6.2 Distortion of Interface Waves

The interface wave profile generally approximates to a sine wave for the case of welding of similar metals, however, the wave profile deviates from sine wave for the case of dissimilar metals. Asymmetry in wave shape has been noted by Hunt [106], Godunov et al. [100], Reid [88], Gupta and Kainth [117], Botros and Groves [118] and Onzawa and Ishii [90]. Godunov et al. [100] mentioned that the asymmetry in wave shape is due to the difference in curvature of the two portions of the wave. Reid [88], Gupta and Kainth [117] and Botros and Groves [118] used Birkhoff's wake oscillator model for two different fluids and they find that asymmetry in wave shape is due to the difference in density of metal plates. Onzawa and Ishii [90] found experimentally that wave distortion depends on density ratio.

1.6.3 Size of Obstacle

Although the ratio $c = h/\lambda$ is independent of obstacle size, but the amplitude h and wavelength λ depend upon the size of obstacle. Also for estimating the Reynolds number for hydrodynamic model of explosive welding, the characteristic length of barrier is needed. Usually the barrier height is considered proportional to the thickness of the re-entrant jet and the proportionality constant is estimated in the range of 1 to 5 [110]. Considering the

obstacle bounded by the stagnation streamlines for the case of collision of two jets, Reid and Sherif [120, 127] developed the following equation for diameter of obstacle in an ideally symmetric situation.

$$d = 0.88\, t\, \beta \qquad (1.5)$$

1.7 FLUID BEHAVIOUR OF METALS

Rosenfield and Hahn [128] have defined four regions of metal behaviour depending on the range of strain rate (10^{-4} sec^{-1} $<$ $\dot{\gamma}$ $<$ 10^{+5} sec^{-1}) and temperature (77 K $<$ T $<$ 293 K). In the region IV, with strain rate in the range 10^{-4} to 10^{-5} sec^{-1}, the metal behaves as a viscous fluid. Robinson [129] considered an additional region V of inviscid fluid behaviour for strain rates greater than a critical strain rate $\dot{\gamma}$ defined by

$$\tau = \mu\, \dot{\gamma} \qquad (1.6)$$

where τ is the theoretical yield shear strength and μ is the viscosity of fluidized metal. Robinson estimated the critical strain rate as 10^{7}/sec using inviscid calculations. Considering a local melting and viscous energy dissipation, he estimated the viscosity of copper as 10^{2} - 2.2×10^{2} N s m^{-2}.

Hunt [106] showed that the high pressure zone is of finite extent. The limited extent of the region within which fluid like behaviour occurs in explosive welding is not usually emphasised.

A knowledge of the viscosity of the fluidized jet is essential for estimating Reynolds number which governs the wave formation in explosive welding. Robinson [87] mentioned that the viscosity of the fluid can damp out the shear layer instability in explosive welding. Some information is available on the influence of the viscosity of the fluidized metal jet on jet formation process [130].

1.8 EXPLOSIVE WELDING PARAMETERS AND WELDABILITY WINDOW

Various research workers [131-153] have studied the parameters for explosive welding. Previous studies show that important welding parameters are

1. Explosive loading, e/m
2. Plate velocity, V_p
3. Obliquity angle, β
4. Collision velocity, $V_c = V_p/\beta$
5. Material properties of plate/s such as density and strength of metal.

On the basis of the past research work it can be concluded that the following conditions need to be satisfied to obtain a successful weld.

1. Collision velocity V_C should preferably be less than sonic velocity V_S in the plate material, though some welds have been achieved upto a value $V_C/V_S = 1.25$.

2. As the formation of the re-entrant jet is essential for welding, impact angle β should exceed a limiting value β_L below which a jetless configuration exists.

3. The stand off distance in parallel arrangement should preferably exceed half the flyer plate thickness to allow the flyer plate to achieve its terminal velocity.

4. Plate velocity V_P should exceed a certain value $V_{P_{min}}$ to ensure the minimum value of contact pressure for dynamic yielding. Minimum value of the plate velocity is given by [148].

$$V_{P_{min}} = K_1 \sqrt{\frac{H_V}{\rho}} \qquad (1.7)$$

where ρ and H_V are density and Vicker's Hardness Number of the material and K_1 is a constant which varies between 0.6 to 1.2 depending upon surface cleanliness[80].

5. Plate velocity V_P should be below a certain value $V_{P_{max}}$ to avoid melting and formation of intermetallic compounds. Maximum value of plate velocity is given by [148].

$$V_{P_{max}} = \frac{1}{N} \frac{(T_{mp}\, C_b)^{1/2}\, (K\, C\, C_b)^{1/4}}{V_C (\rho\, t)^{1/4}} \qquad (1.8)$$

where, T_{mp} is the melting point, C_b the bulk sound speed, K the thermal conductivity, C the specific heat, V_C the collision point velocity, ρ the density of the flyer plate, t the thickness of the flyer plate, and N is a constant.

It is evident that explosive welding is possible only within a limited range of explosive welding parameters. The region of weldability is usually termed as weldability window or explosive welding window.

Weldability windows have been plotted by various research workers in the following ways.

1. Obliquity angle β versus collision velocity V_C
2. Obliquity angle β versus plate velocity V_P
3. Collision energy E_C versus collision velocity V_C
4. Explosive loading e/m versus collision velocity V_C
5. Plate velocity versus collision velocity V_C.

1.9 METALLURGY OF EXPLOSIVE WELDS

Metallurgical effects in explosive welding are less severe than in fusion welding processes as demonstrated by Lucas et al. [154]. However, in some cases, under incorrect welding conditions molten layer leads to formation of brittle intermetallic compounds.

In explosive welding, shock waves and high collision pressure cause severe plastic deformation resulting in hydrodynamic flow. Williams et al. [155] have observed metastable phases in the welded region. Rapid cooling associated with intense metal flow at extremely high strain rates produces [156] high dislocation density ($10^{11}/cm^2$) and other lattice defects [157]. In addition to mechanical twinning, phase changes could occur in the vicinity of the interface [158]. Slip also occurs during shock deformation and slipline notices are fine and more closely packed [159].

A sizable amount of the jet is captured in the swirls or eddies on either side of the wave crest. Lucas et al. [155], by means of electron microscopy, found clear evidence of melting in the vortex area. Using X-ray microanalyser and X-ray diffraction, Onzawa and Ishii [160] studied the formation of alloys on the bonded boundary of explosively welded dissimilar metals.

Ezara reported [161] that, at higher energy levels, molten pockets coalesce to form a continuous molten layer due to trapping of large amount of jet. Nagarkar and Carpenter [157] mentioned that solidified melt zones show columnar grain structure typical of cast metals. Extremely high hardness with the solidified melt zone may be due to high rates of cooling involving large amount of microstresses, phase transformation possibly of the martensite type [162] and entrapment of oxides, nitrides and carbides [163].

In dissimilar metal welds, thin layer of intermetallic compounds are found [78, 94]. Angelo et al. [164] mentioned that microprobe results of melt zone of a wide variety of dissimilar metal welds gave alloy series midway between the two component metals. The two elementsmix almost independently of their mutual solid solubility [158]. Trueb [165] observed abrupt changes in the microstructure and sharp transition in concentration of element. Balakrishna et al. [166] studied the influence of collision parameters on the width of diffusion zone and concluded that the width influences the bond strength. Micro-indentation tests of explosive welds have also been reported [94, 167].

1.10 STRENGTH OF BOND

Bahrani and Crossland [94] carried out tensile test across the weld interface, tensile shear test, side shear

test as recommended by ASTM and bend test. Salwan et al. [168], Balakrishna et al. [166, 169 to 174] and Singh [175] have also reported some results on bond-test. Wylie et al. [137] have devised an impact test across the plane of weld.

The strength of the welded bond was also studied by other various research workers [93, 131, 176 to 178]. All these tests showed that usually the weld is stronger than the weaker of the two metals. In general, the material after welding is harder and its ductility and fracture toughness is reduced [78]. Welds also show residual stresses which can be reduced [78] by subsequent heat treatment and cold forging [179]. Formation of harmful intermetallic compounds and a continuous cast interlayer is known to reduce the strength of the bond.

1.11 PRESENT STUDY

Mechanism of explosive welding and interface wave generation is quite complex. Eventhough the basic models of explosive welding seem sufficient for practical applications, nevertheless, further analysis of the explosive welding process is essential for better understanding and application.

The present classification of inclined arrangement of explosive welding into symmetric - asymmetric welding seems inadequate to explain certain features of explosive welding. Various types of asymmetries arising from changes in plate

material and explosive are classified and discussed. A hydrodynamic model of explosive welding for general situation is developed.

Many theories have been proposed so far to explain the interface wave formation. These theories, however,do not explain the observed phenomenon of wave distortion satisfactorily. A 'Swinging Wake Mechanism' for interface wave generation in explosive welding is proposed to explain the interface wave distortion for dissimilar metal combination.

Obstacle size governs the interface wave size. Expression for diameter of obstacle is developed for general situation of explosive welding.

The limited extent of fluidized zone in explosive welding within which fluidlike behaviour can be considered has not been sufficiently emphasised in literature. Furthermore, the energy loss during collision in explosive welding is generally ignored. A model based on the limited extent of fluid zone and energy loss is suggested for asymmetric welding and the expressions for permissible obliquity angles within which welding is possible are obtained. Based on this model a selection procedure for explosive welding parameters is suggested.

Experiments on plate cladding,variable angle experiments and tube to tube-plate welding are carried out to demonstrate the applicability of the suggested selection procedure for explosive welding parameters.

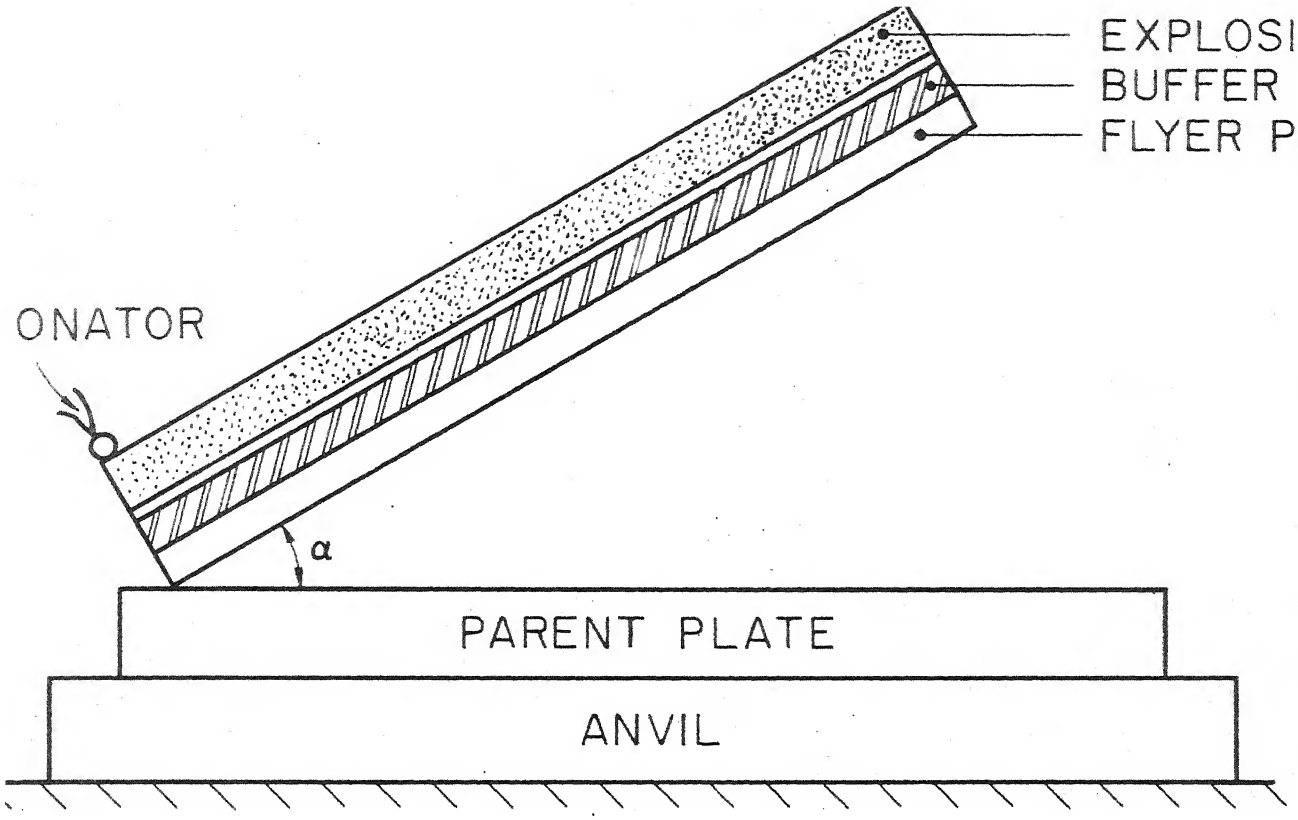

(a) BEFORE DETONATION

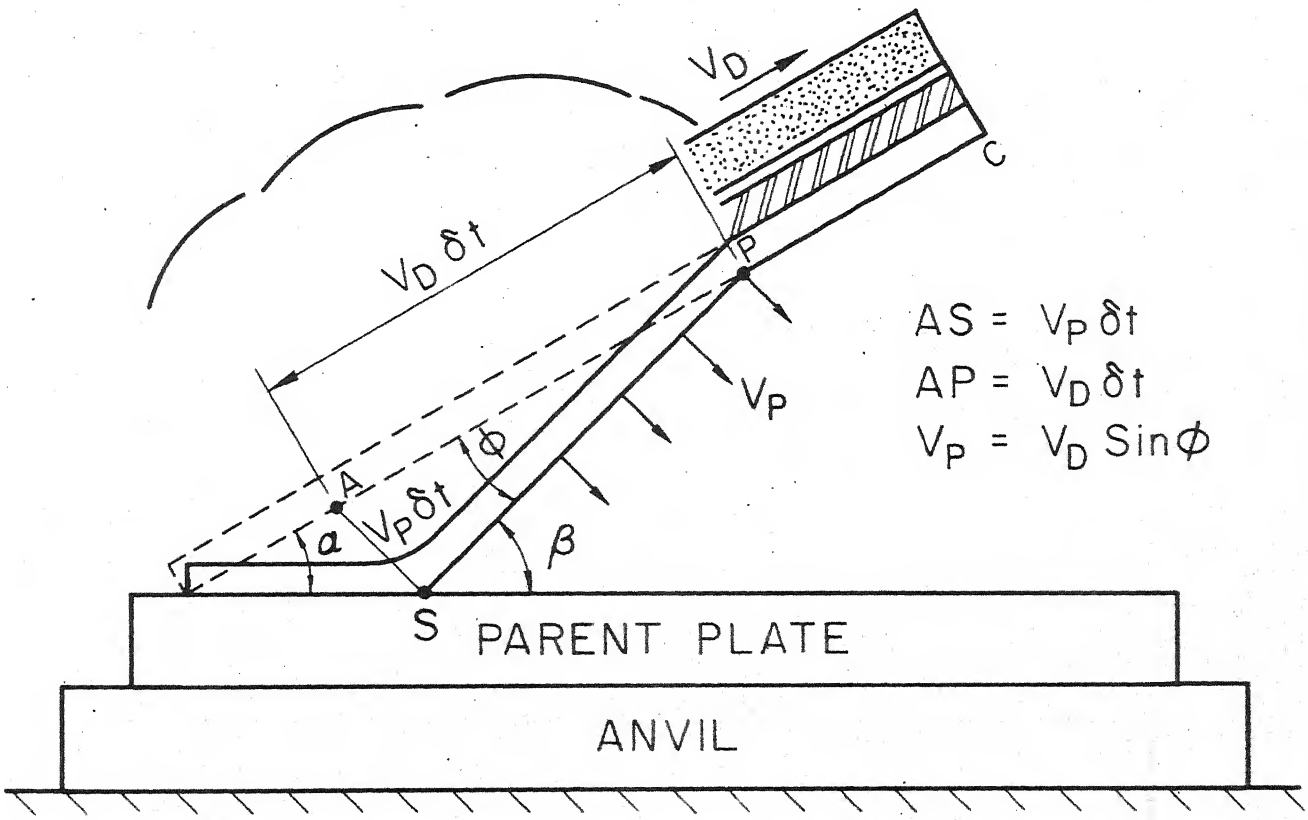

A SHORT TIME AFTER THE INITIATION OF DETONAT

FIG. I.I MODE OF COLLAPSE OF FLYER PLATE

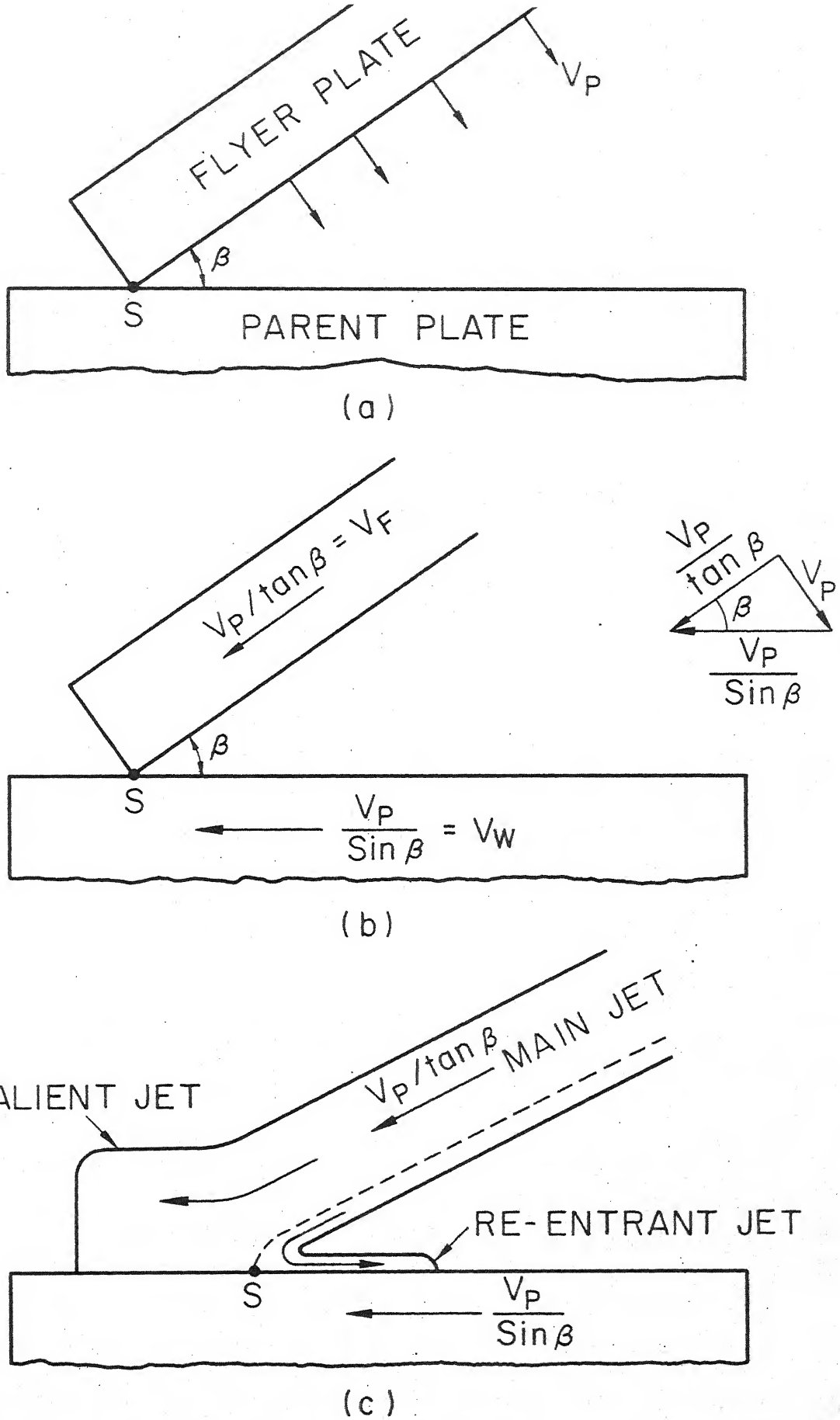

FIG. 1.2 THE FORMATION OF THE METAL JET

(a) RIGID INELASTIC BASE

(b) STATIONARY ELASTIC BASE

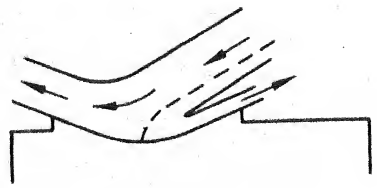

(c) STATIONARY ELASTIC BASE WITH SHEAR

(d) ALLOWING FOR VELOCITY OF THE PARENT PLATE

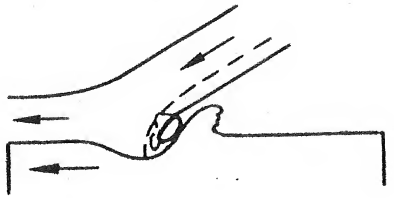

(e) HUMP DEFLECTING RE-ENTRANT JET INTO ONCOMING FLYER STREAM

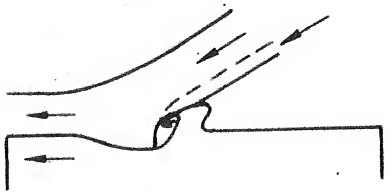

(f) FORMATION OF TAIL BY JET RECIRCULATION

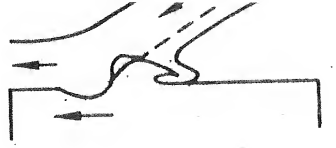

(g) FORMATION OF FORWA TRUNK

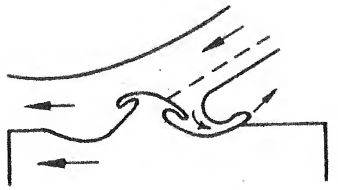

(h) FORMATION OF FRON VORTEX

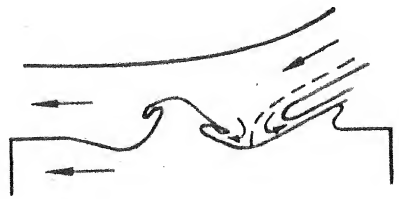

(j) COMPLETION OF PRO

FIG. I.3 SCHEMATIC DIAGRAM OF DEVELOPMENT OF THE WAVE FORMATION DURING THE EXPLOSIVE WELDING OPERAT

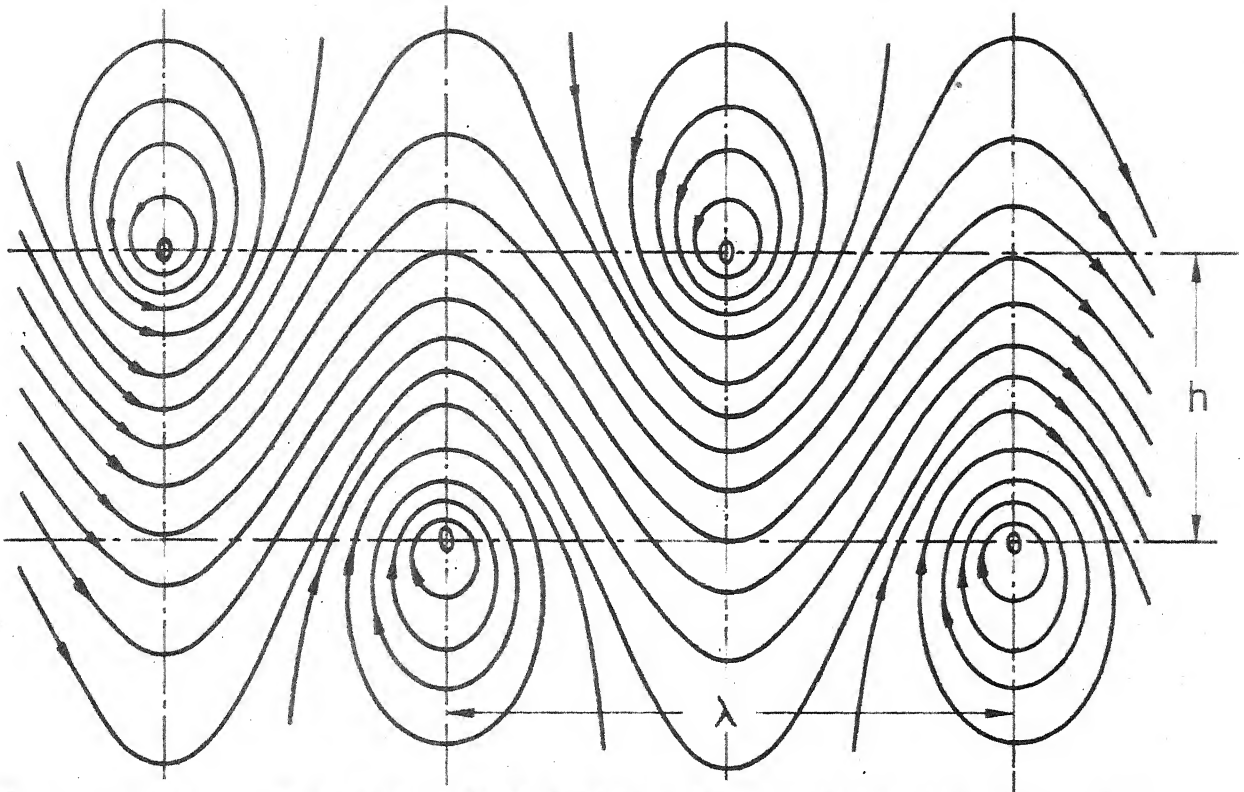

FIG. 1.4 FLOW PATTERN PRODUCED BY VON KARMAN VORTEX STREET

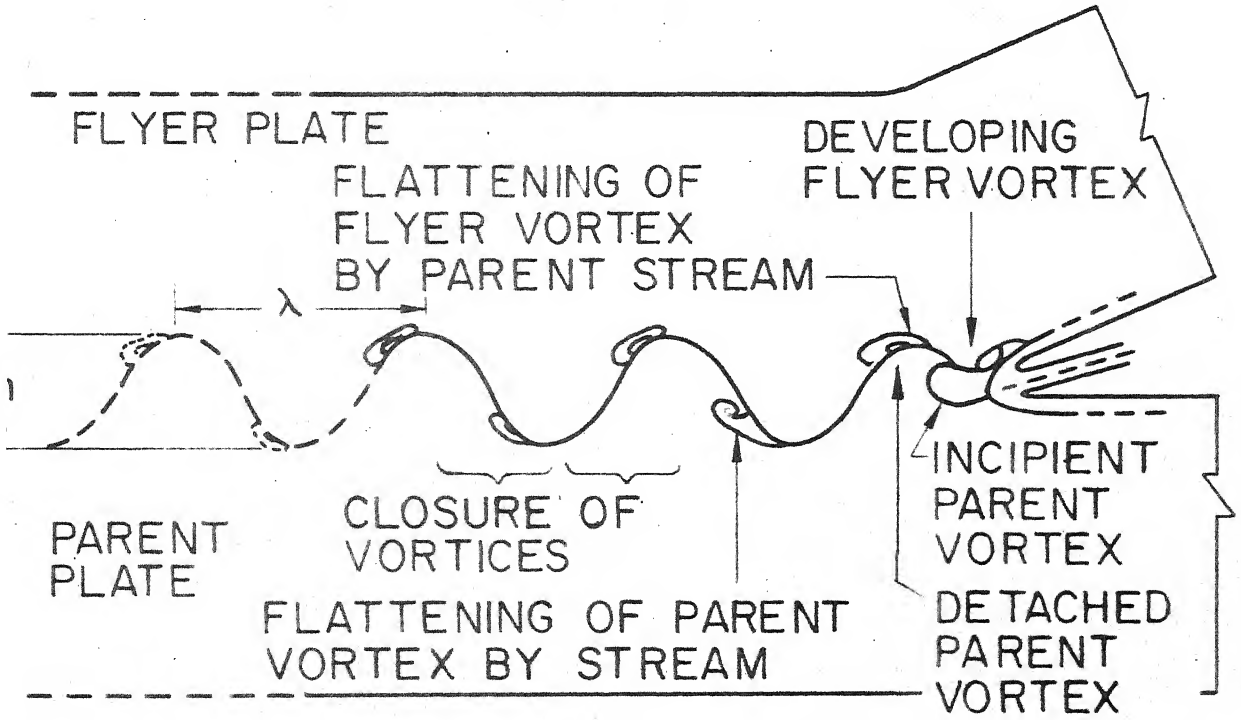

FIG. 1.5 FORMATION OF WAVY INTERFACE IN EXPLOSIVE WELDING (KOWALICK AND HAY [110])

CHAPTER II

A HYDRODYNAMIC MODEL FOR GENERAL ARRANGEMENT OF EXPLOSIVE WELDING

2.1 INTRODUCTION

Explosive welding is usually classified in two broad categories as (i) symmetric welding and (ii) asymmetric welding on the basis whether explosive is laid on both the plates or on one plate only. In order to study the mechanism of explosive welding for general asymmetric situation, various types of asymmetries arising from differences in plate material and explosive charge are classified and discussed.

A hydrodynamic model for general arrangement of explosive welding is presented.

2.2 ASYMMETRIES IN EXPLOSIVE WELDING

It is found from the experimental work of Onzawa and Ishii [90] that in so called symmetric situation if the plates are of different densities the re-entrant jet does not bisect the set up angle and the interface wave is distorted. Strictly speaking, for true symmetric situation of explosive welding (i) the re-entrant jet should bisect the set-up angle and the interface wave ought to be a sine wave. Therefore the above broad classification of explosive welding into symmetric and asymmetric welding does not fully explain the welding mechanism.

In practice, explosive welding is generally applied to welding of two different metals. In view of the need to study the mechanism of explosive welding of two metals and for better understanding of the process parameters, it is necessary to classify various asymmetries in the geometrically symmetric welding situation.

2.3 CLASSIFICATION OF ASYMMETRIES

Various types of asymmetries arising from differences in parameters of plate and explosive charge are classified as follows :

1. Explosive Asymmetries
   - (i) Explosive thickness asymmetry (Fig. 2.1-d)
   - (ii) Explosive type asymmetry (Fig. 2.1-c)
2. Metal Plate Asymmetries
   - (i) Metal plate thickness asymmetry (Fig. 2.1-f)
   - (ii) Metal plate density asymmetry (Fig. 2.1-e)
   - (iii) Metal strength asymmetry
3. Buffer Plate Asymmetry

Explosive Asymmetries and Metal Plate Asymmetries are shown in Fig. 2.1. Usually the buffer plate used on both the metal plates is of the same type and thickness and hence buffer plate asymmetry is of little importance.

In explosive welding there may be one or a combination of these asymmetries. Thus an ideal symmetric situation is such that none of these asymmetries is present.

2.4 DIRECTION OF COLLISION

A general arrangement of explosive welding considering the various asymmetries is shown in Fig. 2.2. Velocities of the plates V_{P1} and V_{P2} are given from eq. (1.2) as

$$V_{P1} = \frac{0.612\ (e/m)_1}{2 + (e/m)_1}\ V_{D1} \qquad (2.1.a)$$

$$V_{P2} = \frac{0.612\ (e/m)_2}{2 + (e/m)_2}\ V_{D2} \qquad (2.1.b)$$

where $(e/m)_1$ and $(e/m)_2$ are the explosive loadings on the two sides, and V_{D1} and V_{D2} are the detonation velocities of the two explosives.

If $V_{P1} \neq V_{P2}$, it is implied that the direction of collision will not bisect the set up angle. If the direction of collision is inclined at α_1 and α_2 relative to plate-I and plate-II, then from velocity and geometry considerations

$$\frac{V_{P2}}{V_{P1}} = \frac{\sin \alpha_2}{\sin \alpha_1} \approx \frac{\alpha_2}{\alpha_1} \qquad (2.2)$$

and

$$\alpha_1 + \alpha_2 = 2\alpha \qquad (2.3)$$

where, 2α is the initial set up angle in general arrangement of explosive welding.

Hence inclination angles α_1 and α_2 are given as

$$\alpha_1 = \frac{2}{1 + V_{P2}/V_{P1}} \alpha \qquad (2.4.a)$$

$$\alpha_2 = \frac{2\, V_{P2}/V_{P1}}{1 + V_{P2}/V_{P1}} \alpha \qquad (2.4.b)$$

In the progressive collapse of the two plates, the collision point S proceeds in the direction SS'. Angle between the direction of collision and the central line bisecting the set up angle is given by

$$\theta_c = \alpha_1 - \alpha = \alpha - \alpha_2$$

or

$$\theta_c = \frac{1 - V_{P2}/V_{P1}}{1 + V_{P2}/V_{P1}} \alpha \qquad (2.5)$$

Since the re-entrant jet is in a direction opposite to that of the salient jet which in turn is opposite to the direction of collision, it can be said that the direction of re-entrant jet and the direction of collision would be same. In case where $V_{P1} \neq V_{P2}$, $\theta_c \neq \alpha$ implying that the re-entrant jet would not bisect the set up angle.

2.5 OBLIQUITY ANGLES IN GENERAL ARRANGEMENT OF EXPLOSIVE WELDING

In general arrangement of explosive welding, $V_{P1} \neq V_{P2}$ and hence the re-entrant jet (collision direction) does not bisect the angle between the two plates. Obliquity angles β_1 and β_2 with respect to the collision direction (Fig. 2.2) for the two plates are given by

$$\beta_1 = \alpha_1 + \phi_1 \qquad (2.6.a)$$

and

$$\beta_2 = \alpha_2 + \phi_2 \qquad (2.6.b)$$

where ϕ_1 and ϕ_2 are the dynamic bend angles (in degrees) of the two plates and are approximately given by

$$\phi_1 = 57.3\, V_{P1}/V_{D1} \qquad (2.7.a)$$

and

$$\phi_2 = 57.3\, V_{P2}/V_{D2} \qquad (2.7.b)$$

Hence from equations (2.6), (2.4) and (2.7)

$$\beta_1 = \frac{2}{1 + V_{P2}/V_{P1}}\,\alpha + 57.3\, V_{P1}/V_{D1} \qquad (2.8.a)$$

$$\beta_2 = \frac{2\, V_{P2}/V_{P1}}{1 + V_{P2}/V_{P1}}\,\alpha + 57.3\, V_{P2}/V_{D1} \qquad (2.8.b)$$

The general arrangement of welding (Fig. 2.2) reduces to (i) asymmetric welding case if $\beta_2 = 0$ and (ii) symmetric welding case if $\beta_1 = \beta_2$.

2.6 A HYDRODYNAMIC MODEL FOR GENERAL ARRANGEMENT OF EXPLOSIVE WELDING

Since the pressure and strain rate encountered in explosive welding are expected to be extremely high, a hydrodynamic model of explosive welding is justified. The impacting plates are considered as impinging jets which divide into salient jet and re-entrant jet as shown in Fig. 2.3. In the hydrodynamic model stagnation streamlines separate salient jets and re-entrant jets. An imaginary obstacle bounded by the two stagnation streamlines and passing through the stagnation point S is considered. The problem thus reduces to the flow of two different fluids meeting at an angle over an obstacle. The obstacle acts as a barrier in the flow resulting in the formation of a wake which swings from side to side like the tail of a swimming fish. The wavy interface in explosive welding would be characterised by the frequency of the swinging wake which in turn depends upon the force on the wake.

2.7 FORCE ON SWINGING WAKE MODELLED AS AN AEROFOIL

Birkhoff obtained expression for force acting on a wake produced behind a cylinder in fluid flow stream by considering the swinging wake as an aerofoil of equivalent

length [115-116]. However, in general arrangement of explosive welding (Fig. 2.3), the wake swings in two different fluids meeting at an angle $(\beta_1 + \beta_2)$.

The lift force on an aerofoil is usually obtained by considering a rotating cylinder in fluid stream. Using a similar approach the lift force on the wake, is obtained by considering the flow of two different fluids meeting at an angle over an equivalent rotating cylinder.

2.7.1 Flow of Two Fluids Over a Rotating Cylinder

It can be shown by potential theory that a flow over a cylinder (without circulation) is obtained by superimposition of the following flows. It is assummed that $V_{F1} = V_{F2} = V_o$ (See page 70).

(i) flow in x-direction, $\phi = -a V_o \cos\beta \cos\theta$

(ii) flow in y-direction, $\phi = a V_o \sin\beta \cos\theta$

(iii) doublet issuing in x-direction, $\phi = \frac{\varkappa}{a} \cos\beta \cos\theta$

(iv) doublet issuing in y-direction, $\phi = \frac{\varkappa}{a} \sin\beta \sin\theta$

where V_o is free stream velocity, β is inclination of the flow with x-axis, a is radius of cylinder, $\varkappa$ is strength of doublet and ϕ is potential function.

Equation for tangential velocity for an inclined flow over the cylinder is obtained from $V_\phi = -\frac{1}{r}\frac{\partial\phi}{\partial\theta}$ and is written as

$$V_\phi = -2 V_o \sin(\theta + \beta) \qquad (2.9)$$

In case of two fluids meeting over a cylinder (Fig. 2.4), the tangential velocity in various regions is given by

$$V_\phi = -2V_o \sin(\theta + \beta_1) \quad \text{for} \quad \beta_2 \leq \theta \leq (\pi - \beta_1) \qquad (2.10.a)$$

$$V_\phi = -2V_o \sin(\theta - \beta_2) \quad \text{for} \quad -(\pi - \beta_2) \leq \theta \leq -\beta_2 \qquad (2.10.b)$$

$$V_\phi = -4V_o \sin(\theta + \overline{\beta_1 - \beta_2}/2) \cos(\beta_1 + \beta_2)/2$$

$$\text{for} \quad \beta_1 \leq \theta \leq -\beta_2 \qquad (2.10.c)$$

where V_o is free stream velocity of both the fluid and β_1 and β_2 are inclination of the upper and the lower fluids respectively.

Net velocity V at the circumference of a rotating cylinder is given by

$$V = V_\phi \mp V_r = V_\phi \mp \frac{\Gamma}{2\pi a} \qquad (2.11)$$

where V_r is peripheral velocity due to rotation, Γ is circulation and 'a' is radius of the cylinder. For the direction of flow shown in Fig. 2.4, the negative sign is used for anticlockwise rotation and positive sign is used for clockwise rotation.

The angular position γ_s of the stagnation point (as shown in Fig. 2.4) is obtained by taking V = 0, such that

$$\gamma_s = \sin^{-1}\left(\frac{V_r}{2V_o}\right) - \beta_2 \qquad (2.12)$$

2.7.2 Lift Force on the Swinging Wake

The lift force L on the swinging wake is obtained by modelling it as an aerofoil equivalent to a rotating cylinder

$$L = -\int_{-(\pi-\beta_2)}^{(\pi-\beta_1)} p\, a \sin\theta \, d\theta \qquad (2.13)$$

where a is the radius of the cylinder; width of the cylinder is taken as unity. The term within the integral denotes the vertical component of the force acting on an elementary area.

Pressure p on the boundary of the cylinder is written from Bernoulli's equation as

$$p = p_1 = p_o + \frac{\rho_1 V_o^2}{2} - \frac{\rho_1}{2}(V_\phi - V_r)^2$$

$$\text{for } -\gamma \leq \theta \leq (\pi-\beta_1) \qquad (2.14.a)$$

$$p = p_2 = p_o + \frac{\rho_2 V_o^2}{2} - \frac{\rho_2}{2}(V_\phi - V_r)^2$$

$$\text{for } -(\pi-\beta_2) \leq \theta \leq -\gamma \qquad (2.14.b)$$

where ρ_1, ρ_2 are the densities of the two fluids; p_1, p_2 are the corresponding pressures in the two fluids regions and p_o is the free stream pressure. Therefore,

$$L = -\int_{-\gamma}^{(\pi-\beta_1)} p_1\, a \sin\theta\, d\theta - \int_{-(\pi-\beta_2)}^{\gamma} p_2\, a \sin\theta\, d\theta \qquad (2.15.a)$$

$$L = L_1 + L_2 \qquad (2.15.b)$$

From equations (2.13), (2.14) and (2.15)

$$L_1 = -a\int_{-\gamma}^{\beta_1}\left[p_o + \frac{\rho_1 V_o^2}{2} - \frac{\rho_1}{2}\left\{-2V_o \sin(\theta-\beta_2)-V_r\right\}^2\right]\sin\theta\, d\theta$$

$$-a\int_{\beta_1}^{\beta_2}\left[p_o + \frac{\rho_1 V_o^2}{2} - \frac{\rho_1}{2}\left\{-4V_o \sin(\theta+\overline{\beta_1-\beta_2}/2)\cos\frac{\beta_1+\beta_2}{2} - V_r\right\}^2\right]$$

$$\sin\theta\, d\theta - a\int_{\beta_2}^{\pi-\beta_1}\left[p_o + \frac{\rho_1 V_o^2}{2} - \frac{\rho_1}{2}\left\{-2V_o \sin(\theta+\beta_1)-V_r\right\}^2\right]$$

$$\sin\theta\, d\theta \qquad (2.16)$$

Equation (2.16) is written in terms of coefficients and integrals as

$$L_1 = (C_o+C_{12}\,\rho_1)\,I_{12} + C_{22}\,\rho_1\,I_{22} + C_{23}\,\rho_1\,I_{23} + C_{24}\,\rho_1\,I_{24} + C_{32}\,\rho_1\,I_{32} + C_{33}\,\rho_1\,I_{33} + C_{34}\,\rho_1\,I_{34} \tag{2.17}$$

Similarly

$$L_2 = (C_o+C_{12}\,\rho_2)I_{11} + \rho_2\,C_{21}\,I_{21} + \rho_2\,C_{31}\,I_{31} \tag{2.18}$$

where the coefficients are given by

$$C_o = -a\,p_o,\quad C_{11} = -a(V_o^2 - V_r^2)/2,\quad C_{21} = 2a\,V_o\,V_r,\quad C_{31}=2a\,V_o^2$$

and $C_{12} = C_{21}$, $C_{22} = C_{21}$, $C_{23} = 2\cos(\frac{\beta_1+\beta_2}{2})C_{21}$, $C_{24} = C_{21}$

$$C_{32} = C_{31},\quad C_{33} = 4\cos(\frac{\beta_1+\beta_2}{2})\,C_{31},\quad C_{34} = C_{31} \tag{2.20}$$

and the integrals are given by

$$I_{11} = \cos\gamma + \cos\beta_2,\quad I_{12} = -\cos\beta_1 - \cos\gamma$$

$$I_{21} = -[\frac{-\gamma}{2}\cos\beta_2 + \frac{\sin(2\gamma+\beta_2)}{4}] - [-\frac{(\pi-\beta_2)}{2}\cos\beta_2 - \frac{\sin\beta_2}{4}]$$

$$I_{22} = -[\frac{\beta_1}{2}\cos\beta_2 + \frac{\sin(2\beta_1+\beta_2)}{4}] - [\frac{-\gamma}{2}\cos\beta_2 + \frac{\sin(2\gamma+\beta_2)}{4}]$$

$$I_{23} = \left[\frac{\beta_2}{2}\cos\frac{\beta_1-\beta_2}{2} - \frac{\sin(2\beta_2+\overline{\beta_1-3_2}/2)}{4}\right] - \left[-\frac{\beta_1}{2}\cos\frac{\beta_1-\beta_2}{2} + \frac{\sin(2\beta_1-\overline{\beta_1-\beta_2}/2)}{4}\right]$$

$$I_{24} = \left[\frac{(\pi-\beta_1)}{2}\cos\beta_1 + \frac{\sin\beta_1}{4}\right] - \left[\frac{\beta_2}{2}\cos\beta_1 - \frac{\sin(2\beta_2+\beta_1)}{4}\right]$$

$$I_{31} = I'_{31} + I''_{31} + I'''_{31}$$

$$I'_{31} = \left[\left(-\frac{\sin^2\gamma\cos\gamma}{3} - \frac{2}{3}\cos\gamma\right)\cos^2\beta_2\right] - \left[\left(\frac{\cos^2\beta_2\sin\beta_2}{3} + \frac{2}{3}\cos\beta_2\right)\cos^2\beta_2\right]$$

$$I''_{31} = \left[-\frac{1}{3}\cos^3\gamma\sin^2\beta_2\right] - \left[\frac{1}{3}\cos^3\beta_2\sin^2\beta_2\right]$$

$$I'''_{31} = \left[-\frac{1}{3}\sin^3\gamma\sin^2\beta_2\right] - \left[-\frac{1}{3}\sin^3\beta_2\sin^2\beta_2\right]$$

$$I_{32} = I'_{32} + I''_{32} + I'''_{32}$$

$$I'_{32} = \left[\left(-\frac{\sin^2\beta_1\cos\beta_1}{3} - \frac{2}{3}\cos\beta_1\right)\cos^2\beta_2\right] - \left[\left(-\frac{\sin^2\gamma\cos\gamma}{3} - \frac{2}{3}\cos\gamma\right)\cos^2\beta_2\right]$$

$$I''_{32} = \left[-\frac{1}{3}\cos^3\beta_1\sin^2\beta_2\right] - \left[-\frac{1}{3}\cos^3\gamma\sin^2\beta_2\right]$$

$$I''_{32} = [-\tfrac{1}{3}\sin^3\beta_1 \sin^2\beta_2] - [-\tfrac{1}{3}\sin^3\gamma \sin^2\beta_2]$$

$$I_{33} = I'_{33} + I''_{33} + I'''_{33}$$

$$I'_{33} = [(-\frac{\sin^2\beta_2 \cos\beta_2}{3} - \tfrac{2}{3}\cos\beta_2)\cos^2(\tfrac{\beta_1-\beta_2}{2})]$$

$$- [(-\frac{\sin^2\beta_1 \cos\beta_1}{3} - \tfrac{2}{3}\cos\beta_1)\cos^2(\tfrac{\beta_1-\beta_2}{2})]$$

$$I''_{33} = [-\tfrac{1}{3}\cos^3\beta_2 \sin^2(\tfrac{\beta_1-\beta_2}{2})] - [-\tfrac{1}{3}\cos^3\beta_1 \sin^2(\tfrac{\beta_1-\beta_2}{2})]$$

$$I'''_{33} = [-\tfrac{1}{3}\sin^3\beta_2 \sin^2(\beta_1-\beta_2)] - [-\tfrac{1}{3}\sin^3\beta_1 \sin^2(\beta_1-\beta_2)]$$

(2.21)

The lift force is now written in the form

$$L = (A + B\ \rho_2 + C\ \rho_1)2\,a\,V_o^2 \qquad (2.22)$$

where

$$A = [C_o(I_{11} + I_{12})]/(2\,a\,V_o^2) \qquad (2.23)$$

$$B = [C_oI_{11}+C_{12}I_{12}+C_{21}I_{21}+C_{31}I_{31}]/(2\,a\,V_o^2) \qquad (2.24)$$

and

$$C = [C_{22}I_{22}+C_{23}I_{23}+C_{24}I_{24}+C_{32}I_{32}+C_{33}I_{33}+C_{34}I_{34}]/(2aV_o^2)$$

(2.25)

If the cylinder is rotating in an opposite direction to that shown in Fig.2.4, the magnitude of the lift force is given by

$$L^{*} = (A^{*} + B^{*} \rho_1 + C^{*} \rho_2)\, 2\, a\, V_o^2 \qquad (2.26)$$

where

$A^{*} = A$

$B^{*} = B$

$C^{*} = C$

provided β_1 and β_2 are suitably interchanged while evaluating the integrals.

For $\rho_1 = \rho_2 = \rho$ and $\beta_1 = \beta_2 = 0$ and taking $p_o = 0$, equation (2.26) reduces to $L = 2\pi a \rho V_o^2$ which is a well known expression for lift force on a rotating cylinder in a fluid flow.

2.8 CONCLUSIONS

Further classification of asymmetries in (geometrically) symmetric situation enables to develop a model of general arrangement of explosive welding. In general arrangement of explosive welding the two plates are inclined at obliquity angles β_1 and β_2 with respect to the collision direction.

In the hydrodynamic model it is generally considered that the wake behind the obstacle swings from side to side producing a wavy interface. The lift force on the wake depends upon the densities (ρ_1, ρ_2) and obliquity angles (β_1, β_2) of both the plates.

EXPLOSIVE WELDING
(INCLINED PLATE ARRANGEMENT)

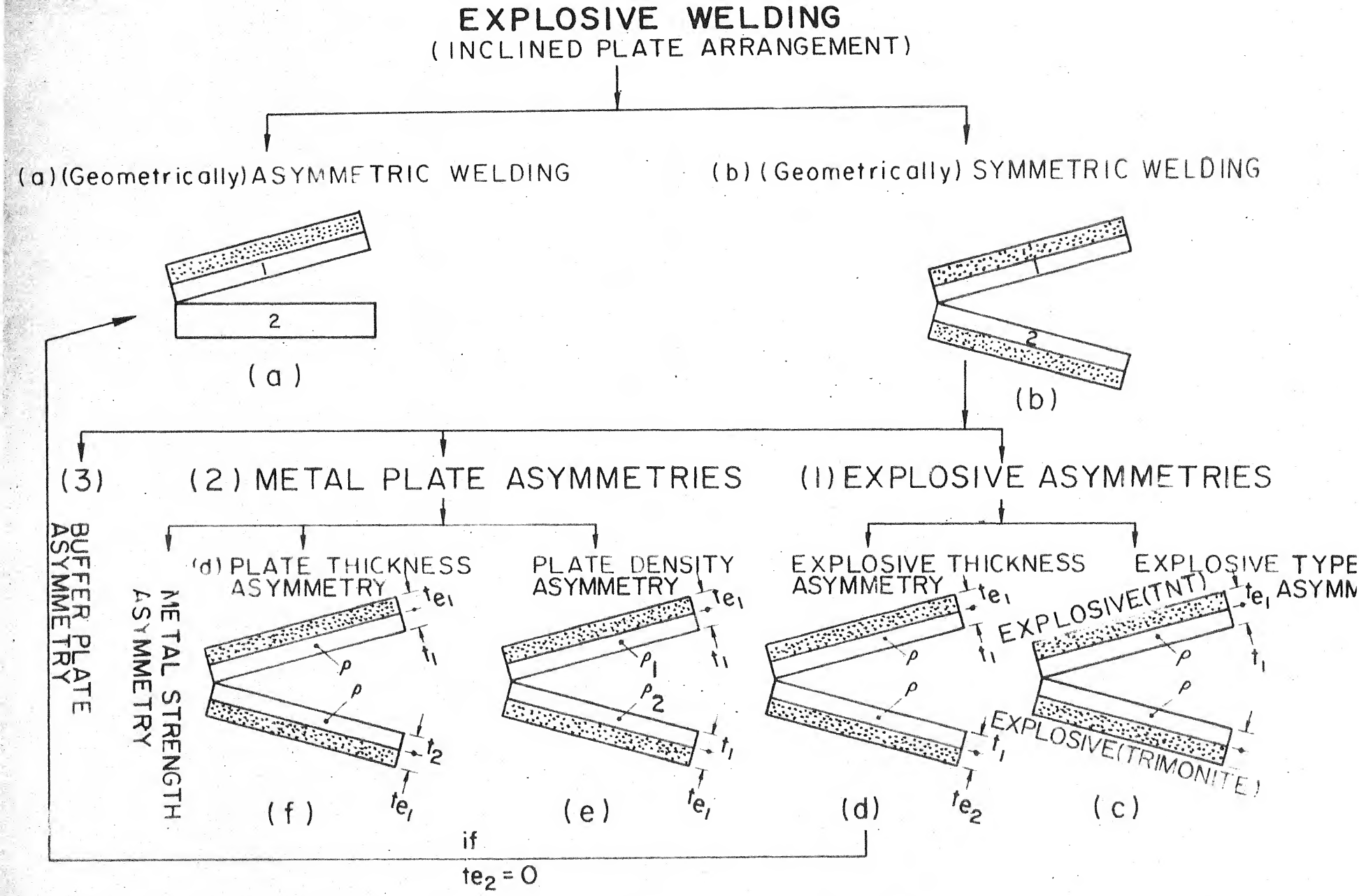

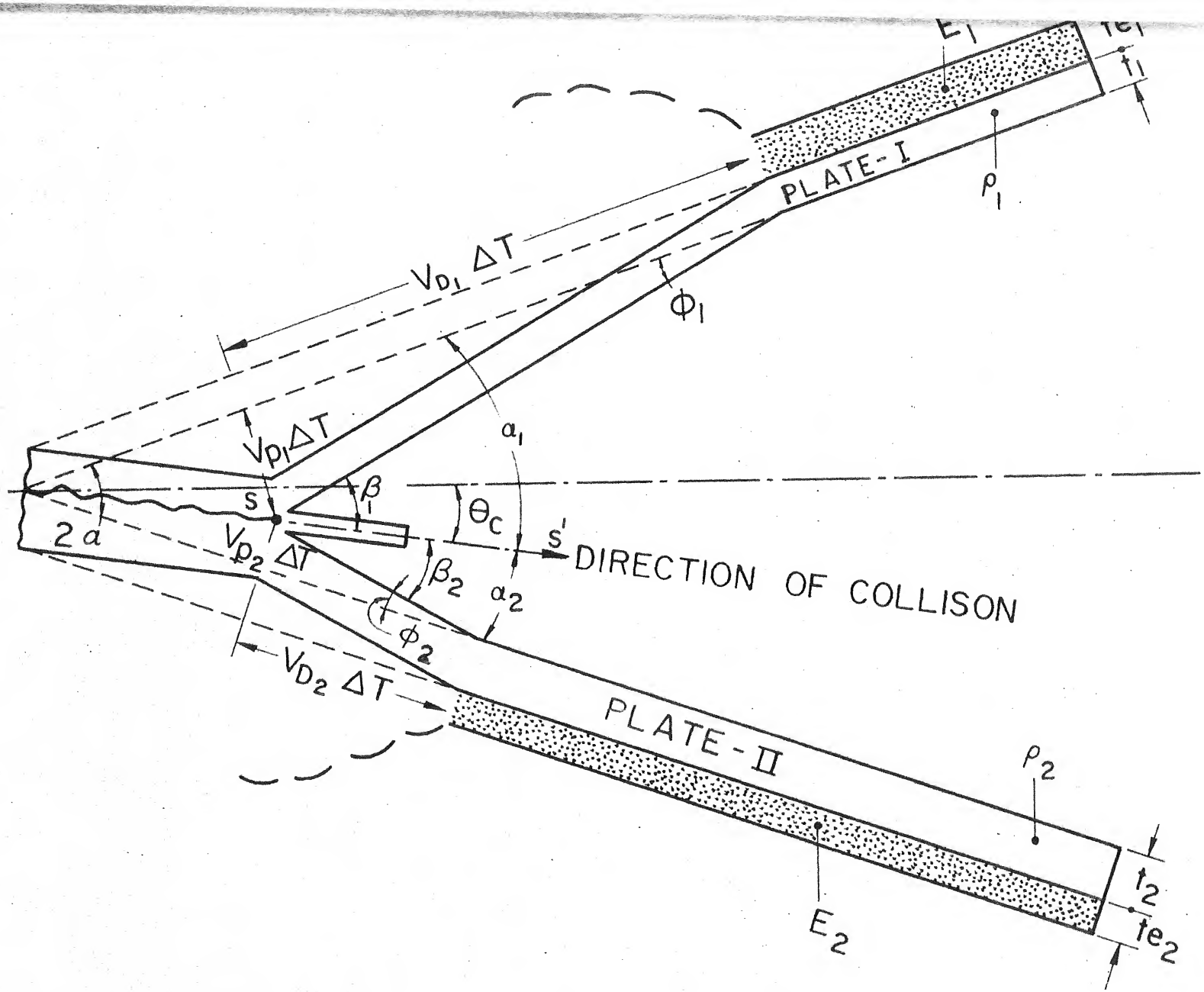
PLATE-I
PLATE-II
DIRECTION OF COLLISON
$V_{D_1}\Delta T$
$V_{P_1}\Delta T$
$V_{P_2}\Delta T$
$V_{D_2}\Delta T$
Φ_1
ϕ_2
α_1
α_2
β
β_2
θ_c
s
s'
2a
ρ_1
ρ_2
E_1
E_2
t_1
t_2
te_2

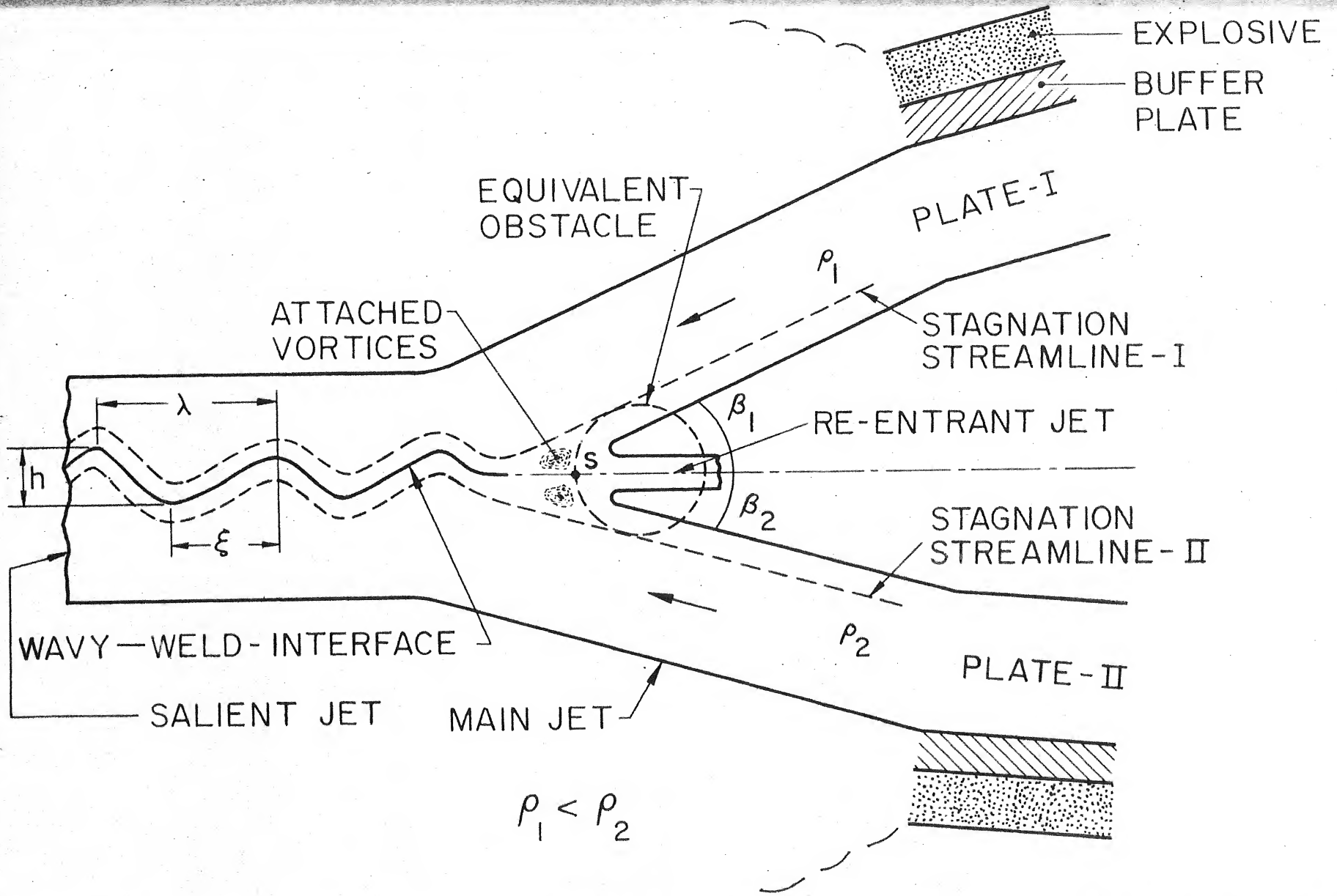

Fig. 2.3 HYDRODYNAMIC MODEL FOR GENERAL ARRANGEMENT

CHAPTER III

SWINGING WAKE MECHANISM FOR INTERFACE WAVE GENERATION IN EXPLOSIVE WELDING

3.1 INTRODUCTION

The interface wave profile approximates to a sine wave for the case of welding of similar metals, however, the wave deviates from a sine wave for the case of welding of dissimilar metals. Inspite of the fact that many theories have been proposed to explain the wave formation, however, it seems that there is yet no complete analogy available which explains the formation of welded interfacial waves and its distortion. In the present chapter, a 'Swinging Wake Mechanism' is proposed to explain the generation of interface wave using Birkhoff's vortex shedding theory.

3.2 SWINGING WAKE MECHANISM

3.2.1 The Hydrodynamic Model of Explosive Welding

Since pressure encountered in explosive welding is much higher than the yield shear strength of the material [59] and strain rates are usually higher than the critical strain rate (10^7/sec) above which the material behaves like an inviscid fluid [87], a hydrodynamic model for general arrangement of explosive welding is considered. Figure 2.3 shows the

hydrodynamic model of explosive welding in which two jets are considered to impinge on each other. Stagnation streamlines separate the main jet into corresponding salient jet and re-entrant jet. By considering an imaginary obstacle bounded by the two stagnation streamlines, the problem is reduced to the flow of two different fluids meeting at an angle over an obstacle. Wake, produced behind the obstacle, swings from side to side like tail of a swimming fish. The frequency of the wavy interface depends on the restoring lift force acting on the swinging wake.

The lift force acting on the wake, modelled as an aerofoil, is obtained in chapter II by considering the flow of two dissimilar fluids meeting at an angle over an equivalent rotating cylinder, by following an approach generally used in fluid dynamics.

Considering that a wake of length 2ℓ is moving from a higher density material (ρ_2) to a lower density material (ρ_1), the restoring lift force F, acting on the wake inclined at an instantaneous tilt θ, is obtained from equation (2.26) by substituting $V_o = V_F$ and $2a = 2\ell\theta$ as

$$F = 2(B^{*}\rho_1 + C^{*}\rho_2) V_F^2 \ell \theta \qquad (3.1)$$

It is assumed that the free stream pressure $p_o = 0$ such that the constant A^{*} in the eq. (2.26) is zero.

When the wake is moving from a material of lower density (ρ_1) into a material of higher density (ρ_2), restoring lift force is given by equation (2.22) as

$$F = 2 (B \rho_2 + C \rho_1) V_F^2 \ell \theta \qquad (3.2)$$

Expressions for the coefficient B, B^* and C, C^* are given in chapter II. A representative value of circulation $\Gamma = 2 \pi a V_F$ is taken for evaluating γ. Using DEC-10 computer, the values of these coefficients are calculated and are plotted in Figs. 3.1 and 3.2. It is seen that the values of C and C^* are an order higher than B and B^*, hence it is concluded that the lift force on the swinging wake depends primarily upon the density of the material from which the wake is moving away.

3.2.2 Swinging Wake Mechanism for Interface Wave Generation in Explosive Welding

An approach similar to the one adopted by Reid using wake oscillator model [88] of Birkhoff is employed to study the interface wave formation quantitatively. However, the present approach differs from Reid's approach in that (i) the lift force is estimated by considering two dissimilar fluids flowing above and below the swinging wake modelled as an aerofoil and (ii) as the mass of the wake is distributed restoring couple instead of restoring force is equated t. the inertia of the wake.

Birkhoff's wake oscillator model is extended as it is able to explain some of the important observed facts. Considering the wake oscillator model (Fig. 3.3-a) and assuming that the lift force is acting at a distance $\ell/2$ from the point of swing [180], the following expression is written for the case when the wake is moving from a fluid of density ρ_2 into a fluid of density ρ_1

$$I\ddot{\theta} = \text{Restoring couple} \tag{3.3}$$

$$\frac{4}{3} m \ell^2 \ddot{\theta} = -(B^* \rho_1 + C^* \rho_2) V_F^2 \ell^2 \theta \tag{3.4}$$

The related frequency of the swinging wake is given by

$$N_1 = \frac{V_F}{2\pi} \sqrt{\frac{3}{4} \frac{(B^* \rho_1 + C^* \rho_2)}{m}} \tag{3.5}$$

The corresponding wave length a_1 is given by

$$N_1 a_1 = (V_F - V_{FS}) = V_F(1 - \varepsilon) \tag{3.6}$$

where V_{FS} is velocity of the vortex street, and the velocity ratio $\varepsilon = V_{FS}/V_F$.

From equations (3.5) and (3.6)

$$a_1 = (1-\varepsilon) \sqrt{\frac{16 \pi^2 m}{3(B^* \rho_1 + C^* \rho_2)}} \tag{3.7}$$

Considering that the wake height h is made up of two materials of densities ρ_1 and ρ_2 and k is the fraction of total wake height occupied by metal of density ρ_1, the mass of the wake is given by

$$m = 2h \quad [k \ \rho_1 + (1-k) \ \rho_2] \qquad (3.8)$$

It is assumed that the length of wake 2ℓ varies from zero to $a_1/2$ giving an average value of $\ell_1 = a_1/8$ [115]. Hence from equations (3.7) and (3.8)

$$a_1 = \frac{4}{3} \frac{\pi^2}{(B^* \rho_1 + C^* \rho_2)} (1-\varepsilon)^2 [k \rho_1 + (1-k) \rho_2]h \qquad (3.9)$$

During movement of the wake in material of lower density ρ_1 from mean position to top position, the contribution to wavelength is $a_1/4$ as shown in Fig. 3.3-b (i).

Similarly, when the wake starts swinging from top position towards material of higher density ρ_2, it contributes a portion of wavelength equal to $a_2/2$ as shown in Fig.3.3-b (ii) such that

$$a_2 = \frac{4}{3} \frac{\pi^2}{(B \rho_2 + C \rho_1)} (1-\varepsilon)^2 [k \rho_1 + (1-k) \rho_2]h \qquad (3.10)$$

When the wake moves from bottom position to top position towards material of lower density ρ_1, it again contributes

a portion of wavelength equal to $a_1/2$ as shown in Fig. 3.3-b (iii).

Thus the interface wave is formed by contributions from upward and downward movements of the wake in both the materials. Combination of various portions of the wave yields the final shape of wavy weld interface as shown in Fig. (2.3).

3.2.3 Distortion of Interface Wave

Welded profile for similar metal combination generally approximates to a sine wave, whereas, for dissimilar metal combination the shape of the profile deviates from a sine wave [90]. The proposed shape (Figs. 2.3 and 3.3-b) broadly agrees with the observed shape of the wavy weld interface given by Onzawa and Ishii [90] (Fig. 3.4).

The characteristic parameters of interface wave (Figs. 2.3 and 3.3-b) λ and ξ are defined as

$$\lambda = (a_1 + a_2)/2 \qquad (3.11)$$

$$\xi = a_2/2 \qquad (3.12)$$

where λ is the wavelength and ξ is the contribution to the wavelength when wake is moving from lower density material to higher density material. If $\rho_1 < \rho_2$, then from equations (3.9) and (3.10) $a_2 > a_1$ and hence $\xi > \lambda/2$.

If density of the top plate is lower than the density of the bottom plate then,

ξ is the distance between crest and neighbouring trough in the direction of the stream. The experimental work of Onzawa and Ishii [90] shows that $\xi > \lambda/2$. Experimental work of Thorpe [181] on flow of two immisible fluids also implies that $\xi > \lambda/2$.

The degree of distortion η is defined in the following manner such that $\eta = 0$ for sinusoidal wave when the ratio of density is unity, and $\eta > 0$ if $\rho_1/\rho_2 < 1$,

$$\eta = \frac{(2\xi - \lambda)}{\lambda} \tag{3.13}$$

From equations (3.9) to (3.13)

$$\eta = \frac{(C^{*} - B)}{(C^{*} + B)} \left[\frac{1 - \frac{C-B^{*}}{C^{*}-B} \frac{\rho_1}{\rho_2}}{1 + \frac{C+B^{*}}{C^{*}+B} \frac{\rho_1}{\rho_2}} \right] \tag{3.14}$$

Theoretical variation of degree of distortion η with density ratio ρ_1/ρ_2 is plotted in Fig. 3.5. Theoretical variation of η with obliquity angle β_1 and with obliquity angle ratio $r_\beta = \beta_2/\beta_1$ are shown in Fig. 3.6. The theory predicts that distortion of interface wave is more if there is a large difference between the densities of the two metals (lower density ratio ρ_1/ρ_2). The theory also indicates

(Fig. 3.6) that even the welded interface for similar metal combination ($\rho_1/\rho_2 = 1$) produced by asymmetric welding is slightly distorted. Available experimental evidence shows that there is a slight distortion in the wavy weld interface even for welding of similar metals.

3.2.4 Amplitude to Wavelength Ratio

Klein [108] found experimentally that the amplitude to wavelength ratio has an average value of approximately 0.3. Von Karman vortex shedding theory predicts the ratio $h/\lambda = 0.281$. Birkhoff's theory [116] predicts the ratio $h/\lambda = 0.35$, which is close to the values quoated above. Taking the amplitude of the interface wave equal to the height h, the amplitude to wavelength ratio h/λ is obtained from equation (3.9), (3.11) as

$$\frac{h}{\lambda} = \frac{3}{2\pi^2(1-\varepsilon)^2} \frac{(B+C\,\rho_1/\rho_2)\,(B^{*}\,\rho_1/\rho_2 + C)}{[(B+C^{*})+(B^{*}+C)\,\rho_1/\rho_2][(1-k)+k\,\rho_1/\rho_2]} \tag{3.15}$$

3.2.5 Swinging Wake Model Using Simplified Lift Force Equation

In the above analysis of swinging wake model, the lift force is obtained from equations (2.22) and (2.26). The values of B, B^{*} and C, C^{*} are comparatively difficult to

evaluate. However, use of a simple lift force equation enables us to develop simple formulae for η and h/λ. Figures 3.1 and 3.2 show that there is a little effect of β_1 and the ratio β_1/β_2 on the value of the coefficients B, B^* and C, C^*.

Ignoring the effect of β_1 and β_2, the following simplified expression for the lift force on the swinging wake is obtained from equations (2.22) or (2.26) using a representative value of circulation $\Gamma = 2\pi\, a\, V_F$ and assuming free stream pressure $p_o = 0$, taking $\beta_1 = \beta_2 \approx 0$.

$$F = 2\, \ell\, \theta\, V_F^2\, [\pi\, a - 0.21(\rho_a - \rho_b)] \qquad (3.16)$$

where ρ_a is the density of the fluid from which the wake is moving away and ρ_b is the density of the other fluid. As the contribution of the second term is small (less than 7 %), equation (3.16) is further approximated as

$$F = 2\pi\, \rho_a\, V_F^2\, \ell\, \theta \qquad (3.17)$$

Using equation (3.17) and an approach similar to that adopted in the previous sections, the following simple expressions for a_1, a_2, η and h/λ are obtained.

$$a_1 = 4\pi(1-\varepsilon)^2\, [k\, \rho_1 + (1-k)\, \rho_2]h/(3\, \rho_2) \qquad (3.18)$$

$$a_2 = 4\pi(1-\varepsilon)^2\, [k\, \rho_1 + (1-k)\, \rho_2]h/(3\, \rho_1) \qquad (3.19)$$

$$\eta = \frac{1 - \rho_1/\rho_2}{1 + \rho_1/\rho_2} \tag{3.20}$$

$$\frac{h}{\lambda} = \frac{3}{2\pi(1-\varepsilon)^2} \frac{\rho_1/\rho_2}{(1 + \rho_1/\rho_2)[(1-k)+k\,\rho_1/\rho_2]} \tag{3.21}$$

Variation of degree of distortion obtained from simplified equation (3.20) is also plotted in Fig. 3.5 (dotted line) which shows that the simplified equation (3.20) is reasonably accurate.

3.3 EXPERIMENTAL EVIDENCE AND DISCUSSION

The values of the degree of distortion η and amplitude to wavelength ratio h/λ from experimental results of Onzawa and Ishii [90] and Crossland et al. [75, 78] are plotted in Figures 3.7 and 3.8.

Predicted values of degree of distortion η (Eq.(3.20)) are also plotted in Fig. 3.7. The predicted values show reasonable agreement with the experimental results. The degree of distortion decreases with increase in the ratio ρ_1/ρ_2. It may be noted that the distortion is defined in a manner such that $\eta = 0$ for a sinusoidal wave when the ratio of densities is unity.

To plot the theoretical variation of h/λ with ρ_1/ρ_2 (Eq. (3.21)) values of ε and k are needed. Values of ε

ranging from 0.03 to 0.4 have been suggested by various workers [116]. According to Onzawa and Ishii [90], in the case of dissimilar metals, most of the metal re-entrant jet generates from the stream of lower density meterial. This implies that the wake would be probably be made up, of material, largely, taken from the metal of higher density. Thus the value of k is expected to be in the range of k = 0 to k = 1/2 depending upon the density ratio. Predicted values of amplitude to wavelength ratio h/λ (Eq. (3.21)) are plotted for k = 0, 1/2 and ε = 0.03 to 0.4 in Fig. 3.8. It is observed that most of the experimental values fall within the predicted range. The average theoretical variation is also plotted for average values of k = 0.25 and ε = 0.215.

The scatter in experimental values of h/λ is due to expected variation of k and ε which are likely to be affected by explosive welding parameters. The limited extent of the region within which fluid like behaviour occurs [106] during explosive welding needs further investigation to establish the behaviour of k and ε with variation in welding parameters. The ratio $\varepsilon = V_{FS}/V_F$ depends on Reynolds number [116] which is difficult to determine accurately in explosive welding.

3.4 CONCLUSIONS

The 'Swinging Wake Mechanism' adequately explains the generation and distortion of wavy weld interface.

The degree of distortion depends upon the density ratio. The lower the value of ρ_1/ρ_2 the larger is the deviation of wavy interface from a sine wave. The degree of distortion is marginally affected by the obliquity angle ratio β_2/β_1. Thus it can be concluded that it is only the 'metal-plate-density asymmetry' which causes significant distortion of interface wave, and all other types of asymmetries leading to the condition $\beta_1 \neq \beta_2$, do not produce any significant wave distortion.

The average value of amplitude to wavelength ratio of interface wave for dissimilar metal combination is expected to be lower than that for similar metal combination.

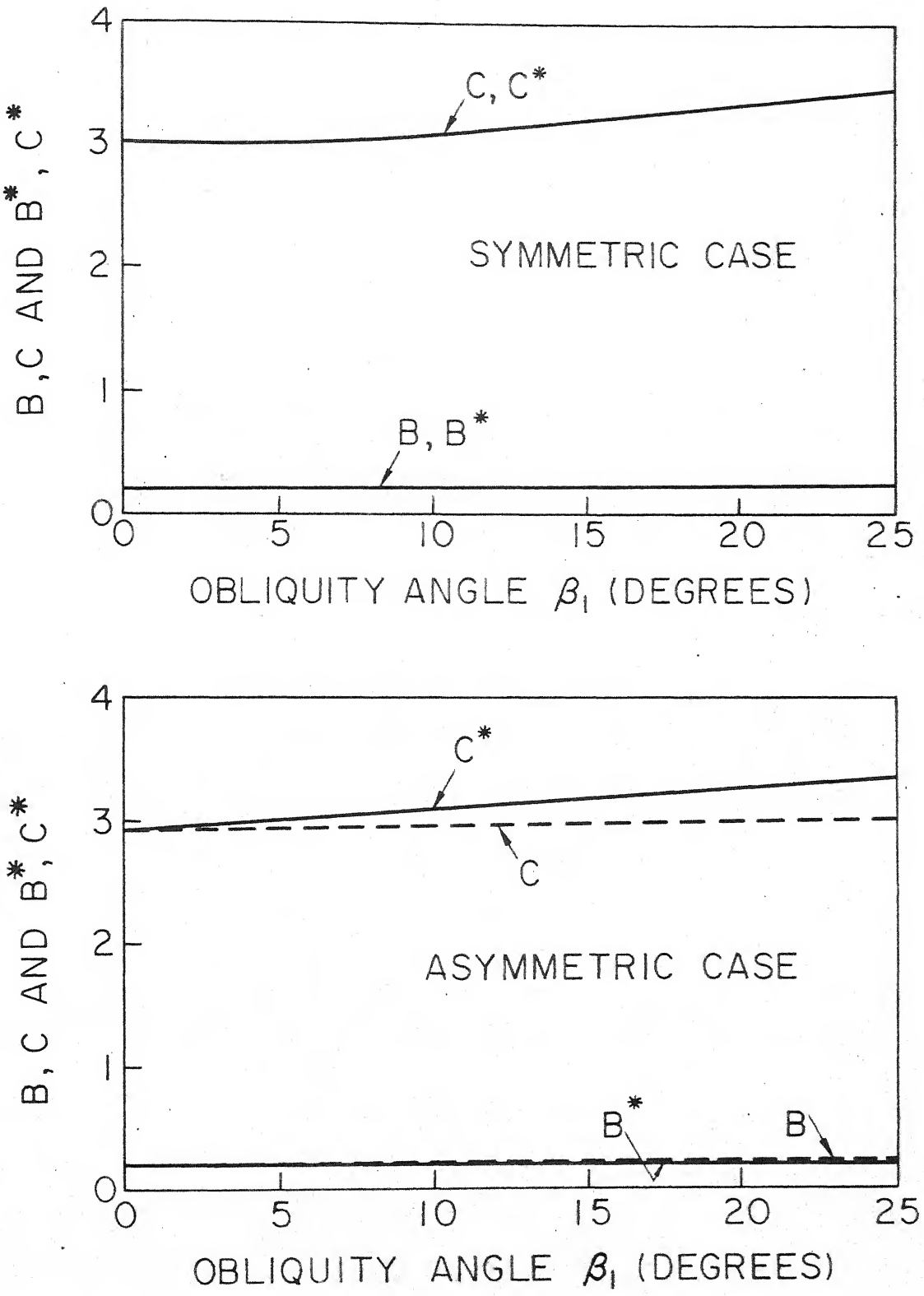

FIG. 3.1 VARIATION OF CONSTANTS B, C AND B^*, C^* WITH OBLIQUITY ANGLE

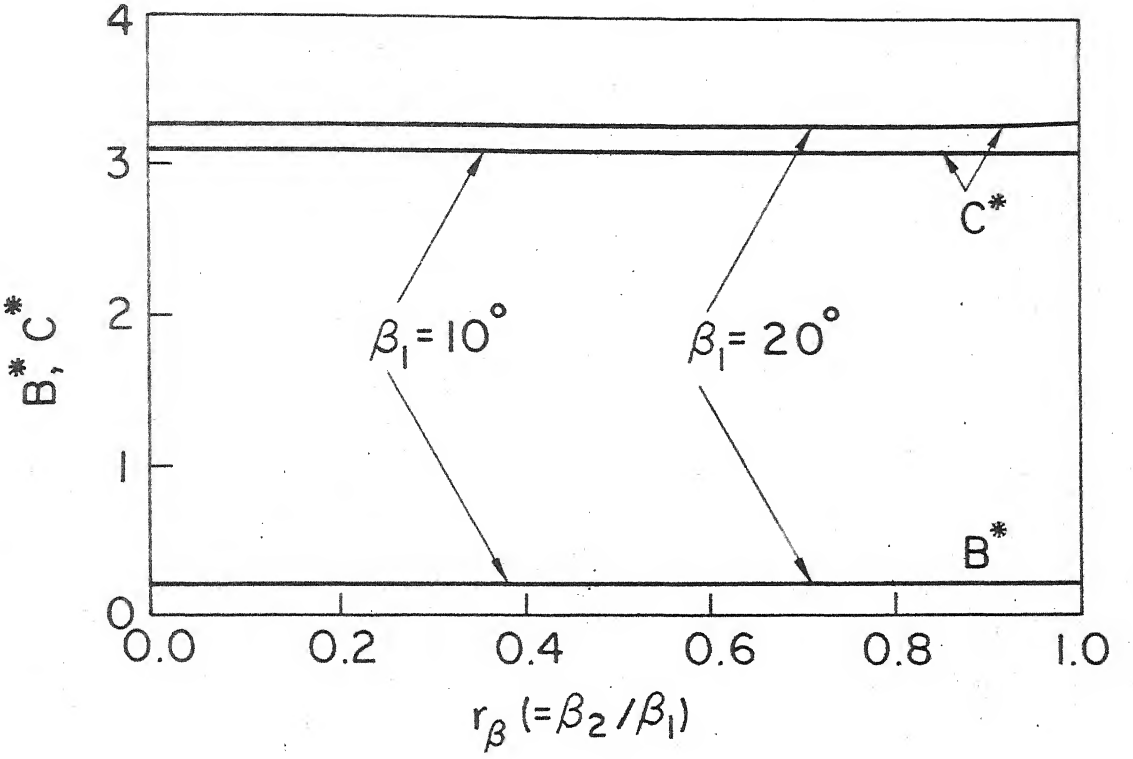

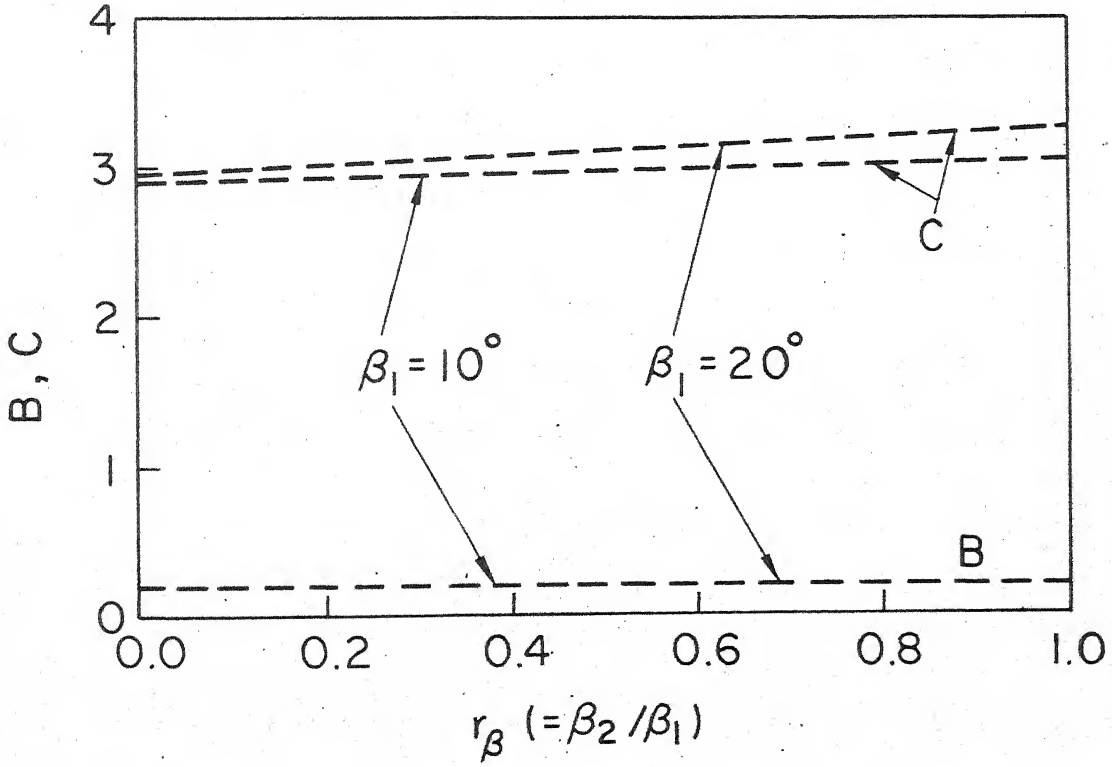

FIG. 3.2 VARIATION OF CONSTANTS B, C AND B*, C* WITH OBLIQUITY RATIO r_β

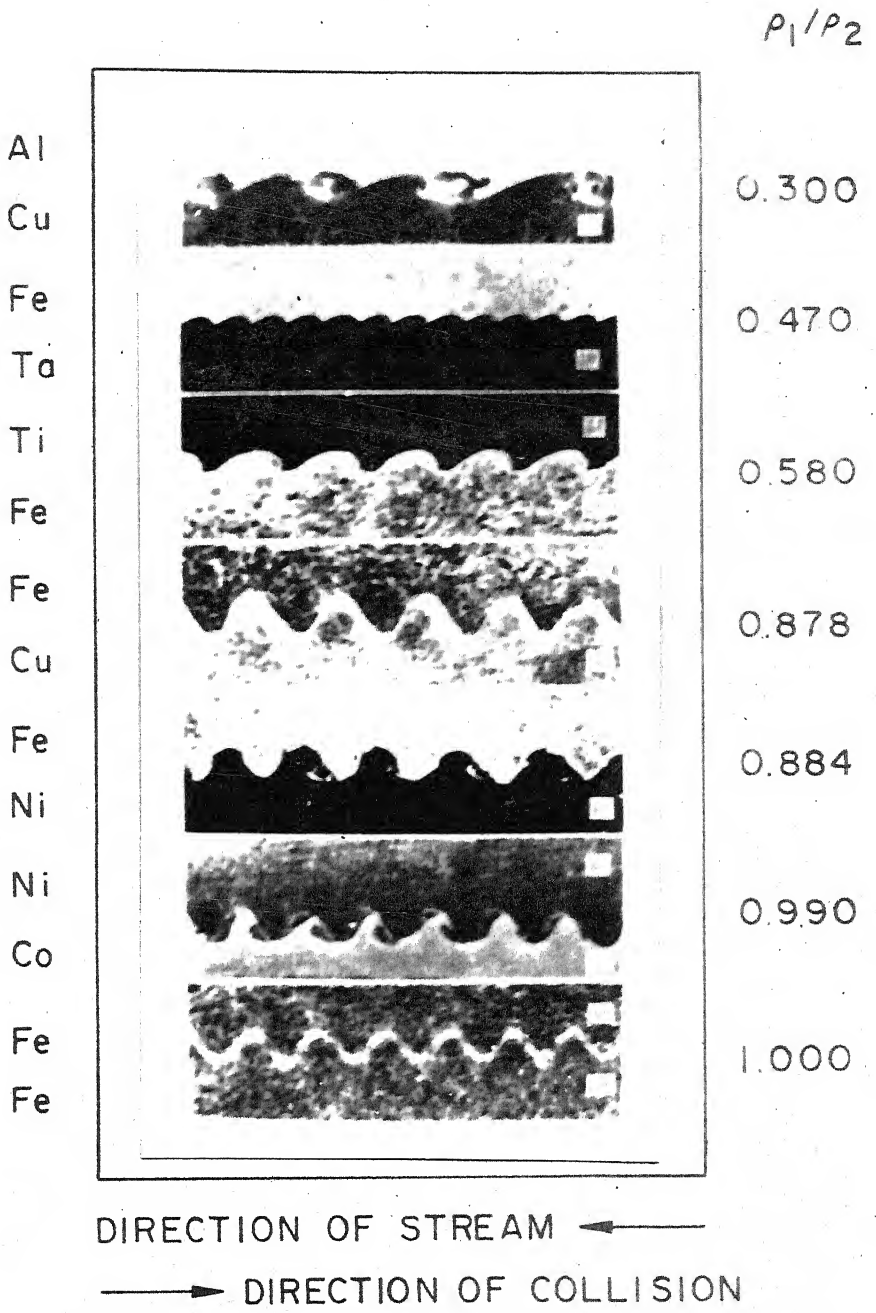

FIG. 3.4 BONDED INTERFACE OF VARIOUS METAL COMBINATIONS (AFTER ONZAWA AND ISHII) [90]

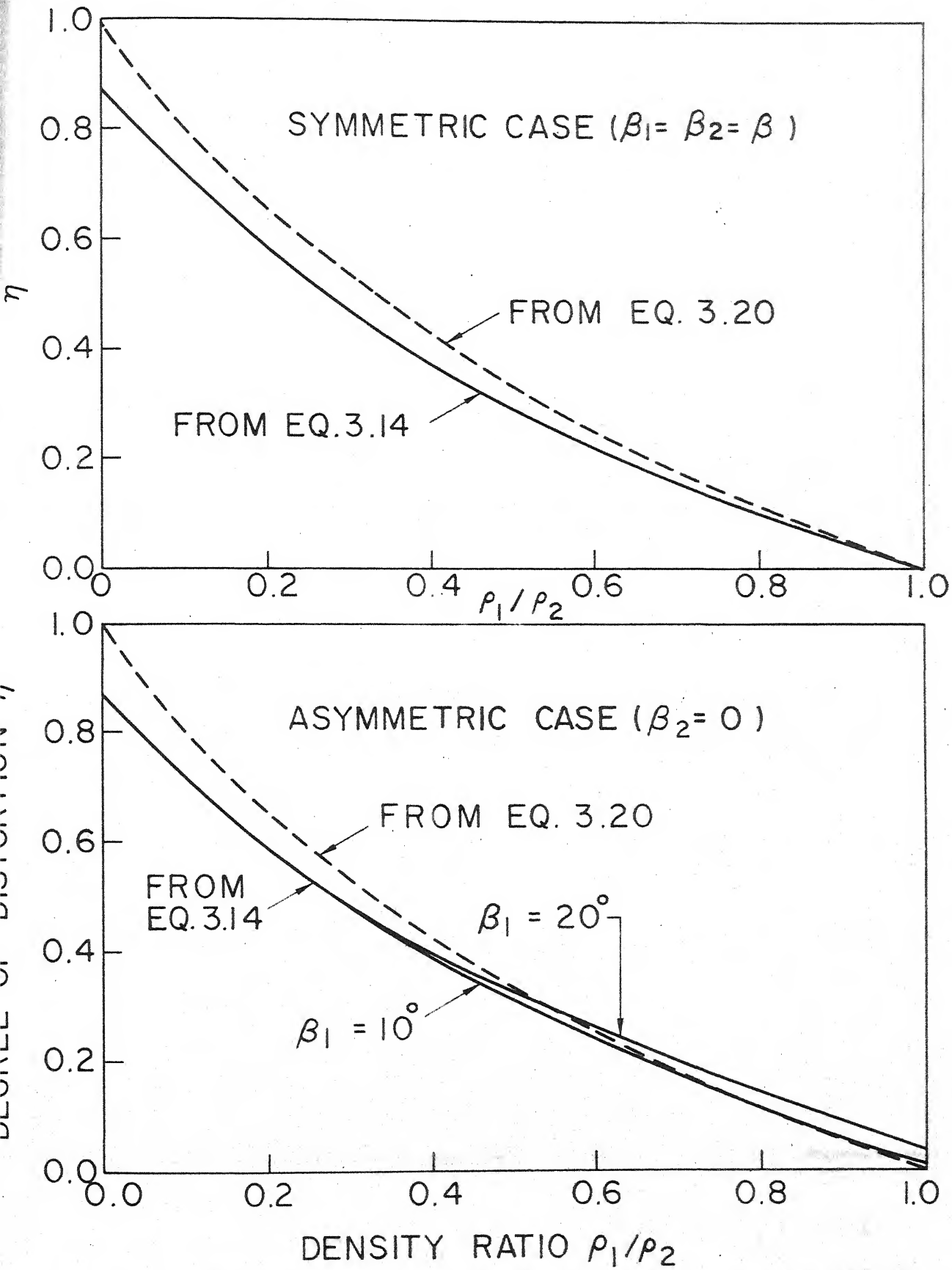

FIG. 3.5 DEGREE OF DISTORTION VERSUS DENSI
RATIO ρ_1/ρ_2

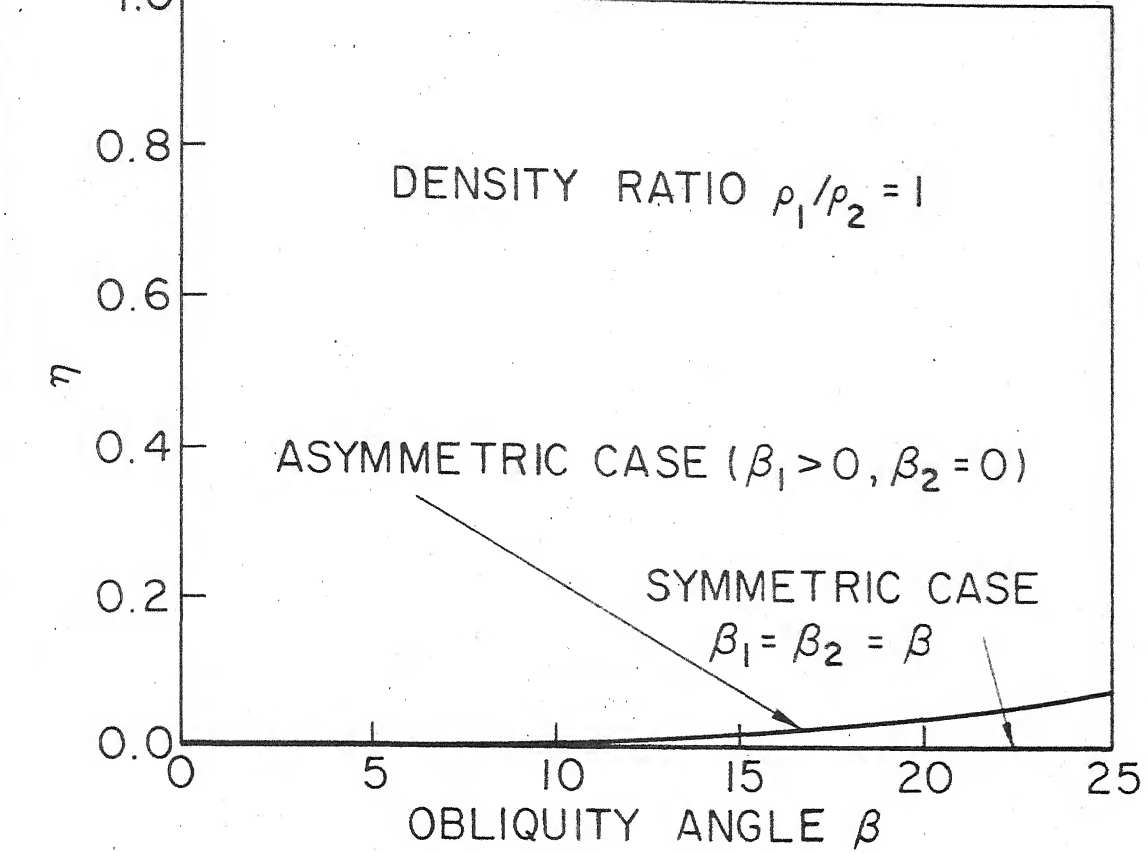

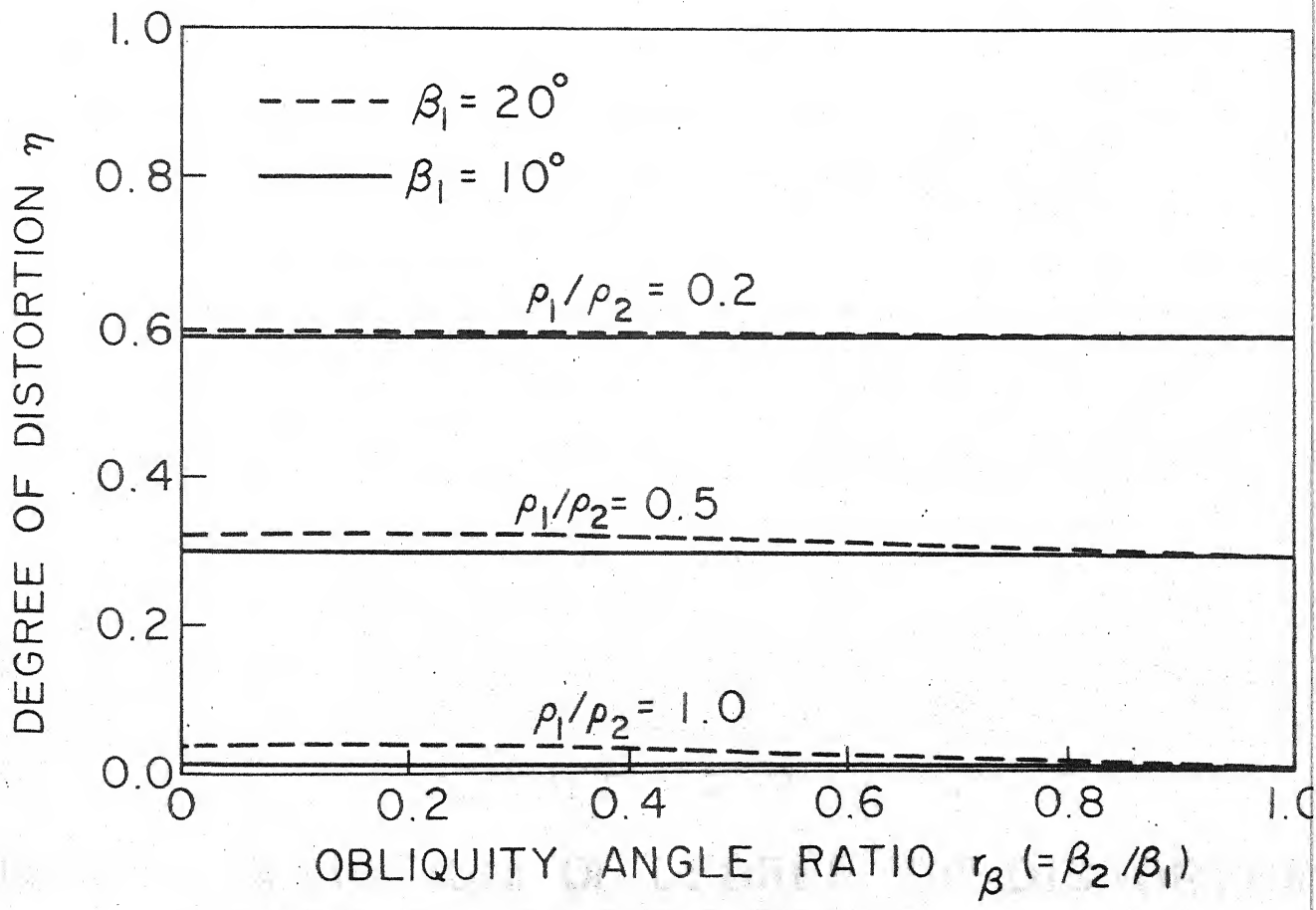

FIG. 3.6 DEGREE OF DISTORTION η VERSUS OBLIQUITY ANGLE RATIO r_β AND

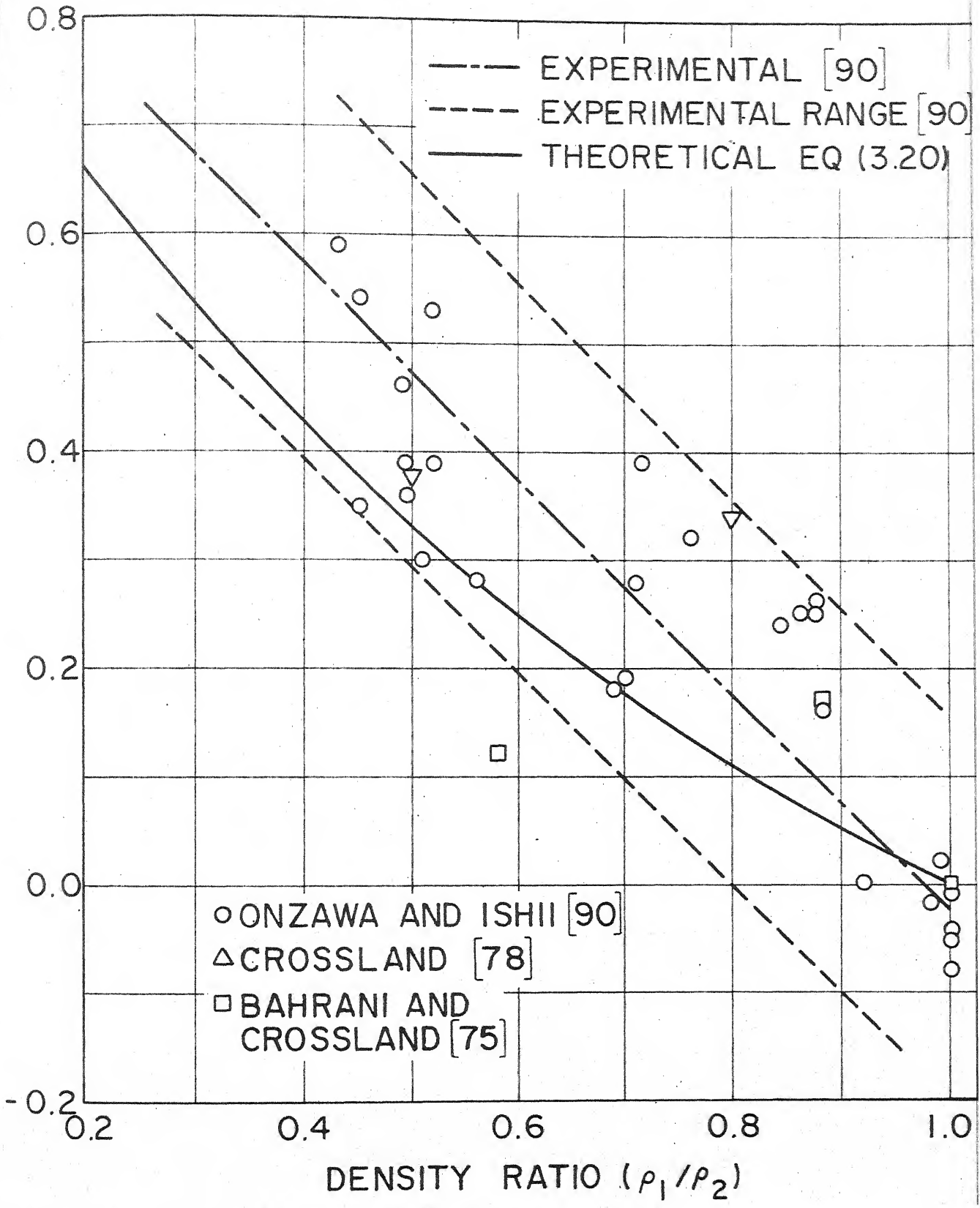

FIG. 3.7 VARIATION OF DEGREE VERSUS DENSITY RATIO

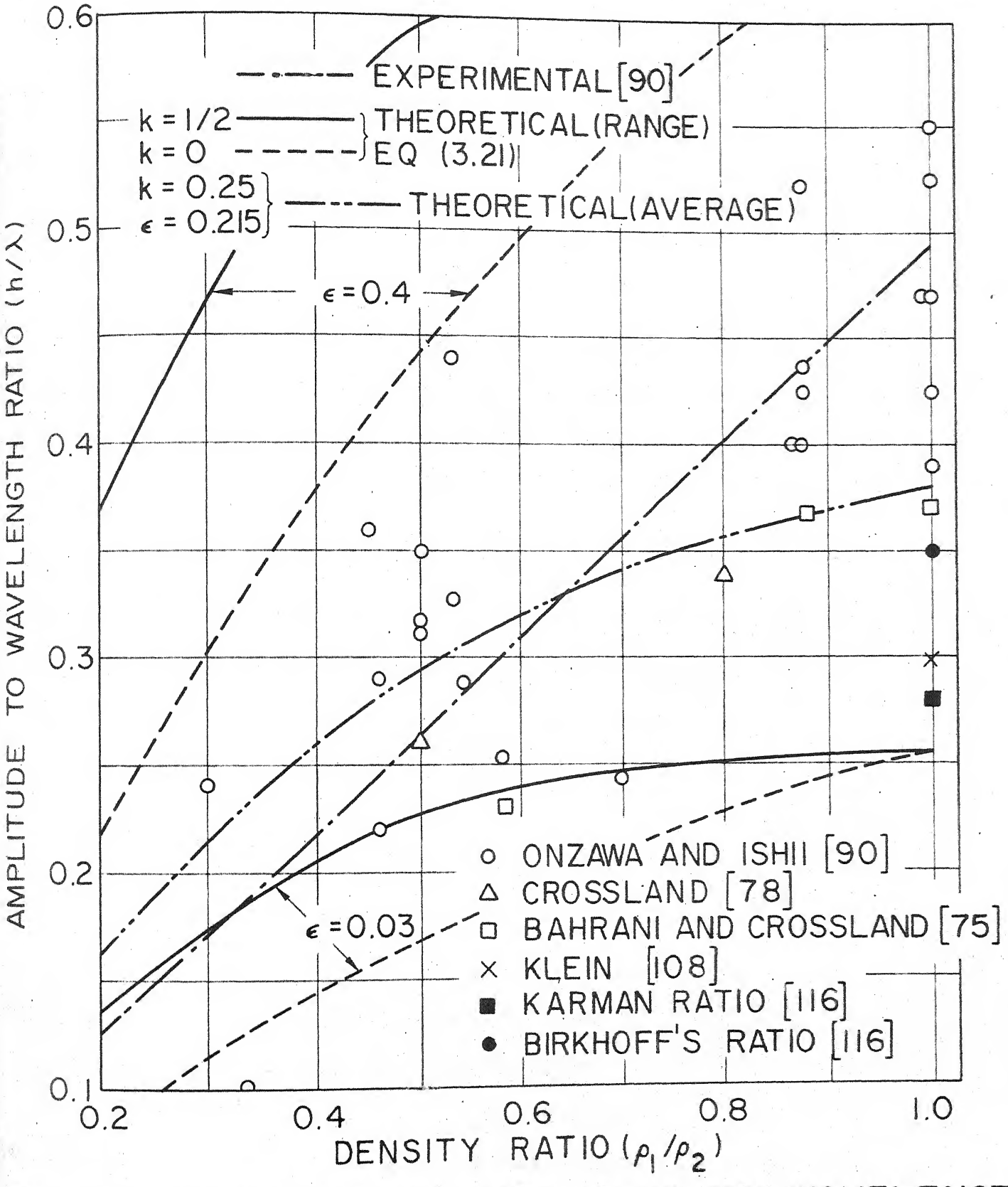

FIG. 3.8 VARIATION OF AMPLITUDE TO WAVELENGTH RATIO VERSUS DENSITY RATIO

CHAPTER IV

SIZE OF OBSTACLE AND INTERFACE WAVE

4.1 INTRODUCTION

In the previous chapter, the swinging wake mechanism of explosive welding is discussed. The model considers that the wake behind the obstacle swings from side to side producing a wavy interface. Size of the obstacle governs the wave size. Expression for size of the obstacle for general arrangement of explosive welding is developed in this chapter.

4.2 AMPLITUDE AND WAVELENGTH OF INTERFACE WAVE

For Von Karman vortex street, amplitude of the interface wave is taken equal to the transverse spacing of vortices h (wake height) where amplitude to wavelength ratio $h/\lambda = 0.281$. From free streamline theory, height of wake is 1.25 times the diameter 'd' of the obstacle. In the case of viscous fluids, mean longitudinal spacing is invariant and the ratio h/λ varies due to variation in h [115]. Since there is a finite extent of fluid zone in explosive welding, the flow is possibly confined and h/λ would be less than 0.281 due to wall effect [115] which implies that h should be less than 1.25d. In cases where centres of vortices can be identified in real fluid flow and also in weld interface, wave amplitude is found to be greater than wake height h [120].

However, in the present analysis, the amplitude of the interface wave is considered equal to total height of wake corresponding to transverse spacing of vortex street and is given by

$$h = 1.25\, d \tag{4.1}$$

The ratio of h/λ is written as

$$h/\lambda = c \tag{4.2}$$

According to vortex shedding theory, $c = 0.281$, whereas the swinging wake model predicts a value of c given by equation (3.21).

From equations (4.1) and (4.2), the wavelength λ is given by

$$\lambda = 1.25\, d/c \tag{4.3}$$

4.3 SIZE OF OBSTACLE

Although the ratio h/λ is independent of diameter of obstacle d, the amplitude h and wavelength λ depend upon d. Thus, to estimate h and λ it is essential to know the diameter of the obstacle in the case of explosive welding.

There has been criticism [121] about the existance of a real obstacle in the hydrodynamic model of explosive welding. Although there is no real obstacle, however, expected

velocity distribution [87] in explosive welding is somewhat similar to that obtained for the case of flow over a solid obstacle. The assumption of a solid boundary is justified as the velocity on the stagnation streamline is zero. Hence it is reasonable to imagine an obstacle between the two stagnation streamlines.

Considering complex velocities of jets [182], Reid and Sherif [120] developed the following expression for the diameter of the obstacle for the symmetric case.

$$d = 0.88\, t\, \beta \qquad (4.4)$$

where β is obliquity angle and t is thickness of each plate.

The equation (4.4) developed by Reid and Sherif [120] is for the ideal symmetric case where both the plates are of same material having same thickness and $\beta_1 = \beta_2 = \beta$. But in actual practice β_1 may not be equal to β_2, for example in asymmetric situation $\beta_1 > 0$ and $\beta_2 = 0$. It is therefore necessary to estimate the diameter of obstacle for a general arrangement of explosive welding.

The diameter of obstacle is found by considering collision of jets and establishing co-ordinates of point of intersection of the extention of stagnation streamlines.

4.3.1 Collision of Jets

Reid mentioned that the oblique collision of jets for non-symmetric situation is in general indeterminate [88]. However, according to Birkhoff, the situation is determinate in the case of parallel impinging jets [115] or for an analogous case of parallel outgoing jets. In the hydrodynamic model of general arrangement of explosive welding (Fig. 2.3) the salient jet and the re-entrant jet are considered parallel hence the situation seems to be determinate.

In a situation where $V_{P1} \neq V_{P2}$ and $\beta_1 \neq \beta_2$, the velocities of incomming jets are not necessarily equal. However, considering energy loss in the collision (chapter V), it can be shown that the speed of the outgoing jet is approximately 5 % less than the speed of the incomming jet. Considering equations (1.1.a), (2.8.a) and (2.8.b) it can be shown that $U_1 \approx U_2$ provided $V_{D1} = V_{D2}$, which is true as same explosive is usually used on both the plates in symmetric arrangement. Hence the approach suggested by Reid and Sherif [120] is extended for general situation of explosive welding assuming that the speeds of all the jets are approximately equal.

For the case of collision of two jets of unequal densities, the two estimates of pressure at the stagnation point are obtained by considering the two jets and are given as

$$p_1 = \tfrac{1}{2} \rho_1 U^2 - L_1 \quad \text{and} \quad p_2 = \tfrac{1}{2} \rho_2 U^2 - L_2$$

where L_1 and L_2 are energy losses in the two jets. From energy loss consideration (chapter V) it can be shown that energy loss is higher in the jet moving with higher kinetic energy. Thus it is possible that the energy losses L_1 and L_2 are such that at some point S, p_1 becomes equal to p_2 giving rise to a stagnation point.

Consider an equivalent system of explosive welding such that two incomming jets of thicknesses t_1 and t_2 are colliding as shown in Fig. 4.1. Let the out going jets be of thicknesses t_s and t_r. Let the speeds of bounding free streamlines of all the jets be U. A point (x, y) in the physical plane is denoted by $z = x + iy$ in the complex z-plane, and the fluid velocity at a point is described by the complex velocity $\nu = U\, e^{-i\theta}$ where U is the fluid speed and θ is the direction of velocity. The stagnation point S is the origin in both physical and in complex plane. The relationship between z and ν is given as [182]

$$\pi z = U\left[\frac{t_1}{t_2}\log_e\left(1-\frac{\nu}{u_1}\right)+\frac{t_2}{u_2}\log_e\left(1-\frac{\nu}{u_2}\right)\right.$$

$$\left.-\frac{t_s}{v_1}\log_e\left(1-\frac{\nu}{v_1}\right)-\frac{t_r}{v_2}\log_e\left(1-\frac{\nu}{v_2}\right)\right] \qquad (4.5)$$

The derivation of the above equation implies that the density of all the fluid jets is same. Such a relationship for the case of colliding jets of unequal densities (ρ_1, ρ_2) does not exist. In the present analysis, for

estimating obstacle size the thicknesses of the two jets t_1 and t_2 are normalised such that $t_1^* = \frac{2\rho_1}{(\rho_1+\rho_2)}\, t_1$ and $t_2^* = \frac{2\rho_2}{(\rho_1+\rho_2)}\, t_2$ are the equivalent thicknesses of jets of average density $(\rho_1 + \rho_2)/2$. Thus considering the thicknesses of incomming jets as t_1^* and t_2^* and of outgoing jets as t_s^* and t_r^*, the following relationship can be written

$$\pi z = U \left[\frac{t_1^*}{u_1} \log_e\left(1 - \frac{\nu}{u_1}\right) + \frac{t_2^*}{u_2} \log_e\left(1 - \frac{\nu}{u_2}\right) + \frac{t_s^*}{v_1} \log_e\left(1 - \frac{\nu}{v_1}\right) + \frac{t_r^*}{v_2} \log_e\left(1 - \frac{\nu}{v_2}\right)\right] \qquad (4.6)$$

Complex velocities of incomming jets are u_1 and u_2 and that of outgoing jets are v_1 and v_2. By substituting $u_1 = -Ue^{-i\beta_1}$, $u_2 = -Ue^{i\beta_2}$, $v_1 = -U$ and $v_2 = U$, equation (4.6) is written as

$$\frac{\pi z}{t_2^*} = -r\, e^{i\beta_1} \log_e\left[1 + e^{-i(\theta-\beta_1)}\right] - e^{-i\beta_2} \log_e\left[1 - e^{-i(\theta+\beta_2)}\right] + r_s \log_e\left[1+e^{-i\theta}\right] - r_r \log_e\left[1-e^{-i\theta}\right] \qquad (4.7)$$

where,

$$r = t_1^*/t_2^*, \quad r_s = t_s^*/t_2^*, \quad r_r = t_r^*/t_2^* \qquad (4.8.a)$$

$$t_1^* = 2\rho_1 t_1/(\rho_1 + \rho_2), \quad t_2^* = 2\rho_2 t_2/(\rho_1+\rho_2) \qquad (4.8.b)$$

$$t_s^* = \frac{1}{2}\left[r + 1 + (r\cos\beta_1 + \cos\beta_2)\right] t_2^* \qquad (4.8.c)$$

$$t_r^* = \frac{1}{2}\left[r + 1 - (r\cos\beta_1 + \cos\beta_2)\right] t_2^* \qquad (4.8.d)$$

Substituting $\theta = \pi + \beta_1$ in equation (4.7) and separating real and imaginary parts,

$$\frac{\pi x}{t_2^*} = r_s \log_e\left(2\sin\frac{\beta_1}{2}\right) - r_r \log_e(2\cos\beta_1)$$
$$- r\cos\beta_1 \log_e\delta + \left(\frac{\beta_1+\beta_2}{2}\right)\sin\beta_2$$
$$- \cos\beta_2 \log_e\left(2\sin\frac{\beta_1+\beta_2}{2}\right) \qquad (4.9)$$

and

$$\frac{\pi y}{t_2^*} = r_s\frac{\beta_1}{2} + r_r \log_e\left(\frac{\pi+\beta_1}{2}\right) - r\sin\beta_2 \log_e\delta$$
$$+ \left(\frac{\beta_1+\beta_2}{2}\right)\cos\beta_2 + \sin\beta_2 \log_e\left(2\sin\frac{\beta_1+\beta_2}{2}\right) \qquad (4.10)$$

where $\delta \longrightarrow 0$ as $\theta \longrightarrow \pi + \beta_1$.

The equation of the upper innermost streamline I_1 is written as

$$x\sin\beta_1 - y\cos\beta_1 = t_2^* c_1/\pi \qquad (4.11)$$

where c_1 is written, by using small angle approximations, as

$$c_1 \approx -\beta_1 \left[\log_e \frac{(\beta_1+\beta_2)^{(1+\beta_2/\beta_1)}}{\beta_1^{(1+r)}} - \frac{(r\,\beta_1-\beta_2)}{2\beta_1} + \frac{\pi}{2}\frac{r_r}{\beta_1} \right] \tag{4.12}$$

Since BS_1 is parallel to AI_1 (Fig. 4.1.a), the equation of the line BS_1 is given as

$$x \sin\beta_1 - y \cos\beta_1 = c_1\, t_2^{**}/\pi - t_{r1}^{**} \tag{4.13}$$

Similarly, equation of line BS_2 is given as

$$x \sin\beta_2 + y \cos\beta_2 = c_2\, t_2^{**}/\pi - t_{r2}^{**} \tag{4.14}$$

where t_{r1}^{**} is the thickness of the re-entrant jet contributed by jet - I and t_{r2}^{**} is the thickness contributed by jet - II. Expression for c_2 is given by

$$c_2 \approx -\beta_2 \left[\log_e \frac{(\beta_1+\beta_2)^{(r+r\beta_1/\beta_2)}}{\beta_2^{(1+r)}} - \frac{(\beta_2-r\beta_1)}{2\beta_1} + \frac{\pi}{2}\frac{r_r}{\beta_2} \right] \tag{4.15}$$

Solving equations (4.13) and (4.14) and using small angle approximations, we get

$$|x_o| = \frac{t^{**}_{r1} + t^{**}_{r2}}{(\beta_1 + \beta_2)} - \frac{t^{**}_2 (c_1 + c_2)}{(\beta_1 + \beta_2)} \qquad (4.16)$$

$$|y_o| = \frac{t^{**}_{r2}\,\beta_1 - t_{r1}\,\beta_2}{(\beta_1 + \beta_2)} - \frac{t^{**}_2 (c_2\,\beta_1 - c_1\,\beta_2)}{(\beta_1 + \beta_2)} \qquad (4.17)$$

4.3.2 Diameter of the Obstacle

The imaginary obstacle should be tangential to the streamlines S_1 and S_2 and it should also pass through the stagnation point S (Fig. 4.1-b). The diameter of the circular obstacle is given by geometrical considerations, as

$$d = 2(|x_o| + x_1)\,\sec(\beta_1-\beta_2)\,\sin\left(\frac{\beta_1+\beta_2}{2}\right) \qquad (4.18)$$

where the expression for x_1 can be found by considering the triangle GSC such that

$$x_1^2 + \left[y_o + (|x_o| + x_1)\,\tan\left(\frac{\beta_1-\beta_2}{2}\right)\right]^2 = \frac{d^2}{4} \qquad (4.19)$$

From eqs. (4.17) and (4.19) for the ideal symmetric situation ($\beta_1 = \beta_2 = \beta$, $\rho_1/\rho_2 = 1$ and $t_1 = t_2 = t$) $y_o = 0$ and $x_1 = d/2$, as shown in Fig. 4.2-a. Equation (4.18) reduces to $d = 0.88\,t\,\beta$ as also obtained by Reid and Sherif [120].

For the asymmetric situation ($\beta_2 = 0$) $y_o = 0$, $x_1 = 0$ (Fig. 4.2-b), and equation (4.18) becomes

$$d = \left[- \frac{\log_e \beta_1}{\pi} + \frac{3\beta_1}{8} - 0.16 \right] \frac{2\rho_1}{\rho_1 + \rho_2} t_1 \beta_1 \qquad (4.20)$$

4.3.3 Variation of the Diameter of Obstacle With Obliquity Angle and Obliquity Angle Ratio

Expressions for the diameter of the obstacle are solved using computer DEC-10. The results are plotted in Fig. 4.3-a and 4.3-b. It is seen from Fig. 4.3-a that the diameter of the obstacle for asymmetric situation ($\beta_2 = 0$) is independent of thickness ratio ($r = t_1/t_2$) and that it is less than the diameter of the obstacle for symmetric situation ($\beta_1 = \beta_2$). The diameter of the obstacle for the general situation when $0 < \beta_2 / \beta_1 < 1$ can be obtained from Fig. 4.3-b.

4.4 EXPERIMENTAL EVIDENCE AND DISCUSSION

To verify the theoretical analysis for estimation of diameter of the obstacle, the experimental results of Bahrani [183] are used. For asymmetric welding, experimental variation of amplitude (Eq. (4.1)) and wavelength (Eq.(4.2)) are plotted in Fig. 4.4 using the expression for the diameter of the obstacle for asymmetric welding case (Eq. (4.20))

taking c = 0.3 [108]. It is seen that the values of h and λ predicted by the theory are of the same order of magnitude as that of the experimental results.

As the diameter of the obstacle is smaller in the asymmetric situation than in symmetric situation, waves of smaller amplitude and wavelength are likely to be produced in the asymmetric situation.

To study the dependence of wave amplitude on density ratio, variation of amplitude (Eq. (4.1) with Eq. (4.20)) with ρ_1/ρ_2 is plotted in Fig. 4.5. Experimental points have been taken from the work of Bahrani [183] and Cowan et al. [107]. Taking the values of h/λ from the theoretical mean curve of Fig. 3.8, experimental results of Kuzmin et al. [184] are also plotted for β = 12 deg. The theory predicts the experimentally observed trend of the increase in amplitude with increasing density ratio.

4.5 CONCLUSIONS

Expression for the diameter of obstacle is developed for general arrangement of explosive welding.

Diameter of obstacle is expected to be smaller in asymmetric situation than in symmetric situation.

Smaller waves will be produced (a) in asymmetric welding as compared to symmetric welding and (b) for dissimilar metal combination as compared to waves in similar metal combination.

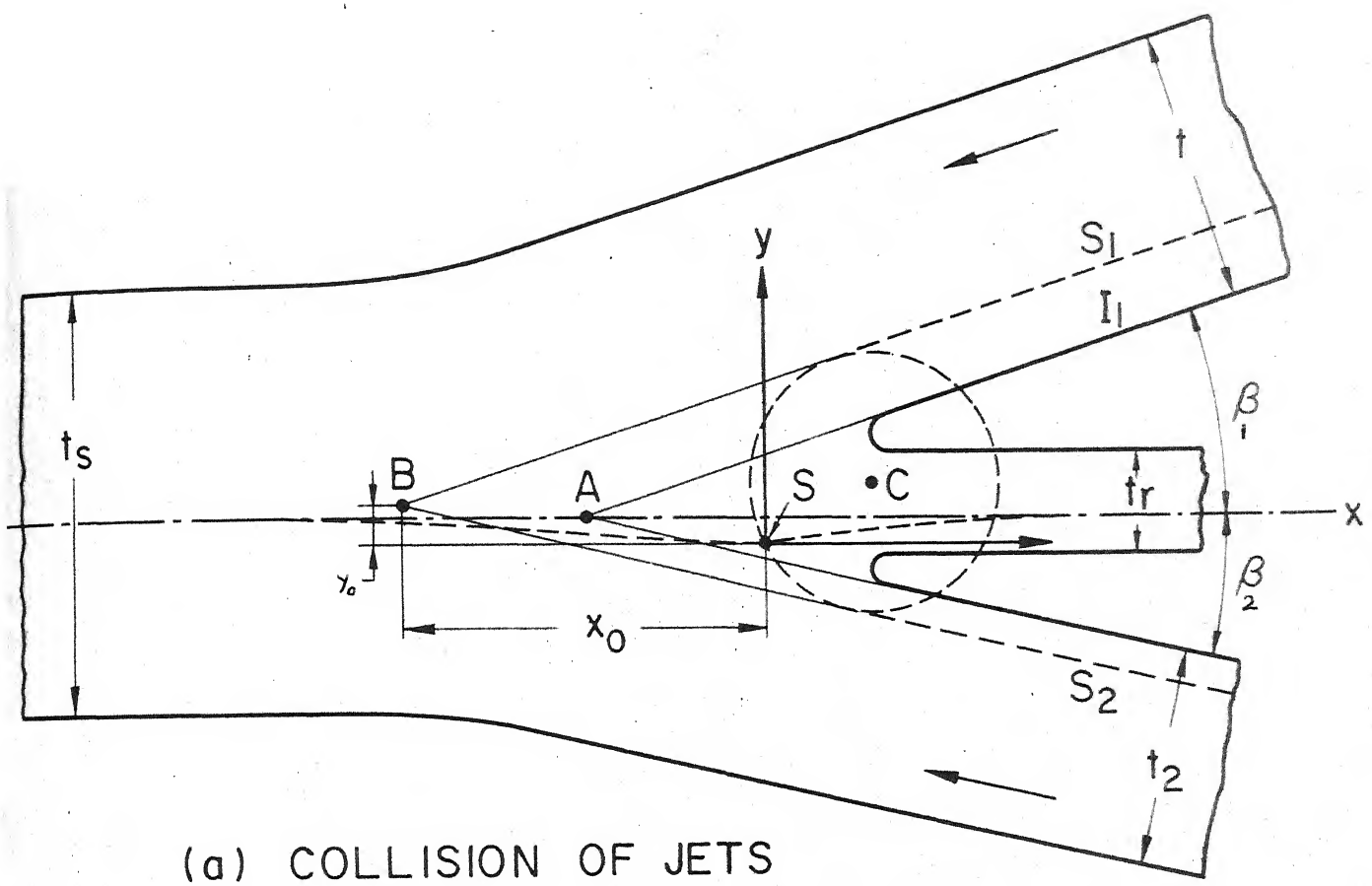

(a) COLLISION OF JETS

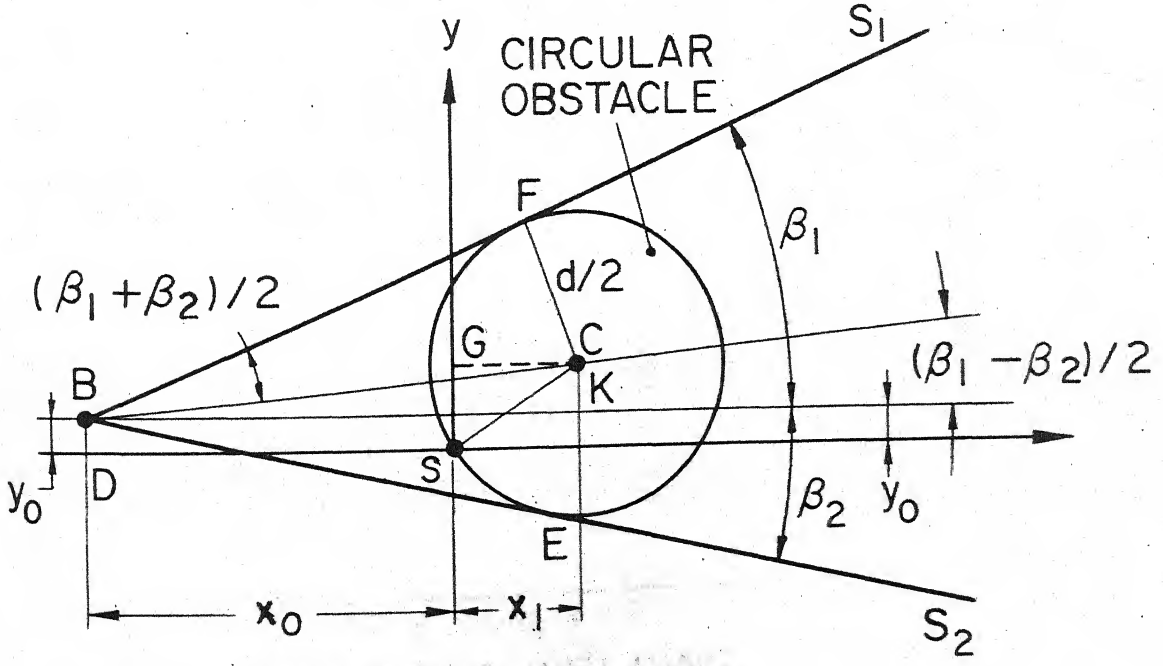

(b) OBSTACLE GEOMETRY

FIG. 4.1 EQUIVALENT OBSTACLE IN HYDRODYNAMIC MODEL OF EXPLOSIVE WELDING

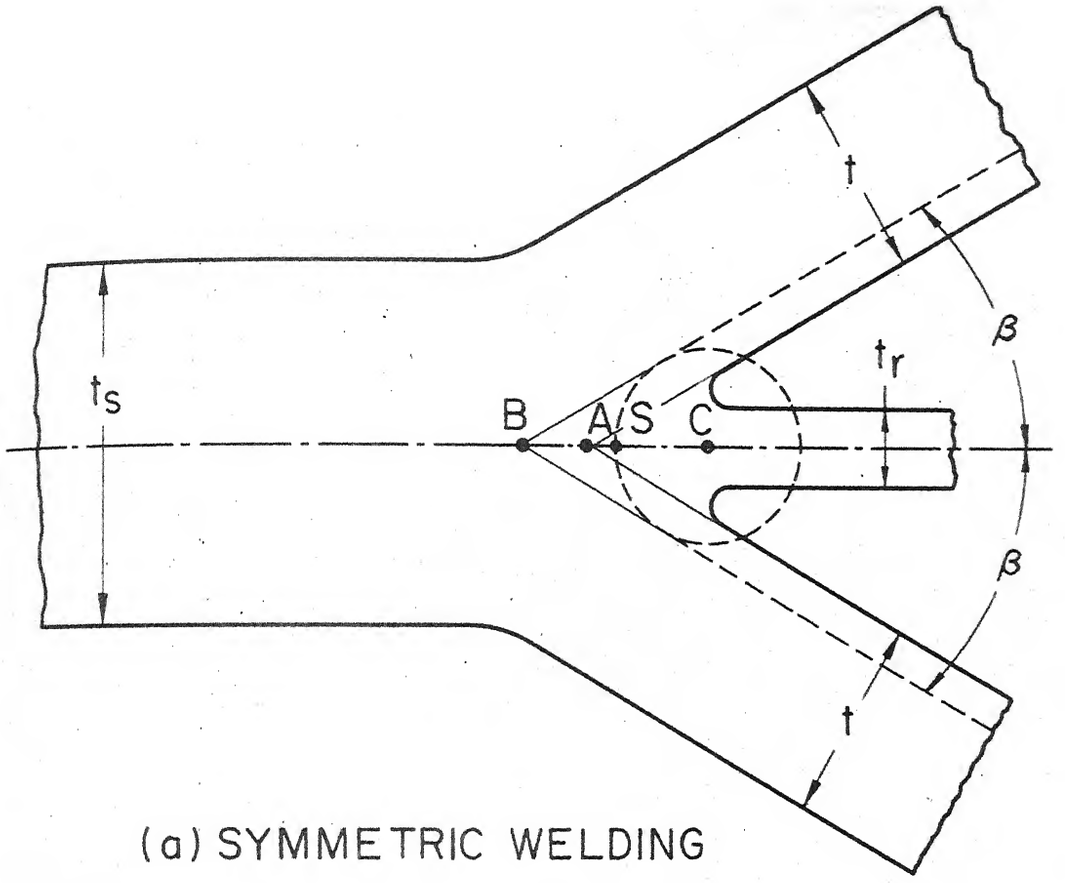

(a) SYMMETRIC WELDING

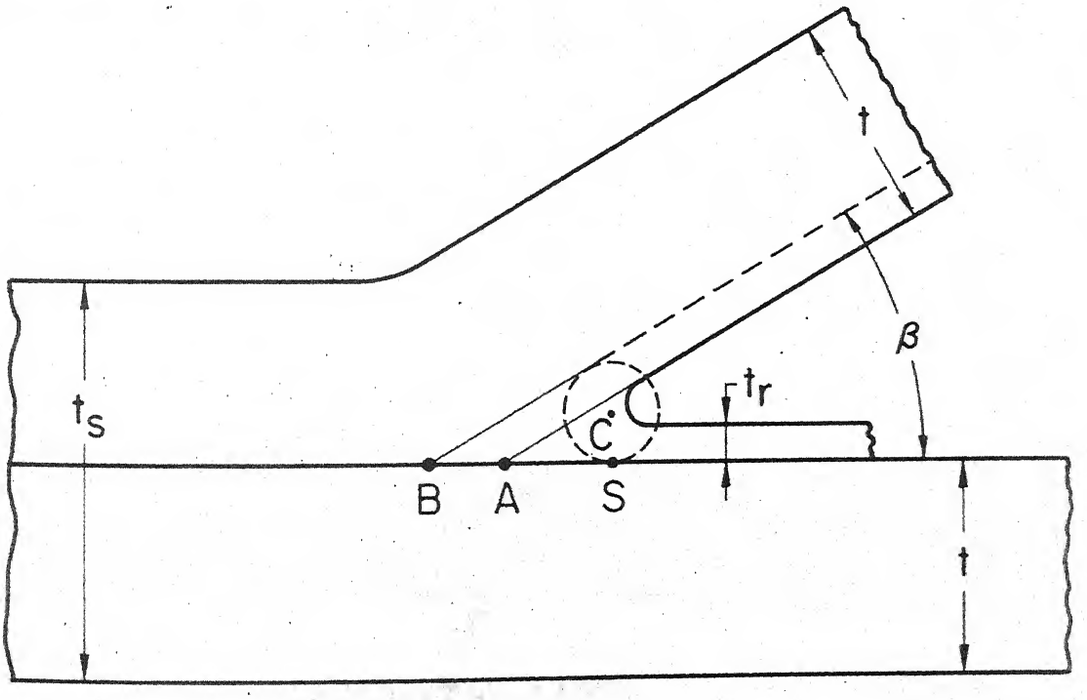

(b) ASYMMETRIC WELDING

FIG. 4.2 ORIENTATION OF OBSTACLE IN SYMMETRIC AND ASYMMETRIC WELDING

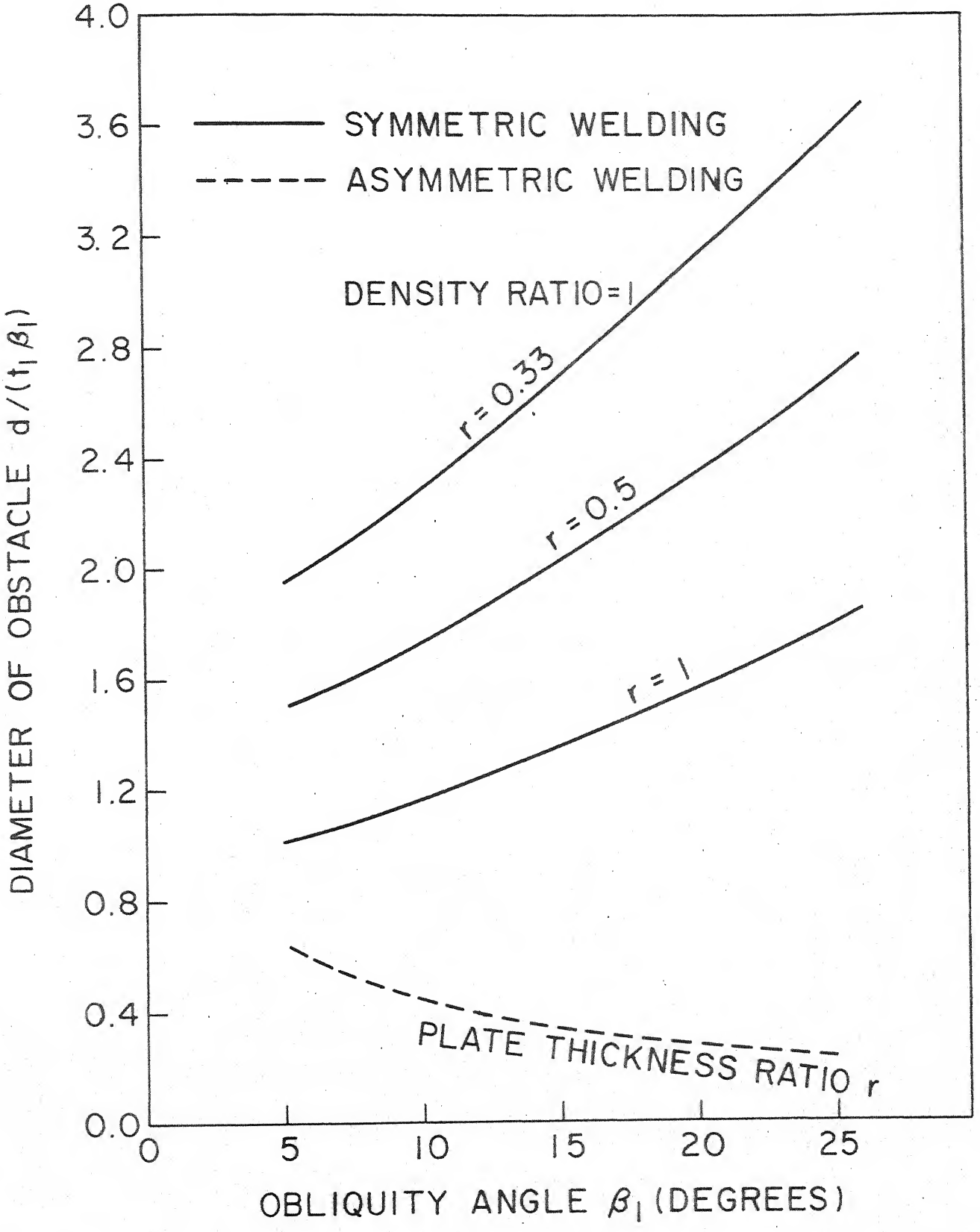

FIG. 4.3a VARIATION OF OBSTACLE SIZE WITH OBLIQUITY ANGLE

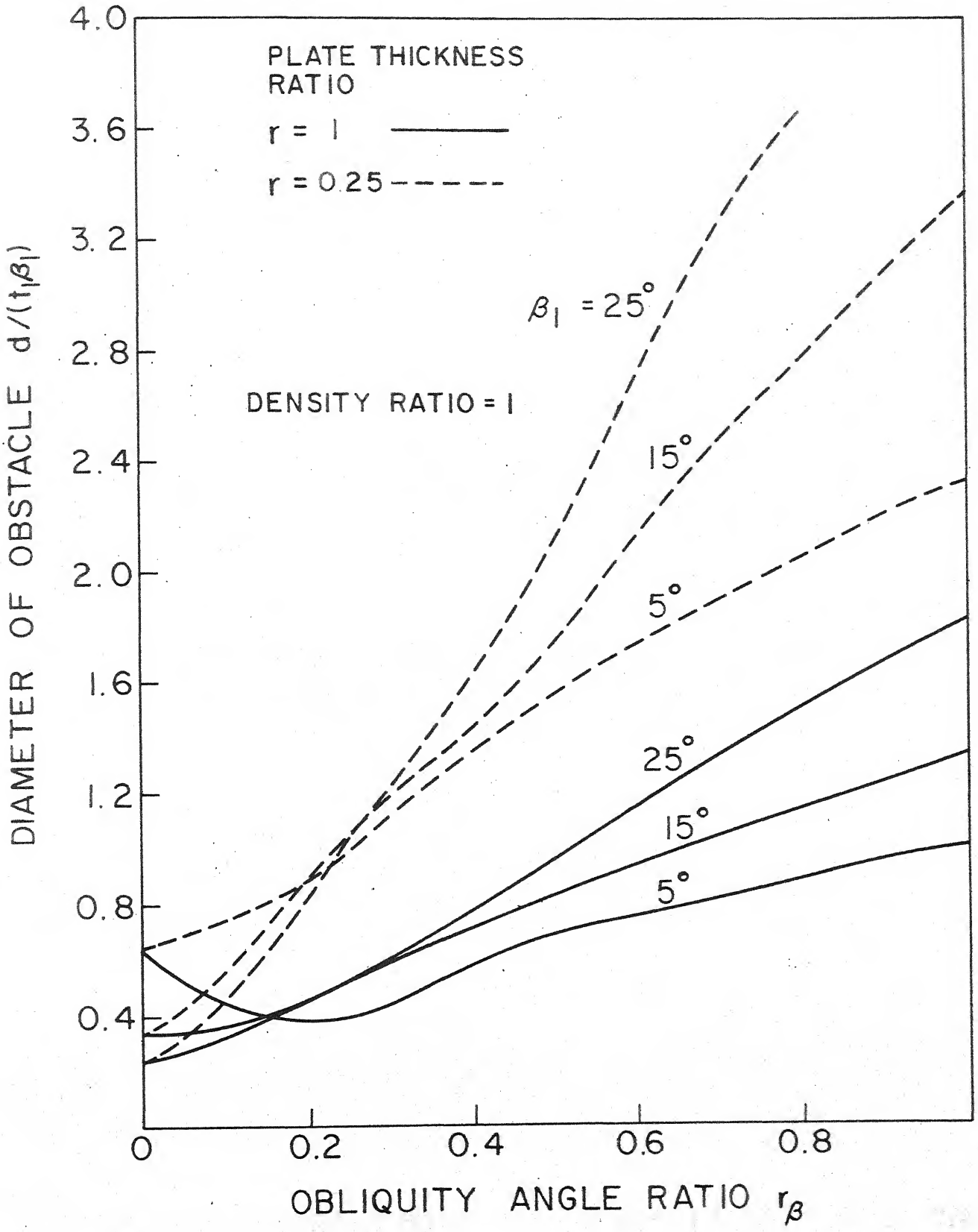

FIG. 4.3b VARIATION OF OBSTACLE SIZE WITH OBLIQUITY ANGLE RATIO

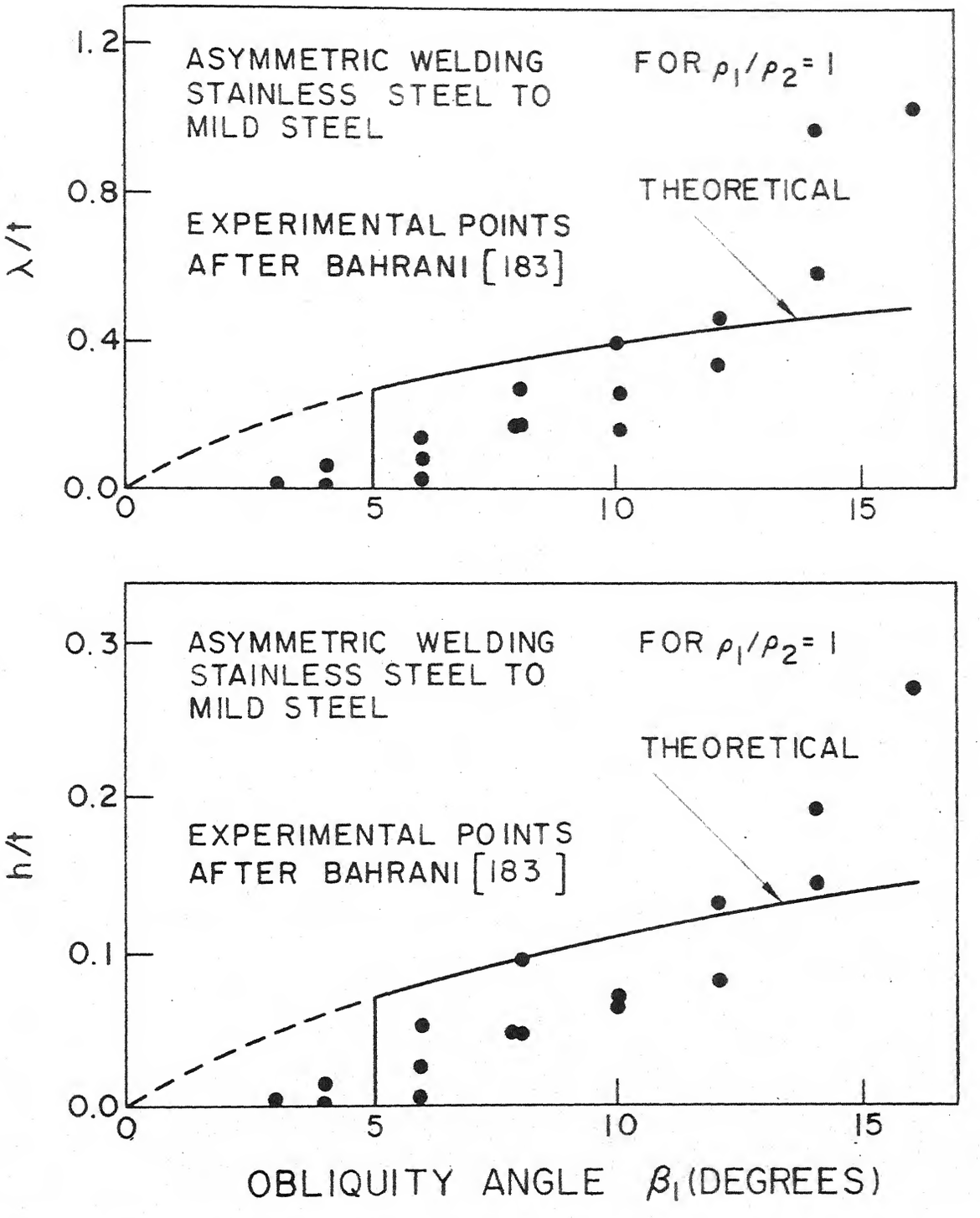

FIG. 4.4 VARIATION OF AMPLITUDE AND WAVE LENGTH WITH OBLIQUITY ANGLE

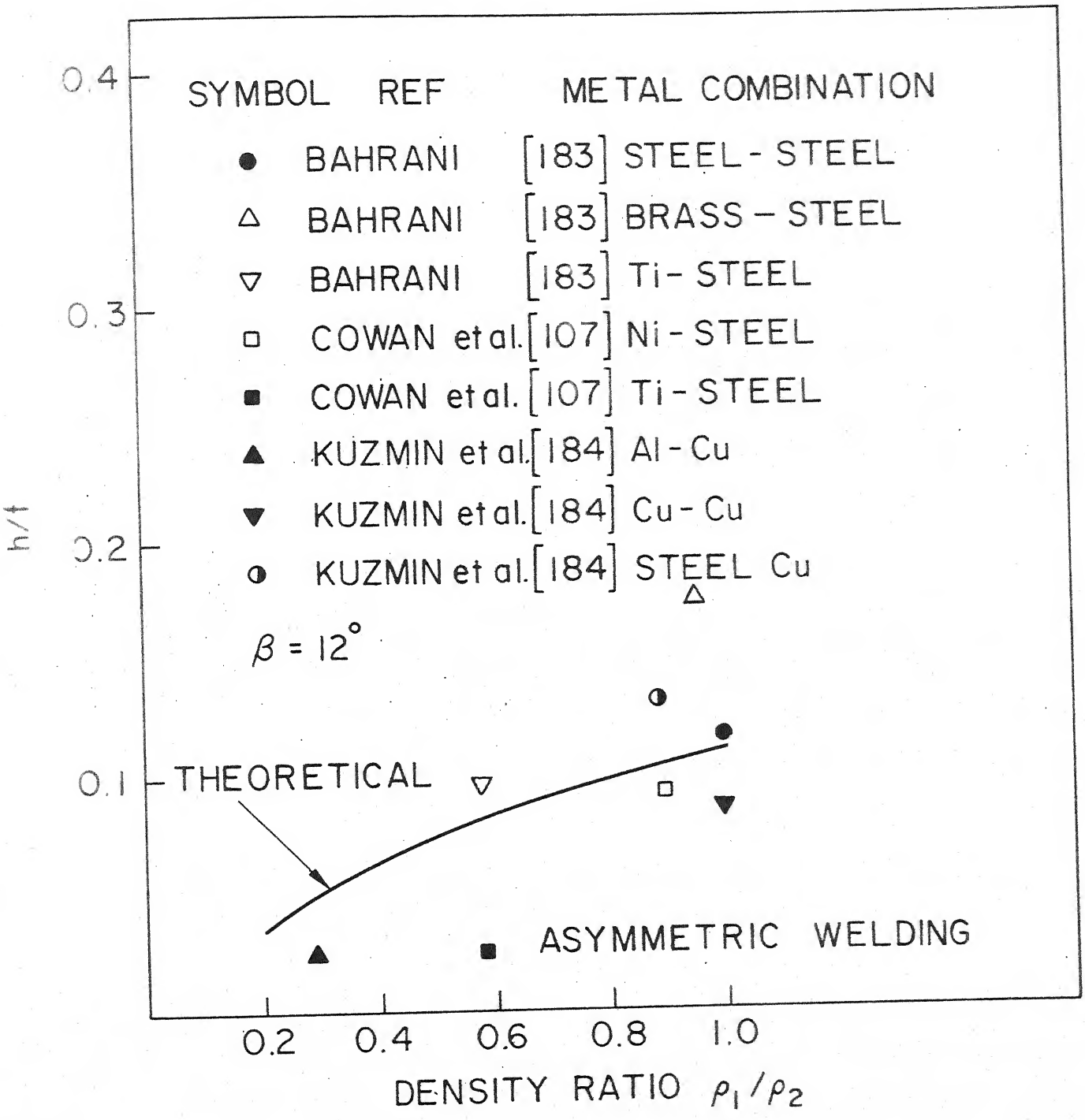

FIG. 4.5 DEPENDENCE OF WAVE AMPLITUDE ON DENSITY RATIO

CHAPTER V

PERMISSIBLE RANGE OF PARAMETERS FOR EXPLOSIVE WELDING

5.1 INTRODUCTION

Bahrani and Crossland [94] carried out explosive welding tests to study the phenomenon of wave formation and its effect on strength of bond. Experimental variations of interface wave amplitude h with obliquity angle β for different explosive loading [94] are shown in Fig. 5.1. The general nature of the curve is also represented in the figure. It is seen that below a critical angle β_L and above an angle β_W wave formation does not occur. However, welding with straight interface may take place upto an angle β_E beyond β_W.

In this chapter a model of explosive welding, based on a limited extent of fluid zone and considering energy loss in collision, is proposed. Expressions for β_E, β_W and β_L are developed. A selection procedure for explosive welding parameters is suggested.

5.2 FLUIDIZED ZONE

Usually in hydrodynamic analogy of explosive welding, total thickness of plate is considered as fluid. However, using Taylor's analysis [185] of oblique impact of an incompressible jet on a plane surface, Hunt [105] showed that there is a limited extent of fluid zone within which fluidlike

form as

$$\frac{w}{t} = \frac{4(1 - \beta^2 p_s)^{1/2}}{\pi \beta^2 p_s^2} \qquad (5.3)$$

Equations (5.1)aand (5.3) are plotted in Fig. 5.2 and it is seen that both the plots are very close. Hence the simpler equation (5.3) is used in the subsequent analysis.

Robinson [87] theoretically predicted pressure distribution around the stagnation point. Pressure and strain rate contours (Fig. 2 of Ref. [87]) are approximately circular. So it is assumed that the fluidized zone is approximately cylindrical in shape. If $w/t < 1$, only a part of the plate thickness is fluidized, if $w/t \geq 1$, total thickness of the plate shows fluidlike behaviour and the width of the fluid zone is equal to or greater than the height of the fluid zone as shown in Fig. 5.2. If t_f is the thickness of the fluidized portion of plate, then t_f/t will always be less than or equal to 1. The variation of t_f/t is also shown in Fig. 5.2, from which it is seen that

$$t_f = t \qquad \text{for } \beta < \beta_0 \qquad (5.4.a)$$

and

$$t_f = w \qquad \text{for } \beta > \beta_0 \qquad (5.4.b)$$

where β_0 is the obliquity angle above which $t_f < t$. For certain values of β the shapes of the fluidized zones are also shown in Fig. 5.2.

Fluid zone factor r_f is defined as the ratio of the fluidized thickness of plate to the total thickness of the plate. Thus $r_f = t_f/t$, hence,

$$r_f = 1 \qquad \text{for } \beta < \beta_0 \qquad (5.5.a)$$

$$r_f = \frac{4(1 - \beta^2 p_s)^{1/2}}{\pi \beta^2 p_s^2} \qquad \text{for } \beta_0 < \beta < \beta_F \qquad (5.5.b)$$

$$r_f = 0 \qquad \text{for } \beta > \beta_F \qquad (5.5.c)$$

where β_0 is the obliquity angle above which only a portion of the plate is fluidized and β_F is the obliquity angle above which the plate does not show any fluidlike behaviour.

The variation of fluid zone factor r_f versus β, and r_f versus V_p, for copper ($p = 1.2 \times 10^9$ N/m^2 [186], $\rho = 8900$ kg/m^3) are shown in Fig. 5.3.

5.3 CONSIDERATION OF ENERGY LOSS IN COLLISION

In explosive welding, the energy loss in collision is usually ignored. Assuming that no energy loss takes place in collision and that the total plate has a fluidlike behaviour,

mass of the re-entrant jet m_r for asymmetric welding is given by equation (1.3.a).

However, whenever there is an impact some energy is always lost. As such in explosive welding too, there will be some energy loss in the collision of jets and it is expected that there will be some reduction in jet velocity after the collision.

Consider that a fluidized jet of thickness t_f and mass $m_f = r_f m$ impinges with a velocity V_F and that it divides into a re-entrant jet of mass m_r and a salient jet of mass m_s each assumed to be moving with a velocity V_J (Fig. 5.4-b), such that

$$m_s + m_r = m_f \tag{5.6}$$

Conservation of horizontal momentum gives

$$r_v\, m_s + r_v\, m_r = m_f \cos\beta \tag{5.7}$$

where, the velocity ratio $r_v = V_J/V_F$.

If L is the kinetic energy lost in collision, conservation of energy yields

$$r_v^2\, m_s + r_v^2\, m_r = m_f - \frac{L}{\frac{1}{2} V_F^2} \tag{5.8}$$

From equations (5.6) to (5.8)

$$m_r = \frac{r_f\, m}{2\, r_v} (r_v - \cos\beta) \tag{5.9}$$

and

$$1 - r_v^2 = \frac{2L}{r_f\, m\, V_F^2} \tag{5.10}$$

Thus the mass of the re-entrant jet is given by

$$m_r = \frac{r_f m}{2} \left[\sqrt{1 - \frac{L}{\frac{1}{2}\, r_f\, m\, V_F^2}} - \cos\beta \right] \Big/ \sqrt{\left(1 - \frac{L}{\frac{1}{2}\, r_f\, m\, V_F^2}\right)} \tag{5.11}$$

For $L > 0$, equation (5.10) suggests that $r_v < 1$ i.e., $V_J < V_F$ which means that there is a reduction in jet velocity after collision. The ratio of 'absolute' value of re-entrant jet velocity to collision point velocity in explosive welding is usually considered equal to 2. However, the experimental study of Onzawa and Ishii [90] shows that this ratio is less than 2. This also reveals that there is some reduction in jet velocity after collision.

For the ideal case of no energy loss $L = 0$, and hence from equation (5.10) $r_v = 1$. The equation(5.11) thus reduces to equation (1.3.a) for $r_f = 1$.

5.3.1 Evaluation of Kinetic Energy Loss in Collision

In the case of collision of two jets, the kinetic energy loss is primarily due to the plastic work done in deforming the plates and viscous losses. These losses are expected to depend mainly upon the material properties of the plates, the velocity and the viscosity of the jets. In view of an inadequate information regarding the viscosity of the fluidized jet of metal and its dependence upon the welding parameters V_p and β, a semi-empirical approach is adopted to estimate the loss of kinetic energy.

Maximum loss of kinetic energy is given from equation (5.11) by taking $m_r = 0$, such that

$$L_{max} = \tfrac{1}{2} r_f m V_F^2 \sin^2 \beta \qquad (5.12)$$

When the energy loss is equal to L_{max}, no re-entrant jet is produced. In general the kinetic energy loss L is written as

$$L = \psi \; L_{max} \qquad (5.13)$$

where ψ is the loss factor such that $\psi \leq 1$.

The loss factor is obtained from Eqs. (5.11) and (5.13) as,

$$\psi = \left[1 - \left\{(r_f m \cos \beta)/(r_f m - 2m_r)\right\}^2\right]/\sin^2 \beta \qquad (5.14)$$

Meyer's experimental data [91] for the mass of the re-entrant jet m_r for various values of plate velocities V_P with $\beta = 16^o$ and m = 24 gms is used to estimate the loss factor ψ. The values of ψ are plotted in Fig. 5.5 against p_s. By fitting a curve relationship $\psi = 0.35\ p_s^{0.5}$ is obtained.

The mass of the re-entrant jet $m_r = 0$ when the loss factor $\psi = 1$. From Meyer's experiments on copper, this condition corresponds to V_P = 200 m/s for β = 16 deg., V_P=350 m/s for β = 30 deg. and V_P = 475 m/s for β = 40 deg. The function $\psi/p_s^{0.5}$ is plotted against β in Fig. 5.5, which gives

$$\psi = 1.25\ \beta\ p_s^{0.5} \qquad (5.15)$$

Using equations (5.12), (5.13) and (5.15), the empirical expression for kinetic energy loss in collision is given as

$$L = 0.625\ \beta\ p_s^{0.5}\ r_f\ m\ V_F^2\ \sin^2\beta \qquad (5.16)$$

5.3.2 Mass of Re-entrant Jet

From equations (5.11) and (5.16), the mass of the re-entrant jet with energy loss consideration is given by

$$m_r = \frac{r_f\ m}{2}\left[1 - \cos\beta / \sqrt{1-1.25\ \beta\ p_s^{\frac{1}{2}}\ \sin^2\beta}\ \right] \qquad (5.17)$$

Using equations (5.2), (5.3) and (5.17), the theoretical variations of the mass of the re-entrant jet is obtained and is plotted against obliquity angle β in Fig. 5.6 for V_p = 350 m/s and 475 m/s, for copper along with the experimental results of Meyer [91] using m = 24 gms. The conventional equation (1.3.a) for mass of re-entrant jet is also plotted. It is seen that there is considerable reduction in the mass of jet when energy loss is considered. The theory predicts that the mass of the jet initially increases with increase in β, reaches a maximum value and decreases with further increase in β giving $m_r = 0$ at a certain angle β_E. Equation (1.3.a), however, predicts a monotonous increase in the mass of jet and does not predict any dependence of mass of re-entrant jet on plate velocity. Thus the present theory is in reasonable agreement with the experimental results of Meyer [91] and predicts the important features of m_r versus β curve.

Corresponding thickness of the re-entrant jet t_r is given from equation (5.17) as

$$t_r = \frac{r_f\, t}{2} \left[1 - \cos\beta / \sqrt{(1-1.25\ \beta\ p_s^{\frac{1}{2}} \sin^2\beta)}\right] \qquad (5.17.a)$$

where r_f is fluid zone factor, t is total thickness of the flyer plate and β is the obliquity angle.

5.4 NATURE OF VARIATION OF WAVE AMPLITUDE WITH OBLIQUITY ANGLE

From swinging wake model proposed in chapter III, amplitude of interface wave h for asymmetric welding of similar metals is given by the equation (4.1) and (4.20) as

$$h = 1.25\left[-\frac{\log_e \beta}{\pi} + \frac{3}{8}\beta - 0.16\right] t\,\beta \qquad (5.18)$$

Since thickness of fluidized plate t_f is not always equal to the thickness of the plate t, the above equation needs to be modified by substituting $t = t_f$. Thus

$$h = 1.25\left[-\frac{\log_e \beta}{\pi} + \frac{3}{8}\beta - 0.16\right] t\,\beta \qquad \text{for } \beta < \beta_0 \qquad (5.18.a)$$

$$h = 1.25\left[-\frac{\log_e \beta}{\pi} + \frac{3}{8}\beta - 0.16\right] \frac{4(1-\beta^2 p_s)^{\frac{1}{2}}}{\pi \beta^2 p_s^2}\, t\,\beta$$

$$\text{for } \beta > \beta_0 \qquad (5.18.b)$$

Variation of t_f, t_r and h with β are plotted in Fig. 5.7 for a representative value of $p_s = 4$ and $t = 1$ mm. Theoretical variation of t_f and t_r with β shows that fluid zone vanishes above an angle β_F and re-entrant jet is absent above an angle β_E. Amplitude of interface wave is maximum corresponding to optimum obliquity angles β_0.

Walsh et al. [60] have shown that below a critical angle β_L jet-less configuration occurs in explosive welding implying h = 0. Thus the wave amplitude plot is slightly modified by line AB in Fig. 5.7.

Kowalick and Hay [110] suggested that below a certain Reynolds number, flow near the obstacle is laminar and a straight bond is obtained. The condition corresponds to the obliquity angle β_W which separates wave-no-wave region (Section 5.5.3). With this consideration the plot of h versus β is further modified as shown by line DW.

5.5 LIMITING OBLIQUITY ANGLES

5.5.1 Fluid Zone-No Fluid Zone Boundary

The obliquity angle β_F (in degrees) above which the plate does not show fluidlike behaviour (Fig. 5.2) is obtained by putting w = 0 in equation (5.3), as

$$\beta_F = 57.3\, p_s^{-\frac{1}{2}} \qquad (5.19)$$

5.5.2 Jet-No-Jet (Weld-No-Weld) Boundary

For explosive welding, re-entrant jet is necessary as it ensures the cleaning of the mating surfaces. Considering that jet-no-jet condition corresponds to weld-no-weld boundary, the following expression for β_E (in degrees) is obtained by putting $m_r = 0$ in equation (5.17)

$$\beta_E = 46\, p_s^{-\frac{1}{2}} \qquad (5.20)$$

5.5.3 Wave-No-Wave Boundary

Kowalick and Hay [110] have opined that in the case of explosive welding flow around an obstacle is governed by Reynolds number given by

$$Re = \frac{V_F\, d\, \rho}{\mu} \qquad (5.21)$$

where V_F is the stream velocity, ρ and μ are the density and viscosity of the fluidized metal stream and d is the diameter of the assumed circular obstacle. They [110] opined that below a certain critical Reynolds number, flow around the obstacle is laminar and straight bond is obtained. Taking $\mu = 2 \times 10^4$ poise for steel, they calculated the critical Reynolds number Re = 2.3 in explosive welding. Cowan et al. [107] defined Reynolds number on the basis of hardness of the metal plates and found that the critical Reynolds number Re = 10. Whereas, for fluid flow Re = 40 has been reported [115].

It is very difficult to estimate the exact viscosity of fluidized metal jet and its dependence on the explosive welding parameters. However a simple approach to find viscosity of the jet can be based upon the criteria that the shear stress between the layers is equal to the theoretical yield

shear strength of the material such that

$$p = \tau_e = \mu \frac{\partial V}{\partial y} = \mu\, a \frac{V_F}{\Delta} \qquad (5.22)$$

where $p = \tau_e$ is the theoretical yield shear strength of the material, μ is the viscosity of the metal, stream velocity V_F is velocity scale, velocity half width Δ is length scale and 'a' is a constant which can be evaluated empirically.

From equations (5.21) and (5.22) the transition collision velocity V_{FW} for wave-no-wave boundary is given by

$$V_{FW} = \sqrt{\frac{Re\ \Delta\ p}{a\ d\ \rho}} \qquad (5.23)$$

It has been shown by Reid [121] that width of disturbance 2Δ is approximately equal to the diameter of the obstacle d, hence

$$V_{FW} = \sqrt{\frac{Re\ p}{2a\rho}} \qquad (5.24)$$

Since $V_{FW} = V_P/\beta_W$ and $p_s = 2p/(\rho V_P^2)$, equation (5.24) can be written as

$$\beta_W = 57.3 \sqrt{\frac{4a}{Re}}\ p_s^{-\frac{1}{2}} \qquad (5.25)$$

where β_W is the critical obliquity angle (in degrees) for wave-no-wave boundary.

5.5.4 Optimum Obliquity Angle for Maximum Wave Amplitude

The obliquity angle β_0 (in degrees) which corresponds to maximum height of interface wave is obtained by equating equations (5.18.a) and (5.18.b)

$$\beta_0 = \frac{114.6}{\sqrt{2\, p_s + \pi\, p_s^2}} \qquad (5.26)$$

5.5.5 Optimum Obliquity Angle for Maximum Thickness of Re-entrant Jet

The obliquity angle β_{0J} (in degrees) which correspond to the maximum mass (or thickness) of re-entrant jet is obtained from equation (5.17) as

$$\beta_{0J} \simeq 30\, p_s^{-\frac{1}{2}} \qquad (5.27)$$

5.6 COMPARISION OF THEORY WITH EXPERIMENTAL RESULTS

Prediction of the theory is compared with the experimental results of Bahrani and Crossland [94], Meyer [91] and Cowan et al. [107].

To calculate specific pressure p_s, the plate velocity V_p is obtained from equation (1.2).

The actual* strength of a material is much less than the theoretical strength due to the presence of impurities and defects. Since the dimensions of wavy interface in

explosive welding are small and strain rates are extremely high, the stress level needed to fluidize the metal is expected to approach the theoretical yield shear strength of the material. Theoretical strength of a material depends upon its crystal structure, modulus of rigidity G and stacking fault energy [186]. Theoretical strength of some of the metals, usually of interest in explosive welding, are given in Table - 5.1. The values of densities used for various materials are also given.

The value of the theoretical strength of metal p is difficult to calculate due to uncertainty of stacking fault energy, variation of crystal structure with temperature and effect of alloying elements on the value of G. However, the values of p given in Table - 5.1 are used to study the effect of specific pressure p_s in explosive welding of metals.

Values of p_s are calculated from experimental data of various workers [91, 94] using equation (5.2) and values of p from Table - 5.1. Theoretical variation of β_E versus p_s (equation (5.20)) is plotted in Fig. 5.8 along with the experimental results of Bahrani and Crossland [94] and Meyer [91]. It is seen that the theoretical predicted values show a good agreement with the experimental results.

The experimental results of Bahrani et al. [94, 97] and Meyer [91], for wave-no-wave condition, are plotted in Fig. 5.9. Cowan et al. [107] found experimentally that wave

Table - 5.1

Values of Theoretical Strength of Metals

Material	Density ρ $10^3 kg/m^3$	Modulus of Rigidity G $10^{10} N/m^2$	Crystal Structure	τ_{max}/G	Theoretical Strength τ_{max} or p $10^9 N/m^2$	Remarks
Iron	7.80	6.0	B.C.C.	0.11	6.6	Taken from Ref. [186]
Copper	8.88	3.08	F.C.C.	0.039	1.2	"
Nickel	8.82	7.8	F.C.C.	0.039	3.0	Calculated using Ref. [187]
Titanium (880°C)	4.52	3.0	H.C.P.	0.087*	2.6	Calculated using Ref. [188]
Aluminium	2.62	2.3	F.C.C.	0.114	2.6	Taken from Ref. [186]

* Taking axial ratio = 1.587.

vanishes at $\beta = 12^{\circ}$ for $V_C = 1365$ m/s and at $\beta = 12^{\circ}$ for $V_C = 1600$ m/s for cladding of Nickel plate where $V_C = \frac{1}{2} V_P / \sin \frac{\beta}{2}$ is collision velocity. These results are also plotted in Fig. 5.9. Theoretical variation (equation (5.25)) of β_W with p_s is of the nature $\beta_W = K\, p_s^{-\frac{1}{2}}$. The experimental variation is represented by

$$\beta_W = 32\, p_s^{-\frac{1}{2}} \qquad (5.28)$$

A comparison with equation (5.25) shows that

$$Re/a = 13 \qquad (5.29)$$

For copper, the value of 'a' is estimated from equation (5.22) by taking a representative value $\mu = 10^3$ poise for $V_P = 350$ m/s and $\beta = 16^{\circ}$ [87]. Taking $2\Delta = d = 0.88\, t\, \beta$ [121], equation (5.22) yields $a = 1.25$. Thus equation (5.29) gives $Re = 16.5$ as the wave-no-wave condition. This is comparable with the values of $Re = 10$ given by Cowan et al. [107], $Re \approx 3$ given by Kowalick and Hay [110] and $Re = 40$ in actual fluid flow situations [115].

Theoretical variations of β_0 and β_{0J} versus p_s (Eqs. (5.26) and (5.27)) are plotted in Fig. 5.10 along with the experimental results of Bahrani et al. [94, 97] and Meyer [91]. The theory shows a reasonable agreement with the experimental results.

5.7 LOWER CRITICAL ANGLE

Walsh, Shreffler and Willing [60] showed that below a certain critical angle β_L, re-entrant jet is absent. Therefore welding does not take place below a critical angle β_L. Although Walsh et al. [60], Cowan and Holtzman [64] and Allen et al. [92] have suggested procedures for evaluating β_L but it is very difficult to calculate β_L for given configuration and material properties. The angles β_E, β_W and β_0 show a dependence on specific pressure p_s, it is expected that β_L would also depend on p_s. A graph between β_L and p_s is shown in Fig.5.11 using experimental data of various workers [91, 92, 94, 97]. A simple empirical equation for β_L is obtained by using least square fit for a power curve as

$$\beta_L = 6\, p_s^{-0.4} \tag{5.30}$$

5.8 PERMISSIBLE RANGE OF OBLIQUITY ANGLE β AND SET-UP ANGLE α FOR EXPLOSIVE WELDING

Permissible range of obliquity angle β for explosive welding is given by

$$\beta_L < \beta < \beta_E \tag{5.31}$$

Using equations (5.20), (5.30), (5.2) and (1.2), the inequality (5.31) is expressed as

$$6\, E_\ell^{0.8}\, E_W^{-0.4} < \beta < 46\, E_\ell\, E_W^{-0.5} \qquad (5.32)$$

where E_ℓ is the explosive loading number and E_W is the explosive welding number, and are defined as

$$E_\ell = \frac{0.612\ e/m}{2 + e/m} = V_P/V_D \qquad (5.33)$$

$$E_W = p/(\tfrac{1}{2} \rho V_D^2) \qquad (5.34)$$

Permissible range of set-up angle α is obtained on the basis of permissible range of β and using the following relationship

$$\beta = \alpha + \phi \qquad (5.35)$$

where dynamic bend angle ϕ (in degrees) is given by

$$\phi \approx 57.3 \frac{V_P}{V_D} = 57.3\, E_\ell \qquad (5.36)$$

From inequality (5.32) and equations (5.35) and (5.36), permissible range of set-up angle is given by

$$(6\, E_\ell^{0.8}\, E_W^{-0.4} - 57.3\, E_\ell) < \alpha < (46\, E_\ell\, E_W^{-0.5} - 57.3\, E_\ell) \qquad (5.37)$$

5.9 SELECTION OF EXPLOSIVE WELDING PARAMETERS

(a) Welding of Copper

Permissible obliquity angles (β_L, β_E) and generated obliquity angle (β) for various conditions, versus plate velocity are plotted in Fig. 5.12 for copper ($p = 1.2 \times 10^9$ N/m^2) using equations (5.20), (5.30), (5.2), (1.2), (5.35) and (5.36). It is implied in the present analysis that the explosive requirement for proper welding is, primarily, a function of material properties of the flyer plate.

Figure 5.12 is used to illustrate the procedure for selecting parameters for explosive welding. Assuming that explosive welding of copper is to be done using parallel arrangement ($\alpha = 0$) and an explosive with $V_D = 5000$ m/s. It is further decided to use an explosive loading such that the plate velocity $V_p = 350$ m/s. The conditions are represented by point A in Fig. 5.12. Thus the corresponding value of β generated falls outside the permissible range and proper welding will not take place. There are three alternatives to remedy the situation.

(i) Increase the explosive loading so that the plate velocity reaches a higher value, say $V_p = 700$ m/s, such that point A moves to point A_1 in the permissible range.

(ii) Use an explosive with lower detonation velocity, say V_D = 4000 m/s, point A moves to point A_2.

(iii) Go in for inclined arrangement so that $\alpha = 10^\circ$ and point A moves to point A_3 which is well within the range of β_E and β_L.

Similar conclusions for explosive welding have been drawn by Crossland [78] on the basis of experimental experience. The present work, however, provides a quantitative basis for selecting alternatives means of carrying out explosive welding successfully.

Variation of β_W with plate velocity, for wave-no-wave condition, is also plotted in Fig. 5.12. A designer may aim at selecting parameters such that $\beta_L < \beta < \beta_W$, so as to ensure the formation of interface wave.

It is interesting to note that a parallel arrangement with V_P = 350 m/s and V_D = 5000 m/s (point A in Fig. 5.12) does not seem to provide suitable condition for cladding of copper whereas using an inclined arrangement ($\alpha = 10^\circ$), welding seems possible even at lower explosive loading (say point A_4). However, it is known from the work of Crossland and various other workers that there is a lower limit of $V_P \simeq 200$ m/s, below which satisfactory welding does not take place. Plate velocity required for parallel arrangement (point A_1) is much higher as compared to inclined arrangement (point A_3).

Thus an inclined arrangement with explosive of high detonation velocity, may be preferred for welding of copper. However, for large plate cladding, parallel arrangement with explosive of low detonation velocity is necessary as in the inclined arrangement a large gap at the free end causes bending of plates [78].

(b) Welding of Steel

Figure 5.13 shows permissible range of obliquity angles for welding of steel ($p = 6.6 \times 10^9$ N/m^2). Consider that explosive welding of steel is to be done using inclined arrangement ($\alpha = 10^o$) with an explosive having V_D = 5000 m/s. It is further decided to use an explosive loading such that plate velocity V_P = 400 m/s. These conditions are represented by point A in Fig. 5.13 which falls outside the permissible range and hence proper welding will not take place. There are three alternatives to remedy this situation.

(i) Increase the explosive loading so that plate velocity is increased to a higher value, say, V_P = 600 m/s, such that the point A moves to point A_1 in the permissible range.

(ii) Use an explosive with higher detonation velocity, say V_D = 7000 m/s, point A moves to point A_2.

(iii) Reduce the set-up angle from 10° to 5°, point A moves to point A_3. Also, by using parallel arrangement ($\alpha = 0$), point A moves to point A_4.

5.10 OPTIMUM EXPLOSIVE LOADING

Maximum amplitude of interface wave is produced if the welding parameters are such that optimum obliquity angle is generated.

Using equations (5.26), (5.2), (1.2), (5.35) and (5.36) values of optimum explosive loading is plotted against detonation velocity in Fig. 5.14.a for $\alpha = 5^{\circ}$ and $\alpha = 10^{\circ}$, for steel and copper as flyer plate materials. It is seen from Fig. 5.14-a that for inclined arrangement of explosive welding use of high detonation velocity explosive and low set-up angle is preferable, as less amount of explosive would be required.

It is evident from Fig. 5.14-a that explosive required to weld steel is more than the explosive required to weld copper. Optimum explosive loading is plotted against explosive welding number E_W in Fig. 5.14-b. It is seen that the explosive requirement is lower for materials having lower explosive welding number. It is concluded that, the plate having lower explosive welding number be made flyer plate if possible, to keep the explosive requirement low.

5.11 MINIMUM AND MAXIMUM PLATE VELOCITY

The minimum plate velocity V_P is obtained on the basis that contact pressure should exceed the dynamic yield strength of the material [148] such that

$$V_{P_{min}} = \sqrt{\frac{\sigma_{ts}}{f}} \qquad (5.38)$$

where σ_{ts} is the ultimate tensile strength and f is the density of the plate.

Higher plate velocity is known to cause spalling of plates, excessive melting at the interface and formation of harmful intermetallic compounds making the joint weaker.

Expression for $V_{P_{max}}$ (equation (1.8)) can be written as [148]

$$V_{P_{max}} = \frac{\sqrt{k_2}}{t_1^{1/8}} \beta^{0.5} \qquad (5.39)$$

where k_2 is a material constant and t_1 is the flyer plate thickness.

For many metals usually used in explosive welding, $V_{P_{min}} \approx$ 200 m/s is generally taken. $V_{P_{max}}$ depends on metal properties, thickness of the flyer plate and obliquity angle. However, a plate velocity less than 800 m/s is

usually used in explosive welding. Thus the plate velocity in explosive welding is such that 200 m/s $< V_P <$ 800 m/s.

5.12 WELDABILITY WINDOW

It is evident from the previous discussion that explosive welding is possible only within a limited range of welding parameters. The region within which welding is possible is usually termed as 'Weldability Window' or 'Explosive Welding Window.

It is known from the results of various workers and from present analysis that, the following conditions need be satisfied to achieve welding.

1 - Collision velocity V_C should be less than sonic velocity V_S in the plate material.

2 - Impact angle β should exceed a limiting value β_L below which a jetless configuration exists.

3 - Impact angle β should be less than β_E above which re-entrant jet vanishes.

4 - Plate velocity V_P should exceed a certain value to ensure minimum contact pressure.

5 - Plate velocity V_P should be below a certain value to avoid the formation of intermetallic compounds and melting at the interface.

In explosive welding the flyer plate collides with the parent plate with a velocity V_P at an inclination β.

Hence, a plot of β versus V_p is possibly of more importance.

For copper, a theoretical weldability window is shown in the graph of β versus V_p (Fig. 5.15) within which welding is possible. Permissible value of obliquity angle β is such that $\beta_L < \beta < \beta_E$. Equation (5.20) is used to plot β_E versus V_p and Eq. (5.30) is used to plot β_L versus V_p (Fig. 5.15). Theoretical transition line (equation (5.28)) corresponding to wave-no-wave boundary is also shown. The weldability window is divided into two regions by the transition line. The region above the line pertains to welding with straight interface and the region below the line corresponds to welding with wavy interface. For minimum and maximum values of plate velocity equations (5.38) and (5.39) may be used. However for simplicity, $V_{P_{min}} = 200$ m/s and $V_{P_{max}} = 800$ m/s are taken. Meyer's [91] experimental plot is also shown in Fig. 5.15. Wave-no-wave boundary for Meyer's experimental results is taken from reference [129]. Experimental plot of β versus V_C as reported by Crossland [80] is suitably re-plotted in Fig.5.15. using $V_C = V_p/\beta$. The theoretical weldability window is found to be in broad agreement with the experimental results.

Weldability window for other materials can be drawn also in a similar way using the above approach.

5.13 CONCLUSIONS

1. In explosive welding, there is a limited extent of fluid zone within which fluidlike behaviour occurs. Above an obliquity angle β_F, there would be no fluid zone.

2. There is some energy loss in collision of plates in explosive welding. The energy loss consideration suggests that there is a reduction in jet velocity after collision. The consideration of energy loss also explains the experimental variation of mass of the re-entrant jet with obliquity angle and plate velocity.

3. For welding to take place, re-entrant jet is necessary and hence the obliquity angle β should be such that $\beta_L < \beta < \beta_E$.

4. Wave-no-wave condition corresponding to a critical Reynolds number represent boundary of wavy interface and straight bond. A wavy interface is formed if $\beta_L < \beta < \beta_W$ and a straight interface is formed if $\beta_W < \beta < \beta_E$.

5. With lower detonation velocity explosive (say $V_D \approx 3000$ m/sec), use of parallel arrangement is recommended whereas for high detonation velocity explosive use of inclined arrangement may be preferred. In general, except for large

plate cladding, inclined arrangement with low set-up angle (say $\alpha = 5^{o}$) may be preferable as compared to parallel arrangement.

6. Besides set-up angle and explosive loading, specific pressure p_s and explosive welding number E_W are important parameters governing welding. In asymmetric situation of explosive welding, the plate with low explosive welding number should be kept as flyer plate.

7. Theoretical weldability window for explosive welding for a material can be constructed which provides permissible range of parameters for explosive welding. Thus suitable values of explosive loading and set- up angle can be selected so as to keep the obliquity angle β and plate velocity V_p within the permissible region.

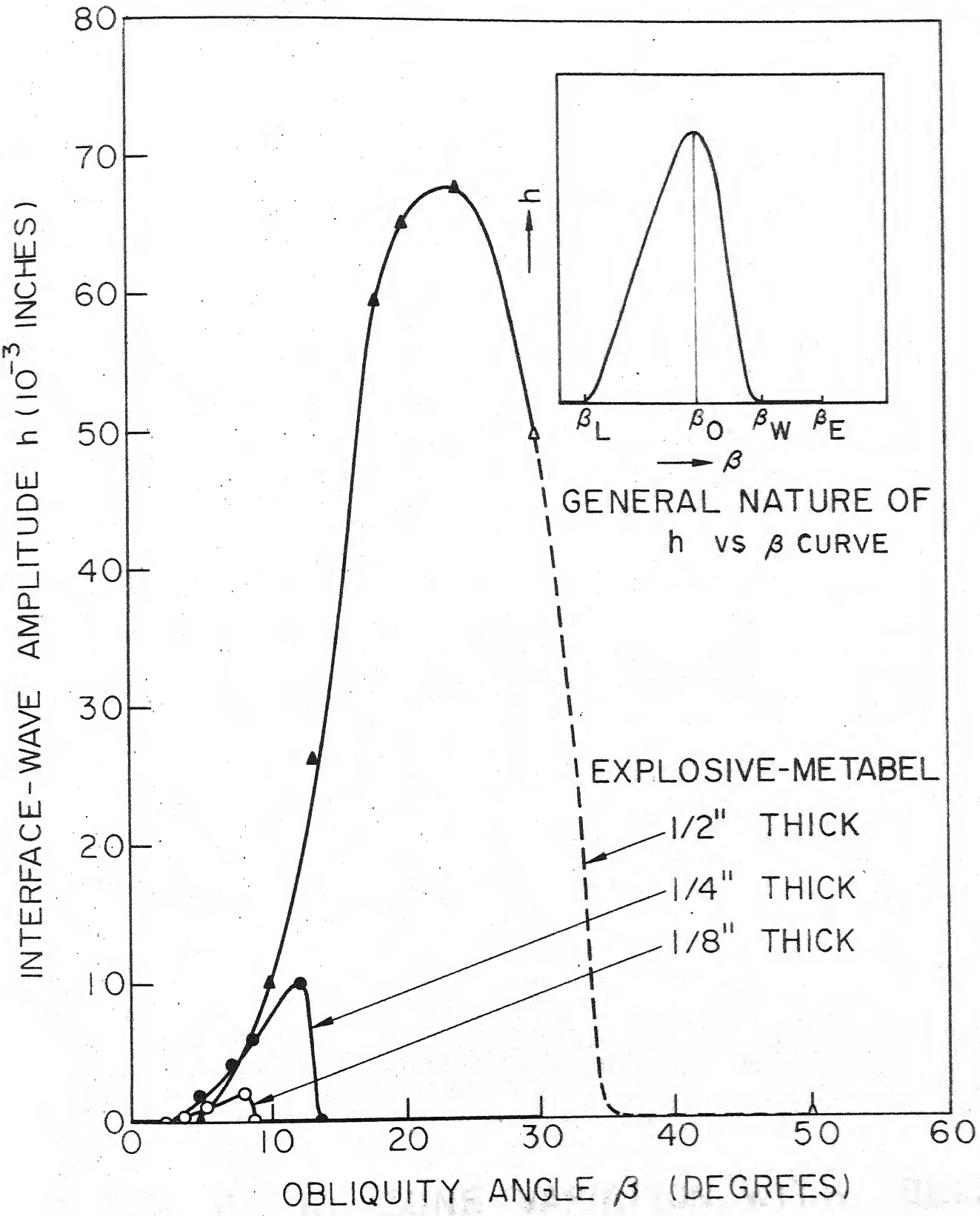

FIG.5.1 VARIATION OF WAVE AMPLITUDE WITH OBLIQUITY ANGLE FOR DIFFERENT EXPLOSIVE LOADING (BAHRANI AND CROSSLAND [94])

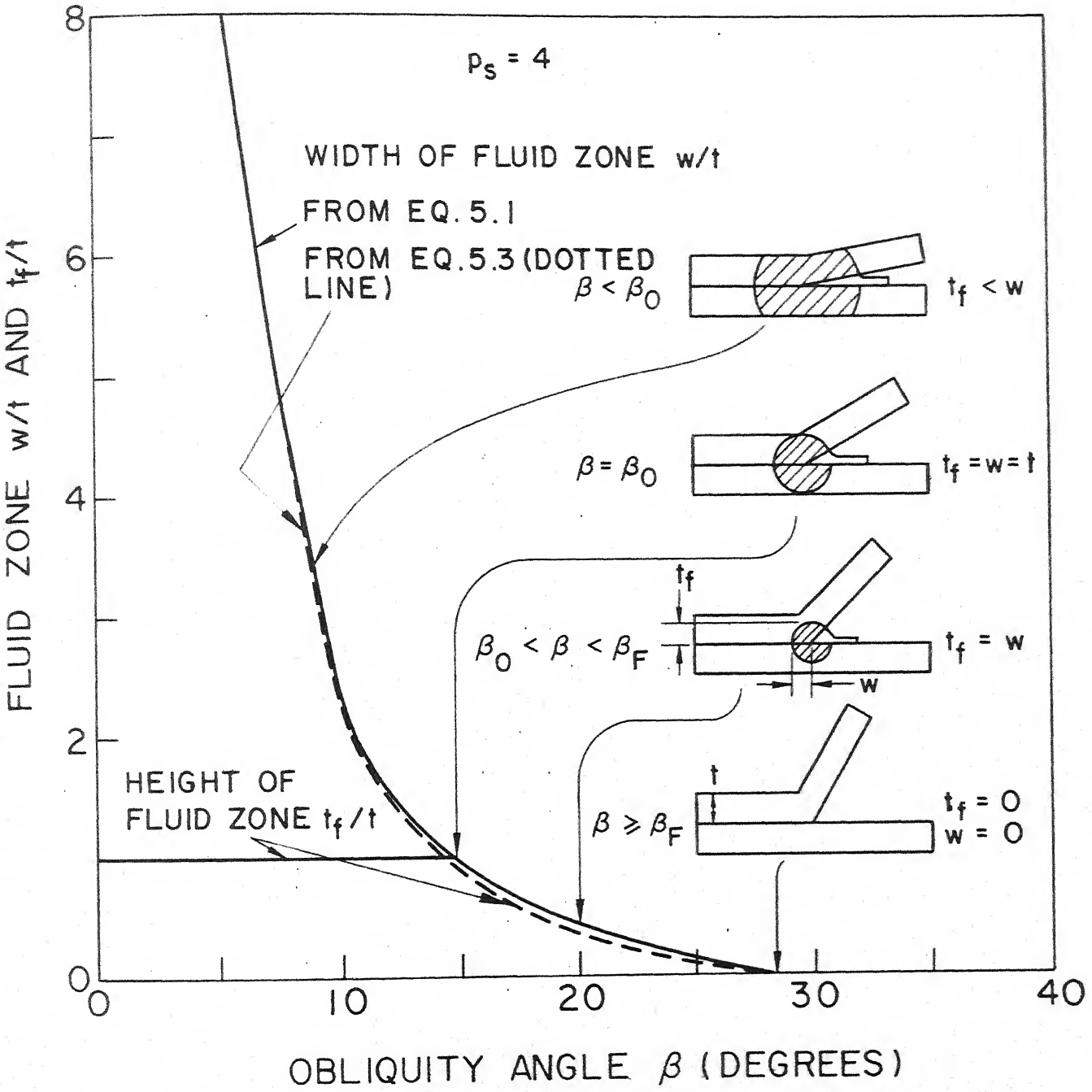

FIG. 5.2 FLUID ZONE VARIATION WITH OBLIQUITY ANGLE

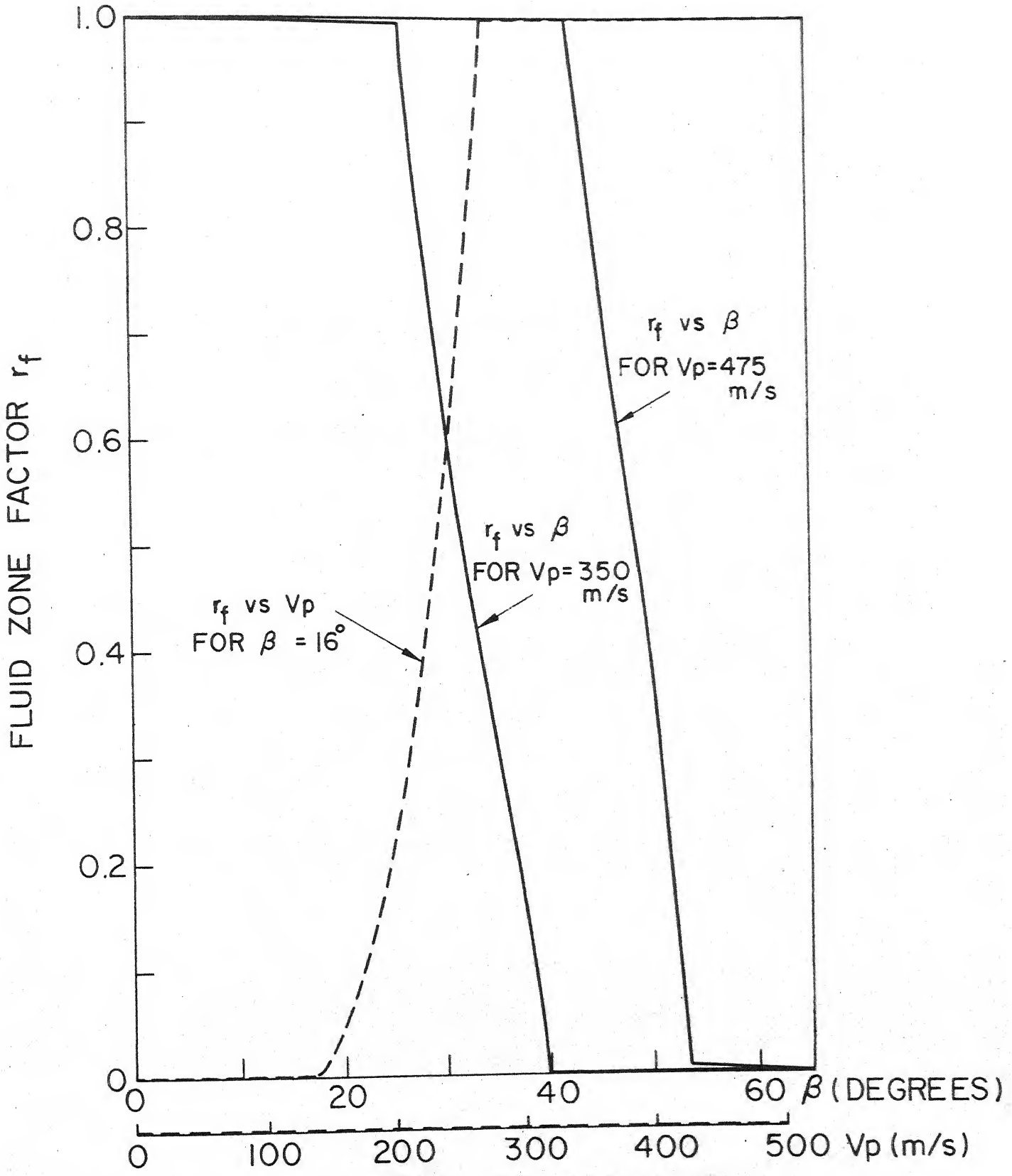

FIG. 5.3 VARIATION OF FLUID ZONE FACTOR WITH OBLIQUITY ANGLE AND PLATE VELOCITY

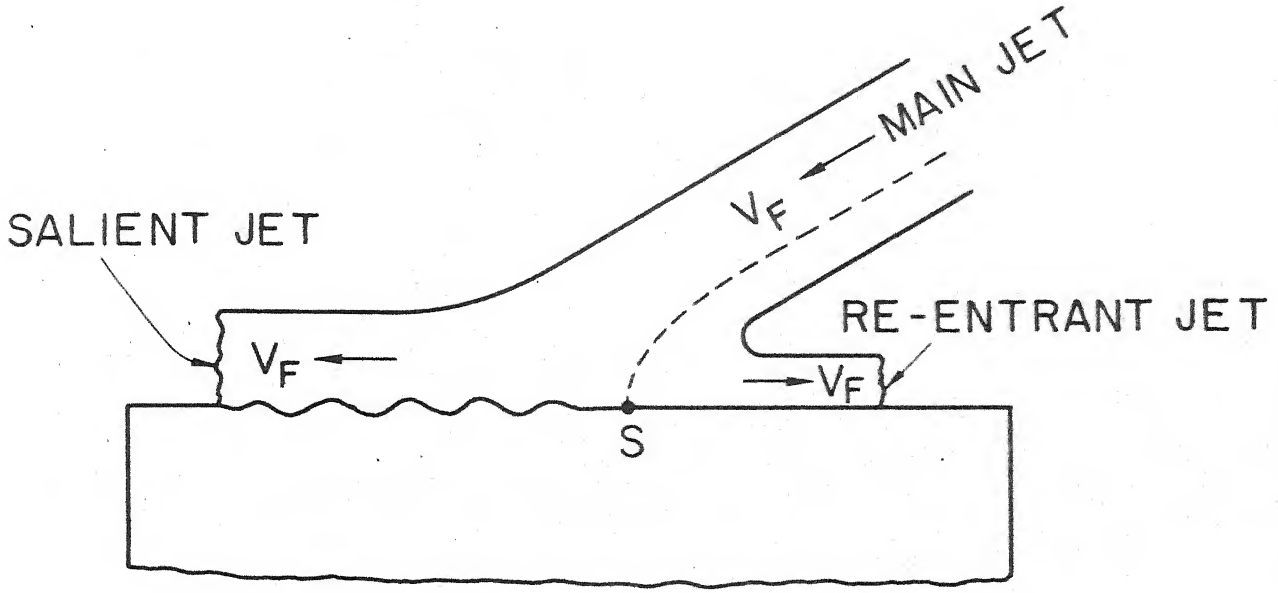

(a) WITH NO ENERGY LOSS

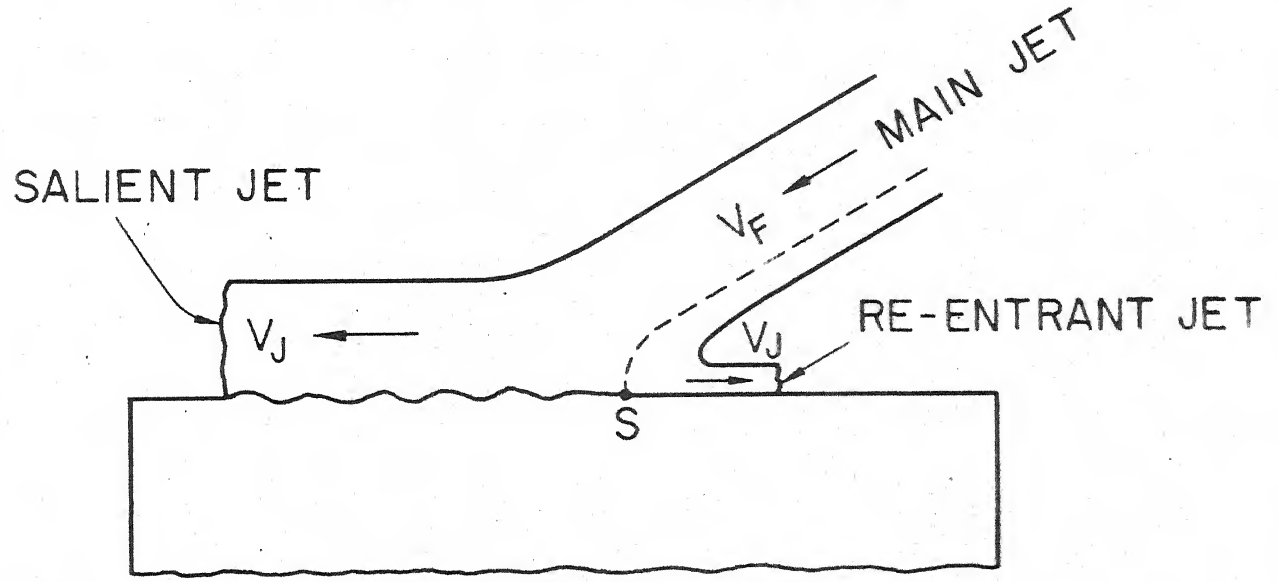

(b) WITH ENERGY LOSS
$V_J < V_F$

FIG. 5.4 DIVISON OF MAIN JET

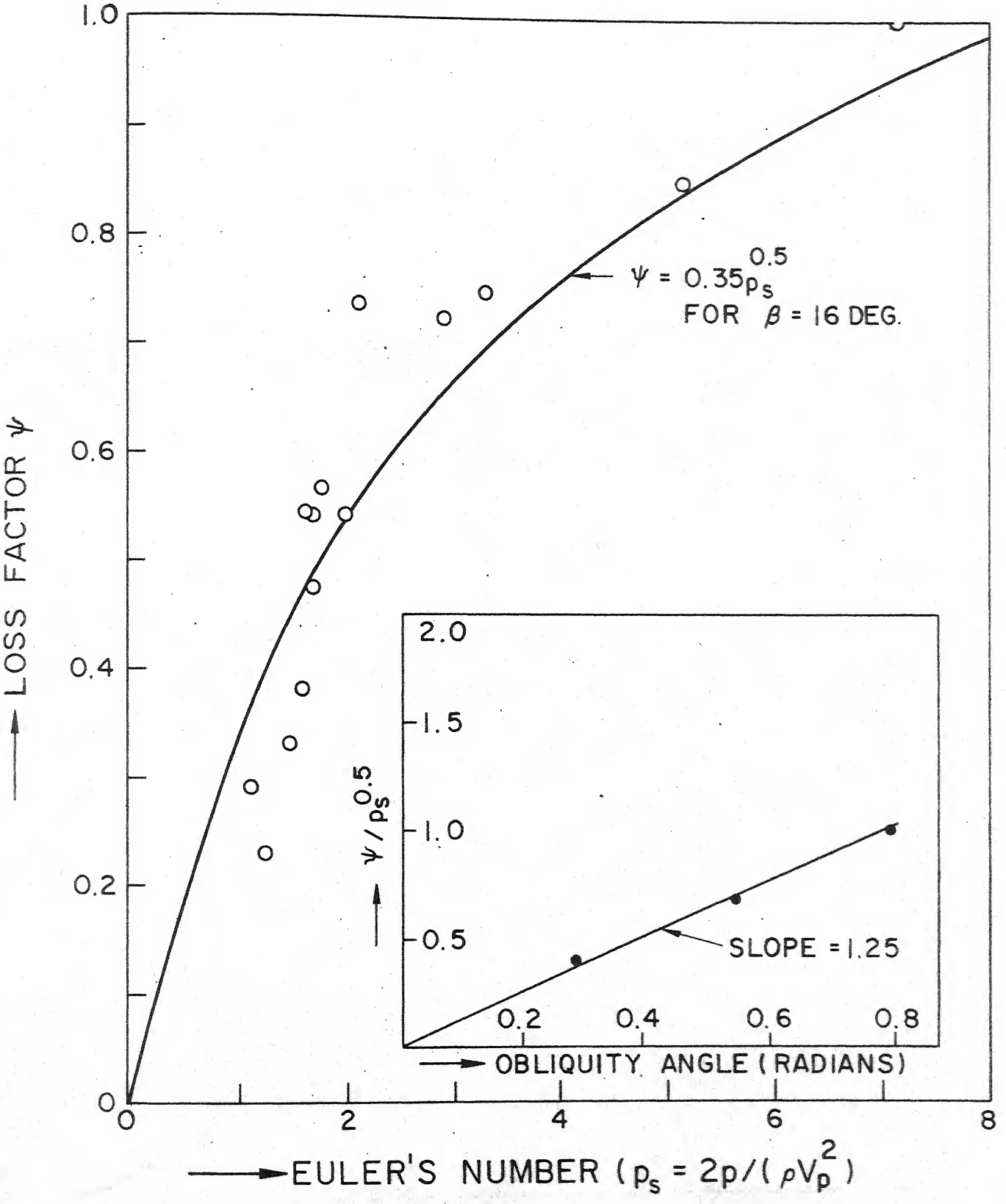

FIG. 5.5 DEPENDENCE OF LOSS FACTOR ON EULER'S NUMBER AND OBLIQUITY ANGLE

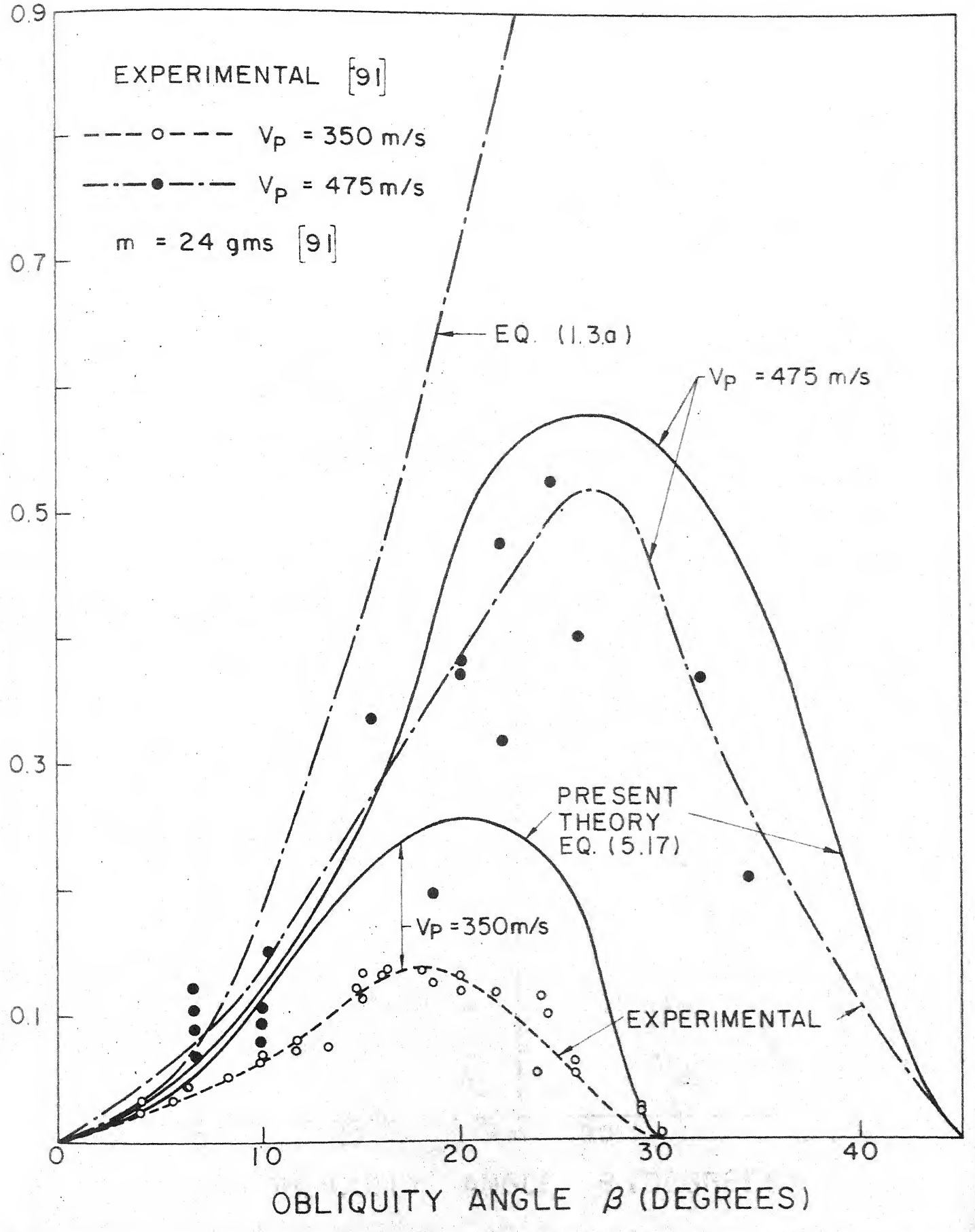

FIG.5.6 VARIATION OF THE MASS OF THE RE-ENTRANT JET WITH OBLIQUITY ANGLE

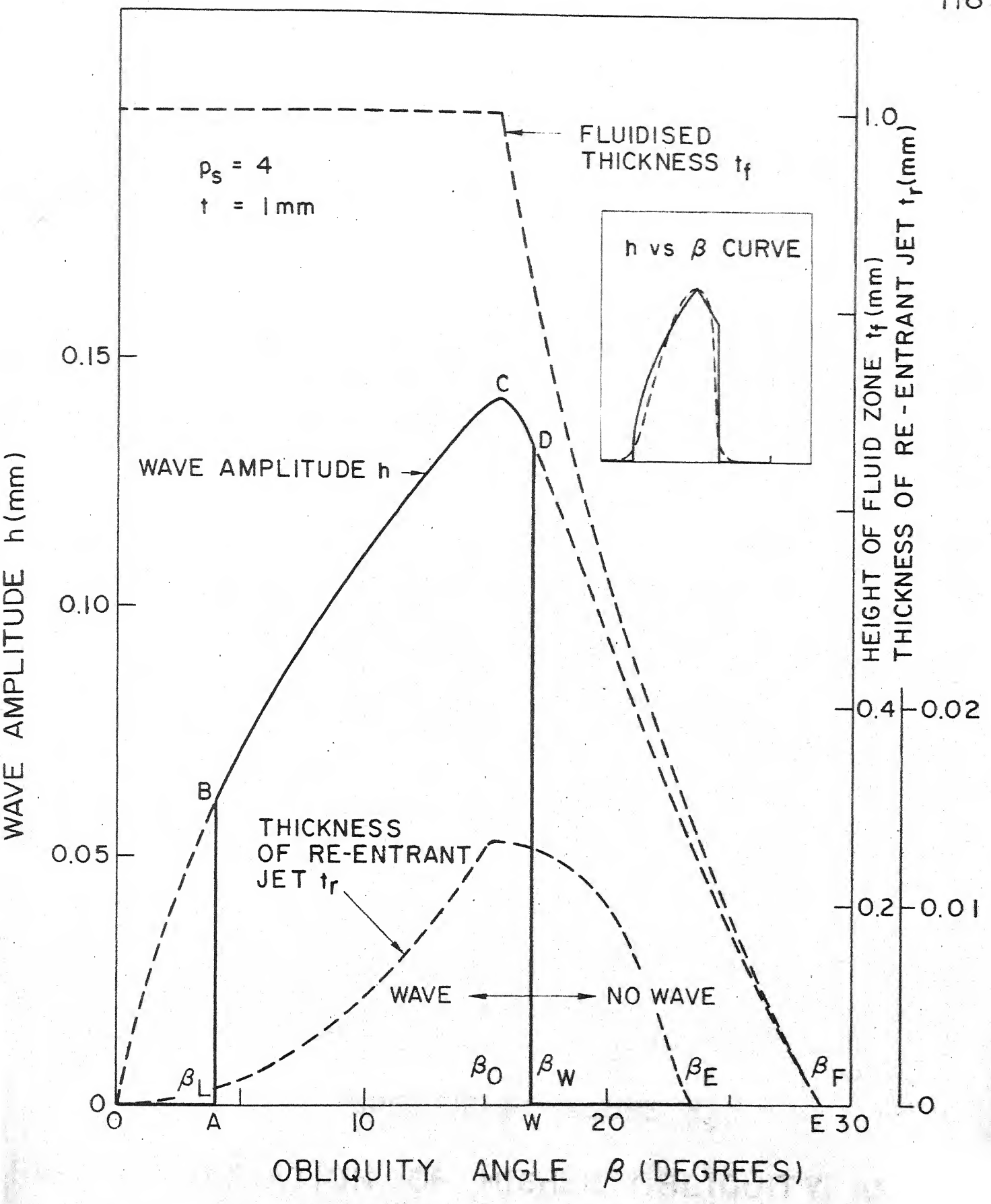

FIG. 5.7 VARIATION OF WAVE AMPLITUDE WITH OBLIQUITY ANGLE

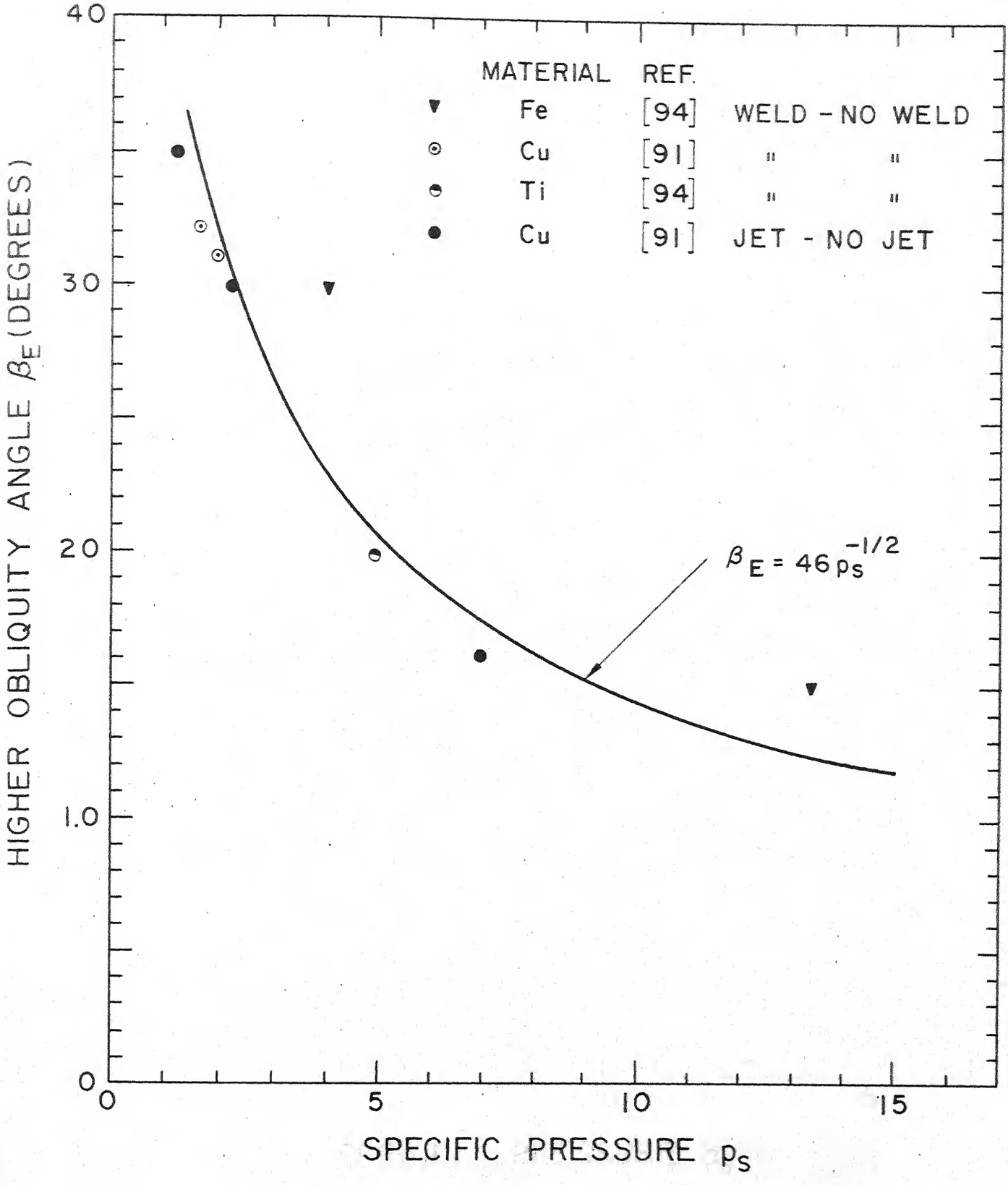

FIG. 5.8 VARIATION OF HIGHER OBLIQUITY ANGLE β_E WITH SPECIFIC PRESSURE

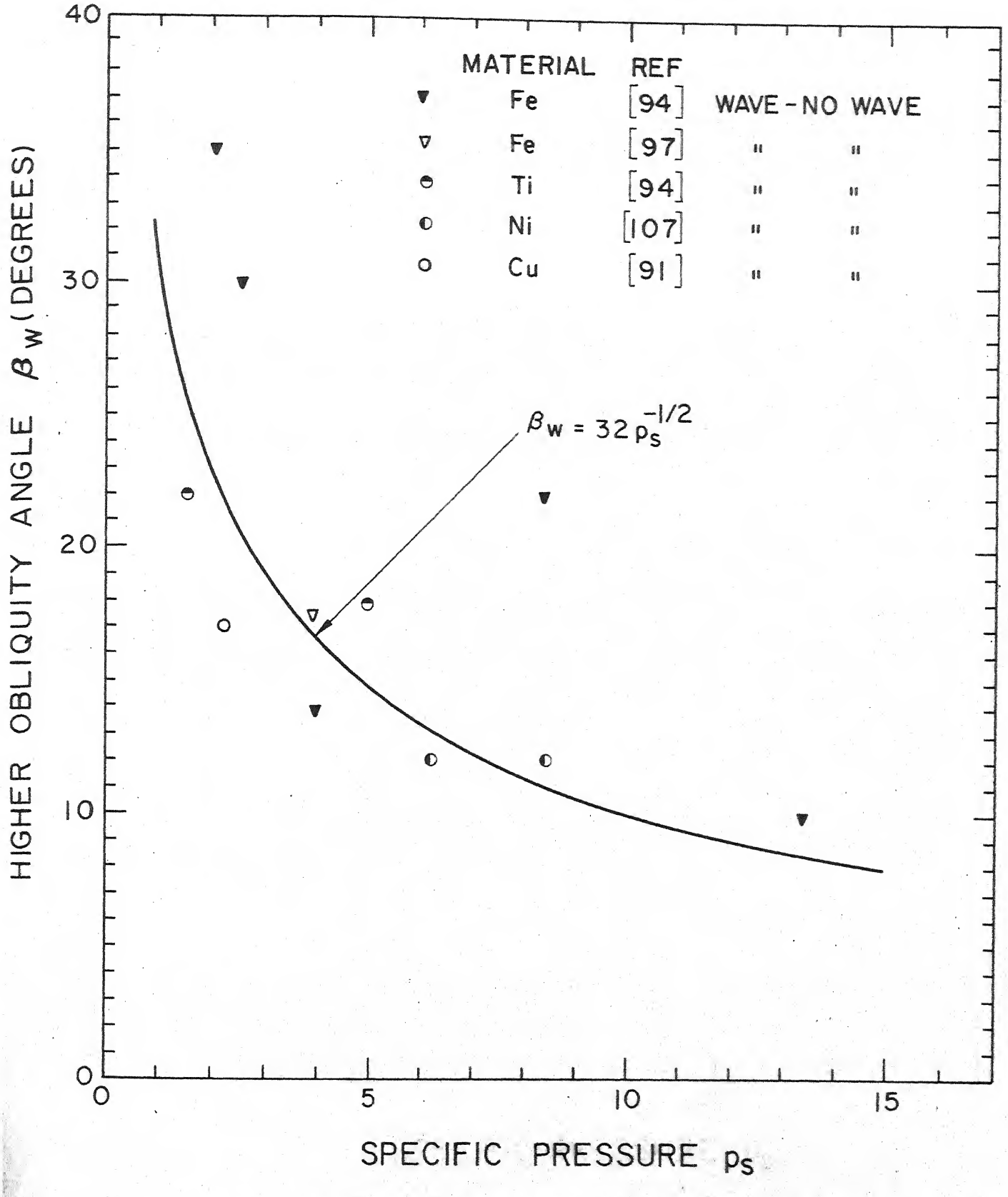

FIG. 5.9 VARIATION OF CRITICAL OBLIQUITY ANGLE β_w WITH SPECIFIC PRESSURE p_s

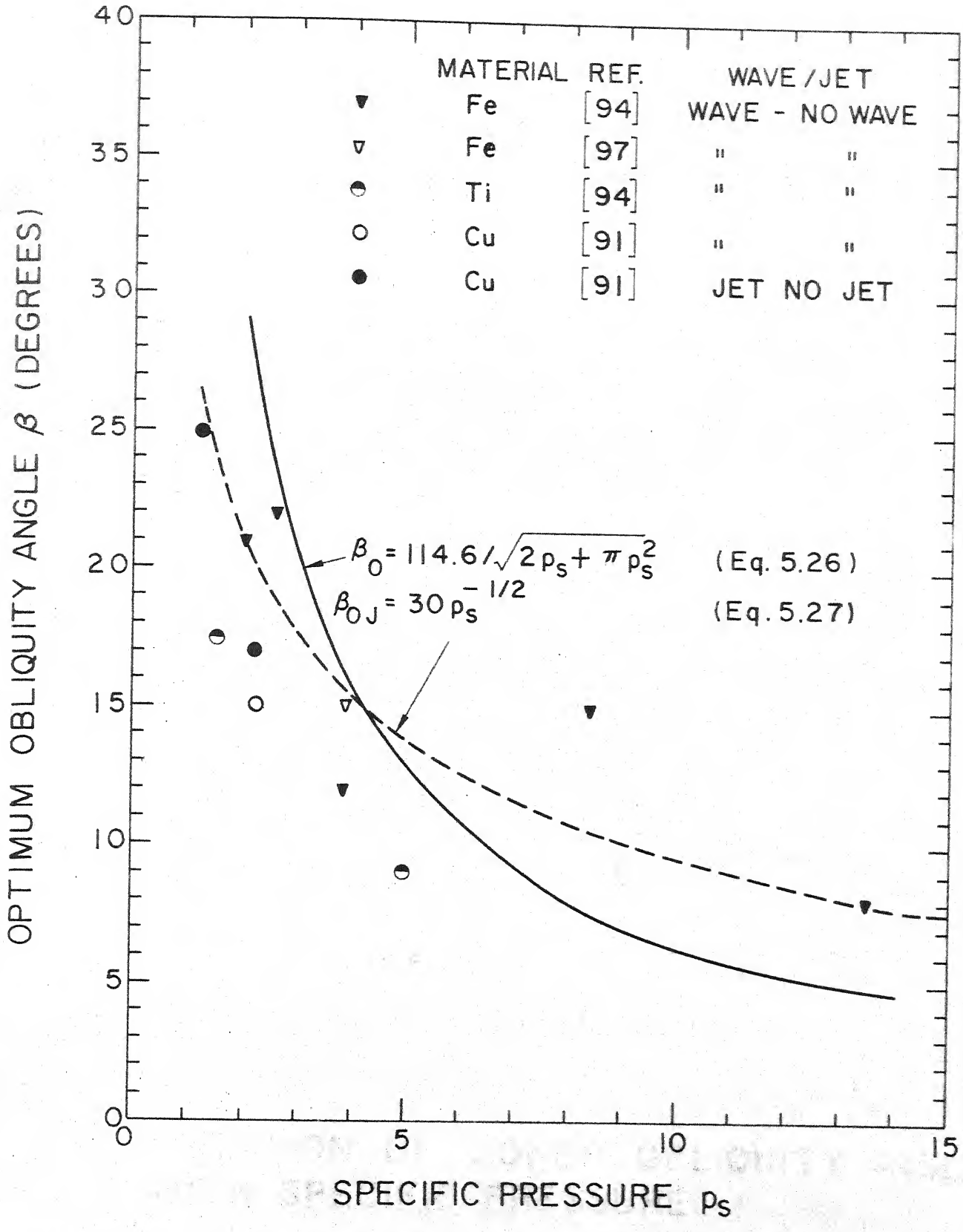

FIG. 5.10 VARIATION OF OPTIMUM OBLIQUITY ANGLE WITH SPECIFIC PRESSURE

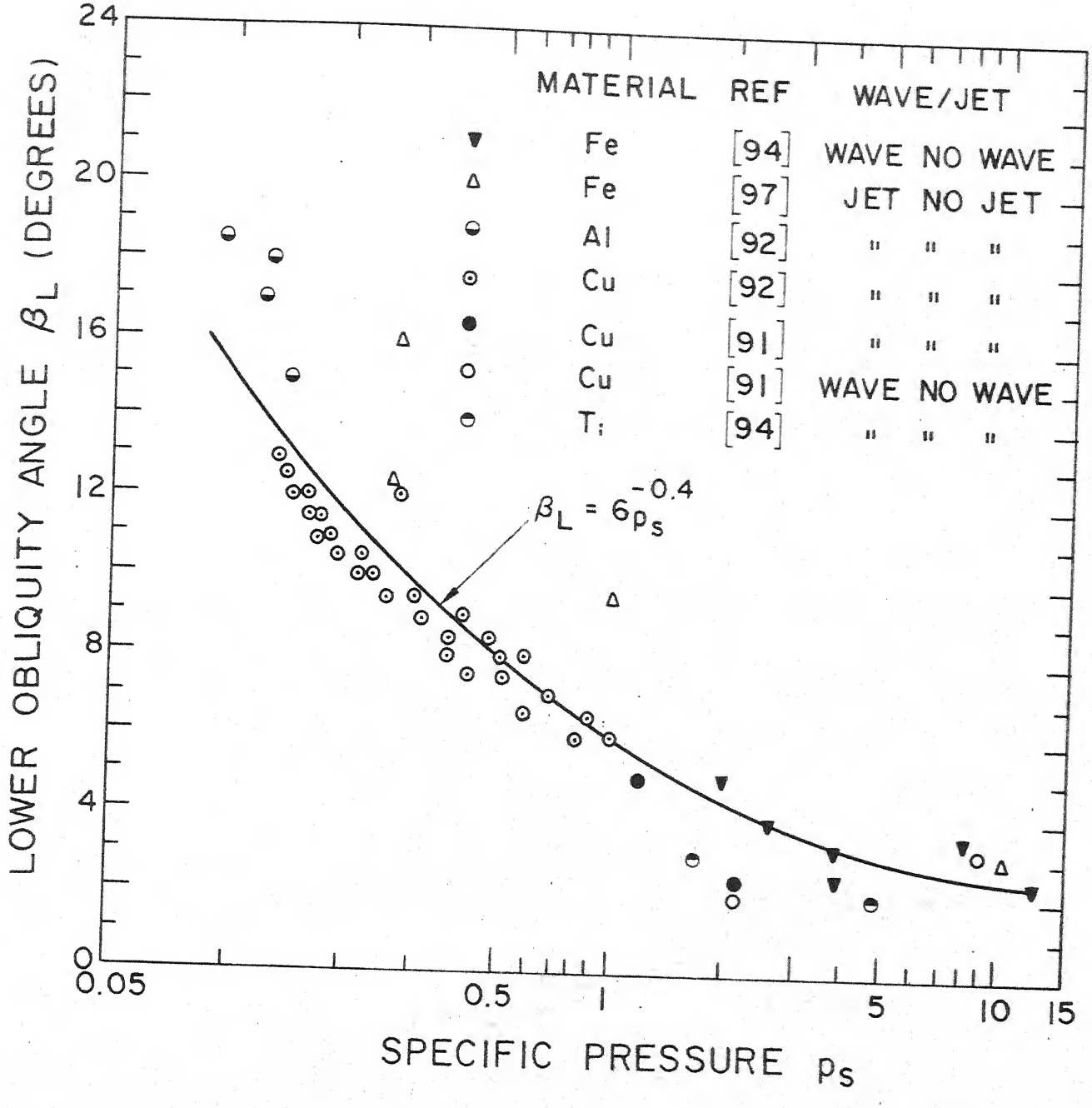

FIG. 5.11 VARIATION OF LOWER OBLIQUITY ANGLE WITH SPECIFIC PRESSURE

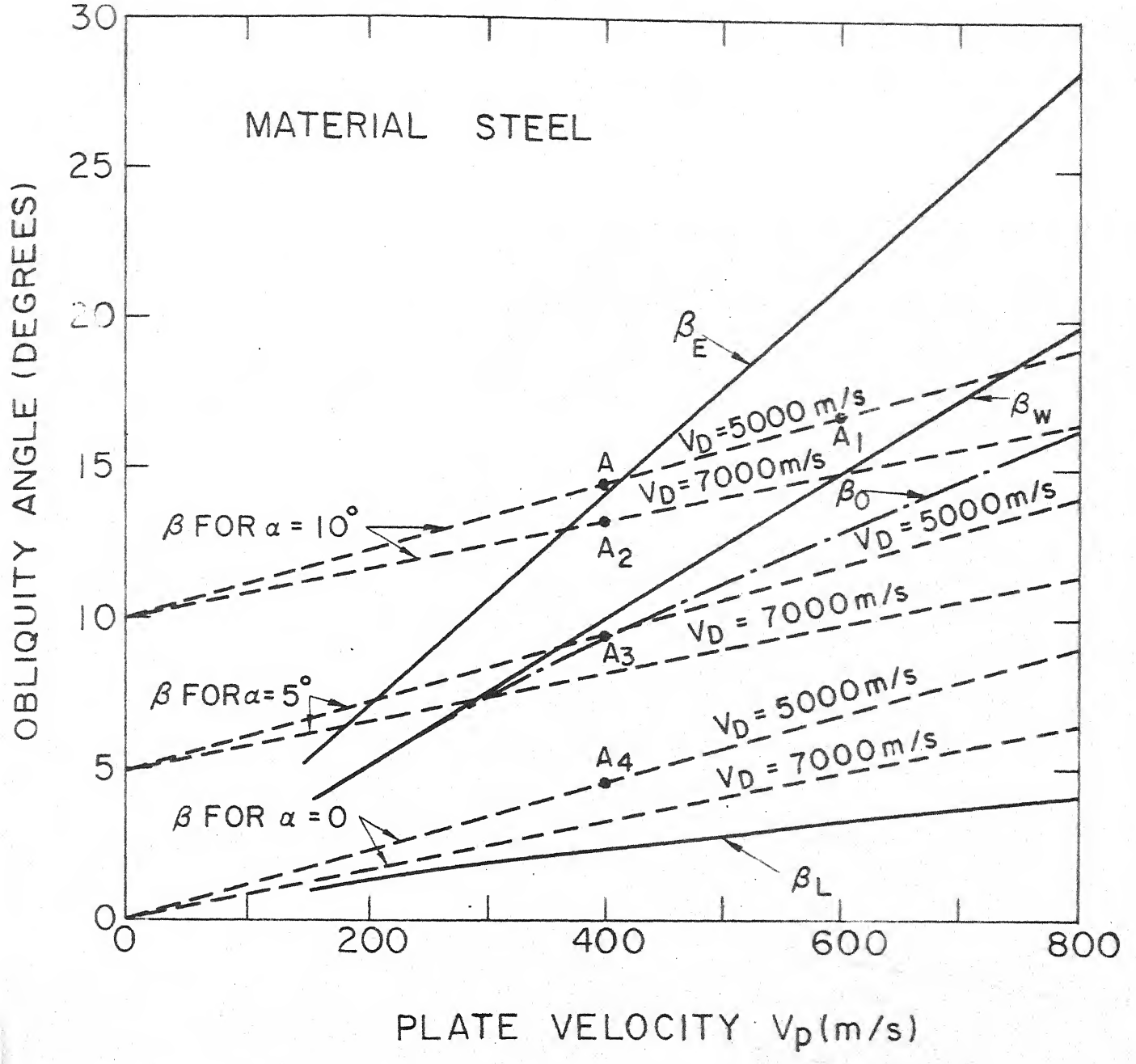

FIG. 5.13 VARIATION OF PERMISSIBLE RANGE OF OBLIQUITY ANGLE AND GENERATED OBLIQUITY ANGLE WITH PLATE VELOCITY FOR STEEL

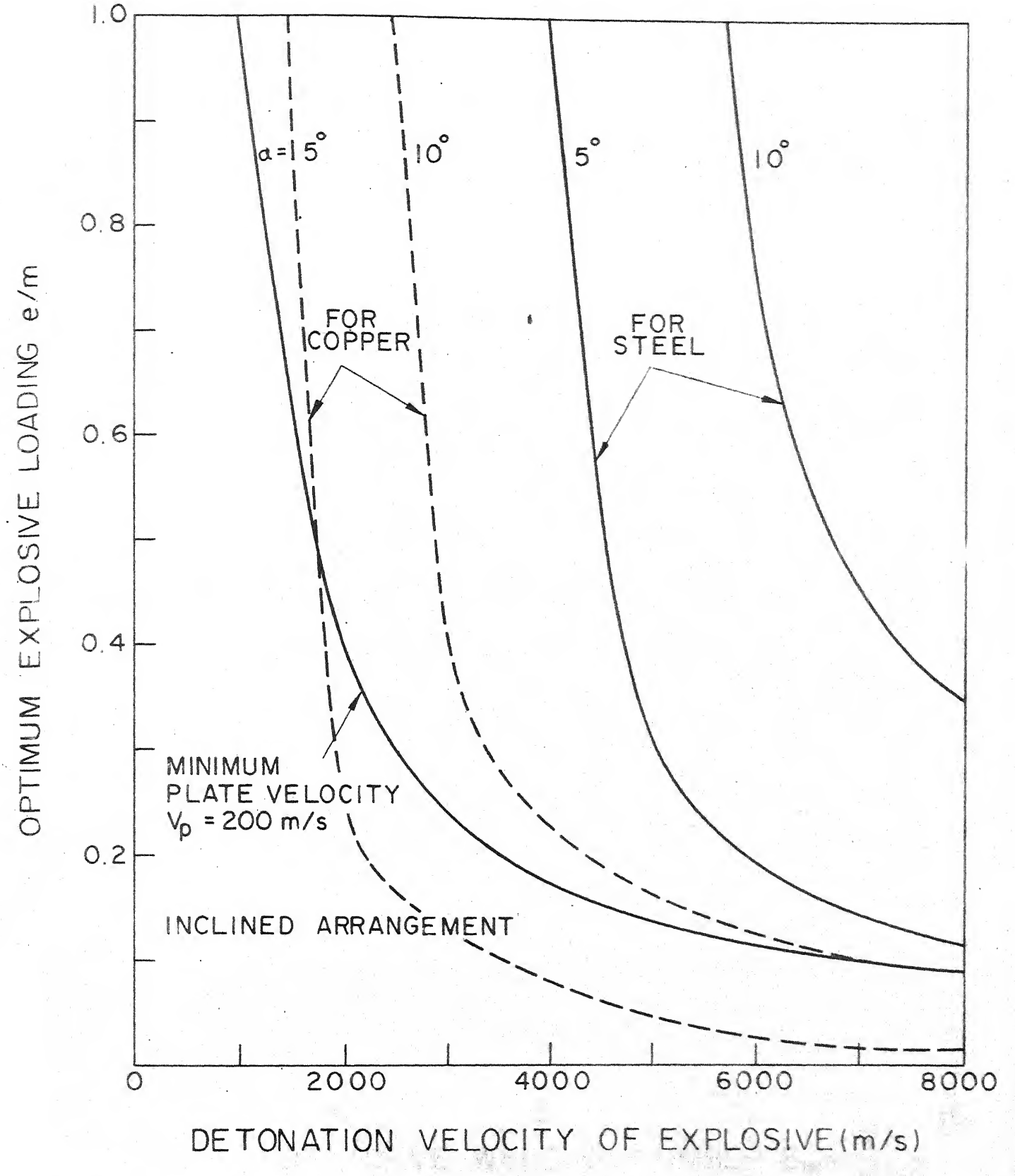

FIG. 5.14 (a) VARIATION OF OPTIMUM EXPLOSIVE LOADING WITH DETONATION VELOCITY

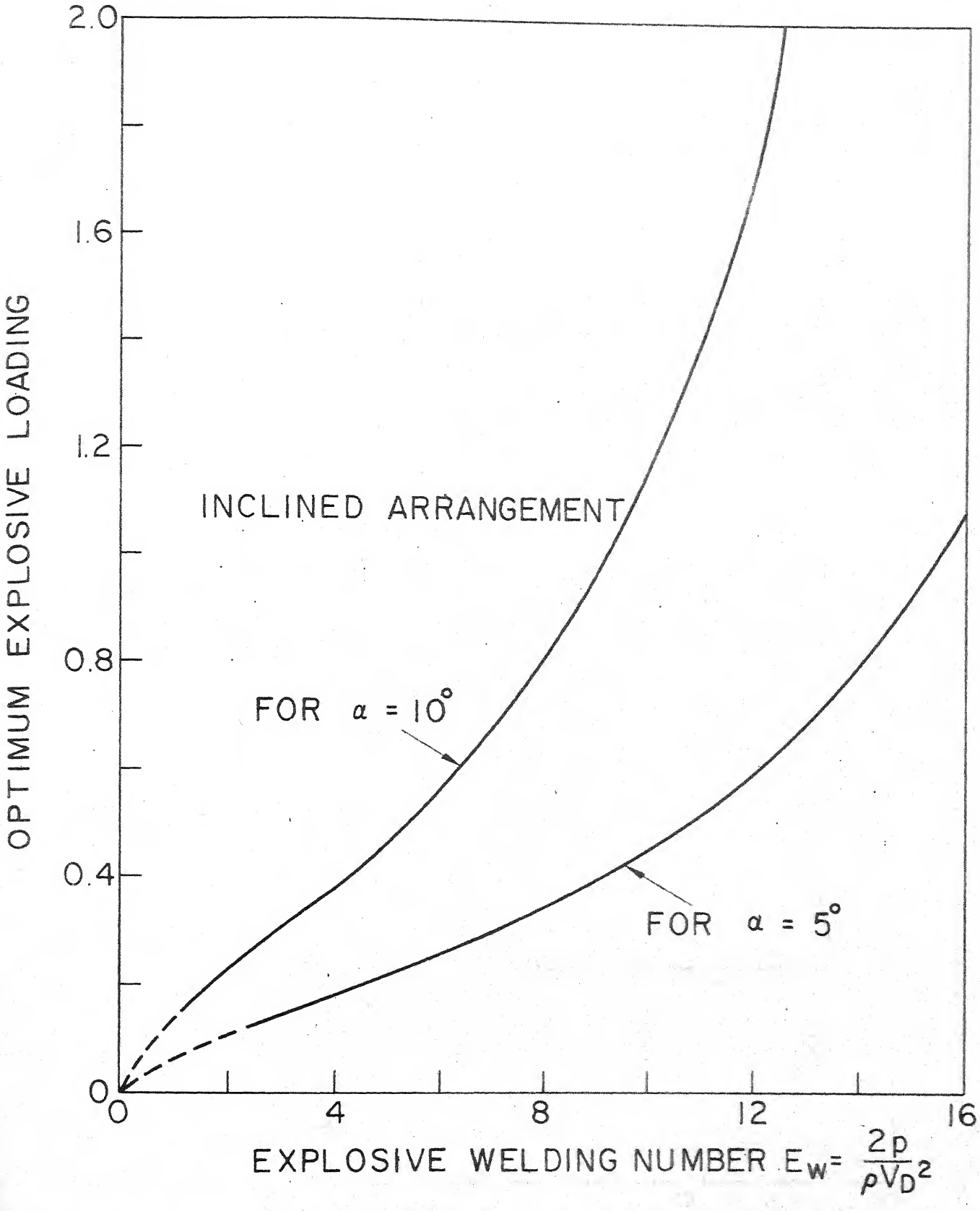

FIG. 5.14(b) VARIATION OF OPTIMUM EXPLOSIVE LOADING WITH EXPLOSIVE WELDING NUMBER

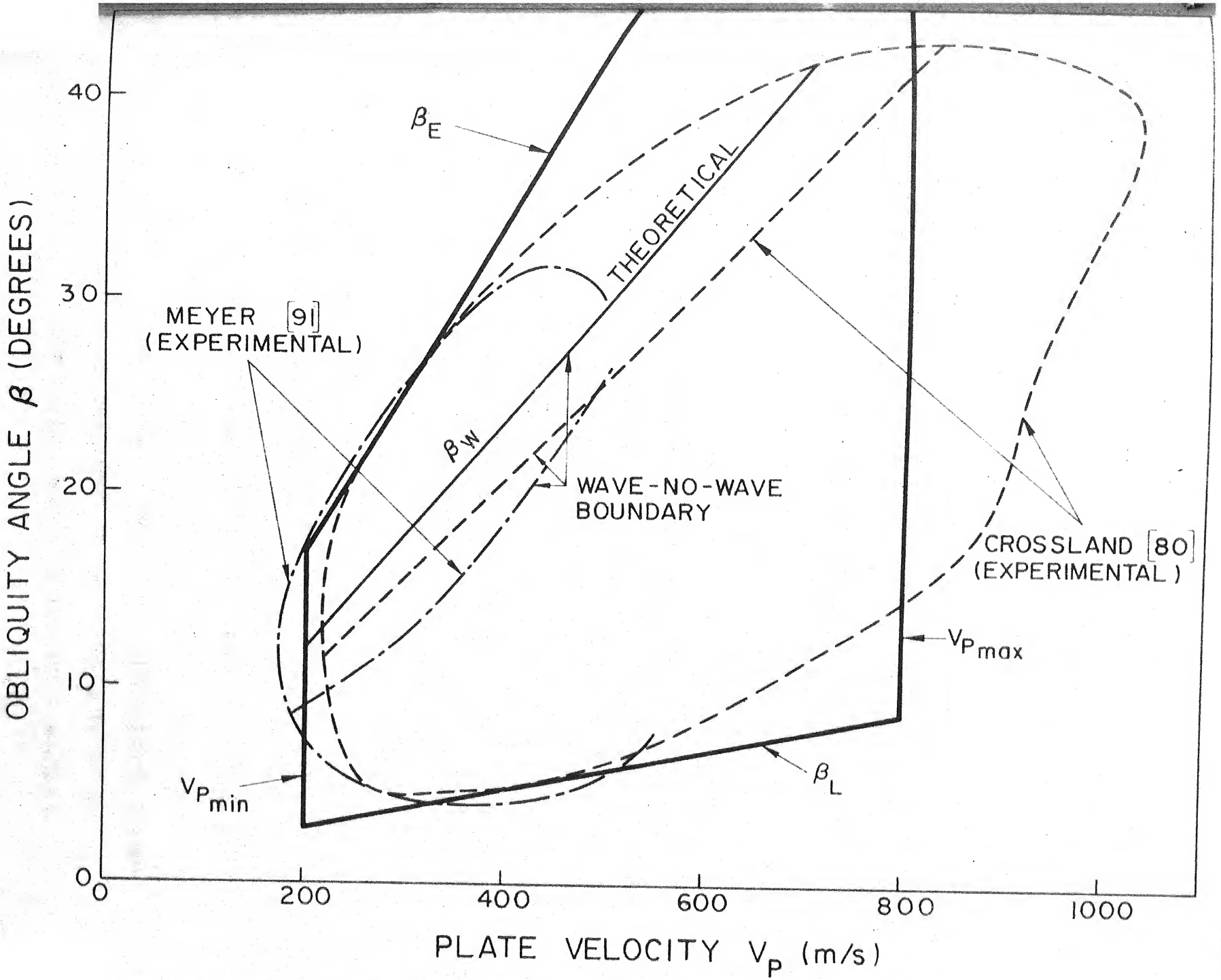

FIG. 5.15 WELDABILITY WINDOW FOR COPPER

CHAPTER VI

EXPERIMENTAL INVESTIGATIONS

6.1 INTRODUCTION

Various research workers have carried out fluid-analogue experiments which show that interface wave generation in collision of two fluid streams is analogous to the generation of weld-interface-wave in explosive welding. The phenomenon of interface wave formation is studied by interposing an obstacle between two fluid streams meeting at an angle, representing the hydrodynamic model of explosive welding.

To demonstrate the utility of the weldability window and selection procedure for explosive welding outlined in the previous chapter, explosive cladding, variable angle experiment and tube to tube-plate welding of various metal combinations is carried out.

6.2 FLUID ANALOGUE EXPERIMENT

Abrahmson [96] carried out experiment on collision of putty and suggested a mechanism of interface wave formation in explosive welding. Cowan et al. [107] investigated interface wave formation by collision of two fluid jets as an analogue to collision of two plates in explosive welding.

Wilson and Brunton [95] carried out experiments by pushing through a cylinder a fluid stream onto another fluid and noticed interface waves. Sobky and Blazynski [122-123] designed a fluid analogue experiment in which two fluid layers are separated at a distance apart. The bottom of the upper container was removed at a certain speed making the top fluid to fall over the bottom fluid. The observed interface wave was found to be similar to the waves formed in explosive welding.

A vortex shedding analogy is usually considered to explain interface wave formation in explosive welding. The vortex shedding experiments is generally carried out by placing a circular obstacle in a fluid stream. The fluid meets the whole circumference of the obstacle. However, in explosive welding, only a portion of the imaginary obstacle is in contact with the fluid (for symmetric situation, fluid contact angle is $180 - 2\beta$). Furthermore, in explosive welding, the top and bottom fluid jets may be of different densities. Fluid analogue experiments have not been carried out for two different fluids. Thorpe [181], however, has studied experimentally the interface wave between two immiscible liquids as a fluid mechanics problem.

An experimental set-up incorporating the following features is designed and fabricated.

1. The two fluids are allowed to meet at an angle over a rounded obstacle.
2. Fluids of different densities can be used in the two channels.

Figure 6.1 shows a sketch of the perspex model. The two streams I and II are considered as salient jets flowing at an inclination $2\beta = 20^{\circ}$ over an obstacle of radius of 0.75 cm. The remaining portion of perspex model serves as inlet and outlet for the fluid flow. The height and velocity of flow are controlled by operating the inlet tap and outlet weir height. Velocity of the flow is calculated from measurement of the time taken for a particle to travel a known distance. For flow visualization, solution of potassium permanganate is injected at certain points in the flow.

6.2.1 Flow of Two Similar Fluids

The two streams of water are allowed to flow in the channels at an inclination. The velocity of the streams is gradually increased by increasing the inlet flow rate. The pattern of wake behind the obstacle changes with velocity. Initially, for very low velocity of the order of $V_F = 1$ cm/sec, vortices are not formed. At a higher velocity say $V_F = 2$ cm/sec, vortices appear and remain attached to the obstacle producing a straight interface. With further increase in velocity ($V_F \approx 3$ cm/sec) the vortices start shedding

alternatively and approximately sinusoidal interface wave is observed. A further increase causes the turbulence in the wake. Figure 6.2-a shows a photograph of the vortices, taken at an angle of 60° from other side of the set up, for V_F = 3 cm/sec. The interface wave is also observed, however, it is not evident in the photograph. General nature of the phenomenon as observed from top is represented in Fig. 6.2-b. The situation shown in Fig. 6.2 corresponds to a Reynolds number Re = 450. It is noted that this critical Reynolds number (450) for hydrodynamic analogue experiment is higher than the critical Reynolds number ($\simeq$ 50) for conventional vortex shedding experiment [115]. The critical Reynolds number for explosive welding has been estimated to be approximately equal to 10 by Cowan et al. [107] and 3 by Kowalickand Hay[110].

The difference in Reynolds number may be attributed to the following factors.

(i) The flow configuration in hydrodynamic analogue is different than that of conventional vortex shedding experiment as explained earlier.

(ii) The velocity measurement is taken at the top fluid layer. The dye flows below the top layer at smaller velocity. Therefore it is quite likely that the vortex shedding might be taking place at a Reynolds number $<$ 450 whereas the calculation based upon the top layer velocity gives Re = 450.

(iii) For the case of explosive welding accurate estimate of the viscosity of fluidized metal jet has not been made.

6.2.2 Flow of Two Dissimilar Fluids

For studying the flow of two different fluids, water and mobil-oil are allowed to flow in the channels at an inclination. It was not possible to maintain equal velocities for the two streams. Vortex formation and shedding was not noticed for the case of flow of two dissimilar fluids. However, it is expected that vortex shedding may take place at certain condition. A further work is needed in this direction.

However, the interface wave was observed. Figure 6.3-a shows a photograph (taken at an angle) of the interface wave formation for V_F(water) = 5 cm/sec and V_F(mobiloil) = 1 cm/sec. General nature of the interface wave formation as observed from top is represented in Fig. 6.3-b. It is seen that the interface wave is distorted and this is in accordance with the actual observation of distorted weld-interface for the case of dissimilar metal combination.

6.3 EXPLOSIVE WELDING EXPERIMENTS

In the previous chapter, selection procedure for explosive welding is outlined. In the present section the utility of the procedure is demonstrated by selecting the

explosive loading e/m and set up angle α such that the obliquity angle β and plate velocity V_p lie within the permissible range.

Following categories of experiments are done

1. Plate cladding
2. Variable obliquity angle experiments
3. Tube to tube-plate welding
4. Half length explosive experiments

Three types of explosives are used namely Nitroglecerene, Cordtex and PEK-I. The properties of these explosives are listed in Table 6.1. Although the detonation velocity of explosives vary with thickness and density of explosive, however, in the present investigation the average values of V_D listed in the table are used. RIHNO exploder with I.C.I. No. 6 electric detonator is used.

Various types of explosives used in the experiments are shown in Fig. 6.4. Details about the packs are given in Table 6.2.

Various metal combinations of copper, stainless steel, mild steel, aluminium and brass are used for explosive welding experiments. No special preparation was done for cleaning of plates. However, the plates were cleaned by 'sanifresh' and emery paper. Cork-sheet, rubber sheet, polythene sheet/tube are used as buffer plate as required.

TABLE 6.1

Properties of Explosive Used

Type of Explosive	Formula	Form	Calorific Value	Density	Detonation Velocity
Nitroglecerene (NG)	$C_3H_5N_3O_9$	Granular	1486 Cal/g	1.4 g/cm^3	2500 m/s
Cordtex (PETN base)	$C_5H_8H_{12}O_4$	Cord	1385 Cal/g	0.103 g/cm*	6500 m/s
PEK-I (Tetryl base)	$C_7H_5N_5O_8$	Gelatine	1120 Cal/g	1.7 g/cm^3	6500 m/s

* amount of explosive/cm.

TABLE 6.2

Preparation of Explosive Packs

Experiment	Explosive	Preparation of Explosive Pack		Remarks
		Step 1	Step 2	
Plate Cladding (Also for Half-length experiment and variable angle experiment)	Cordtex	Cut it to pieces of required length	Pack in miler sheet packet and tape it using a cover miler sheet	One or more layer may be used depending upon requirement
"	NG	Change it to granular form and dry	"	Ram the explosive properly
"	PEK-I	Roll it and cut to required size	"	-
Tube to tube-plate welding	Cordtex	Cut it to pieces of required length	Pack it in a polythene buffer tube. Close the ends with wooden or wax pieces with a hole to insert the detonator	-
"	NG	Make it granular	"	Ram the explosive properly
"	PEK-I	Roll it in cylindrical shape	"	-

6.3.1 Plate Cladding

The set up used for asymmetric welding is shown in Fig. 6.5-a where flyer plate is hung with the help of strings at both the ends. Suitable stand off distance and/or inclination angle is maintained by adjusting screws. The parent plate is kept on the base anvil. Two other arrangements, viz. (i) handing of flyer plate by four strings attached to four corner holes of the flyer plate and (ii) clamping flyer and parent plate at one end, were also tried. However, the above method (Fig. 6.5-a) is found to be most convenient.

An open site is selected at I.I.T. Kanpur campus and experiments are done there. Photograph of the explosion at site is shown in Fig. 6.5-b.

The parameters for the explosive welding are selected as per the following procedure such that the condition corresponding to β and V_P falls within the range (β versus V_P plot given in chapter V).

1. Explosive loading e/m is chosen so as to give a plate velocity $V_P = 0.612\, V_D\, (e/m)/(2 + (e/m))$ in the range 200 m/s $\leq V_P \leq$ 800 m/s.
2. The minimum and maximum permissible obliquity angles (β_L and β_E) are calculated from equations (5.30) and (5.20) (or seen from Figures (5.12) and (5.13)).

TABLE 6.3

Plate Cladding

Sl. No.	Metal Combination	Explosive	α deg.	e/m	V_p	β deg.	Stand off mm
A-1	Stainless steel-Stainless steel	Cordtex	5.0	0.144	267	7.3	1.5
A-2	"	NG	0.0	1.114	547	12.5	3.0
A-3*	"	"	0.0	0.584	346	7.9	2.0
A-4	"	"	0.0	1.000	510	11.7	3.0
A-5	"	Cordtex	4.0	0.204	369	7.3	0.0
A-6	"	"	5.0	0.220	394	8.5	0.0
A-7	"	"	8.5	0.220	394	12.0	0.0
A-8	"	"	0.0	0.142	263	2.3	2.0
A-9	"	"	0.0	0.220	394	3.5	2.0
A-10	"	PEK-I	5.0	0.184	334	8.0	3.0
S-1*	"	Cordtex	6.0	0.110	208	7.8	0.0
S-2*	"	"	6.0	0.110	208	7.8	0.0
A-11**	Copper-Copper	Cordtex	5.0	0.081	137	6.2	3.0
A-12	"	NG	5.0	0.487	300	11.9	3.0
A-13	"	Cordtex	5.0	0.158	291	7.6	3.0
A-14	"	NG	5.0	0.475	294	11.7	0.0
A-15	"	Cordtex	5.0	0.120	227	7.0	0.0
A-16	"	NG	20.0	0.785	431	29.9	0.0
A-17	"	Cordtex	15.0	0.192	349	18.1	7.0

Contd...

Contd. Table 6.3 : Plate Cladding

Sl. No.	Metal Combination	Explosive	α deg.	e/m	V_p	β deg.	Stand off mm
A-18	Copper-Copper	Cordtex	2.0	0.128	240	4.2	5.0
A-19**	"	"	30.0	0.128	240	32.2	5.0
A-20	"	PEK-I	10.0	0.182	331	12.9	5.0
A-21	Stainless steel-Copper	Cordtex	5.0	0.117	220	7.0	0.0
A-22	"	NG	0.0	0.824	447	10.2	4.0
A-23	Stainless steel-Mild steel	Cordtex	5.0	0.128	239	7.1	5.0
A-24	"	"	10.0	0.220	394	13.5	5.0
A-25	Stainless steel-Bronze	"	8.0	0.220	394	11.5	5.0
A-26	Stainless steel-Cast iron	"	6.0	0.220	394	9.5	5.0
A-27	Aluminium-Aluminium	"	4.0	0.150	278	6.5	0.0
S-3	"	"	4.0	0.150	278	6.5	0.0
A-28	Aluminium-Copper	"	4.0	0.150	278	6.5	0.0
A-29	Aluminium-Stainless steel	"	4.5	0.150	278	7.0	0.0
A-30	Brass-Stainless steel	"	5.0	0.155	286	7.5	0.0
A-31	Brass-Brass	"	8.0	0.189	343	11.0	3.0
A-32	Brass-Aluminium	"	10.0	0.189	343	13.0	0.0
A-33	Lead-Lead	"	5.0	0.113	212	6.9	5.0
A-34	Copper-Stainless steel	"	10.0	0.256	452	14.0	7.0
A-35	Copper-Mild steel	"	11.0	0.256	452	15.0	4.0

* Partially welded
A Asymmetric

** Not welded
S Symmetric

3. The dynamic bend angle $\phi = 57.3\ V_P/V_D$.

4. A suitable value of set up angle α is selected so as to give a obliquity angle $\beta = \alpha + \phi$ such that $\beta_L < \beta < \beta_E$.

Details of plate cladding experiments are given in Table 6.3. In general, plates 150 mm long and 50 mm wide are used. The thickness of Copper, Stainless steel, Aluminium, Mild steel, Brass plates are 3 mm, 1.75 mm, 3 mm, 3.25 mm, 1 mm respectively.

The cladded plates are cut all along the periphery to remove material from sides. Then it is cut in several pieces (Fig. 6.6). Pieces (b) and (d) are used to make tensile test specimens and pieces (a) and (c) for shear test specimens (See article 6.4). Central portion (m) is used for microstructural examination.

To study appearance, of the weld interface metallographic examination of the welded pieces is done. The central portion (m) of the welded specimen is polished, suitably etched, and examined under a microscope. Etching reagents used for various metals are mentioned below. For dissimilar metal combination, etching reagent for one of the metal is used.

Microphotographs of some of the specimens are shown in Figs. (6.7) and (6.9).

Metal	Etching Reagent	Composition
Copper	Acqueous Ferric Chloride	Ferric chloride 10 gm, Hydro-chloric acid 30 c.c., Water 120 c.c.
Stainless steel	Marble's reagent	Copper sulphate 4 gms., Hydrochloric acid 20 c.c., Water 20 c.c.
Mild steel	Fry's reagent	Cupric chloride 90 gms., Hydrochloric acid 120 c.c., Water 100 c.c.
Aluminium	Keler's reagent	Water 95 %, Hydrochloric acid 1.5 %, Nitric acid 2.5 %, Hydrofluoric acid 1.0%
Brass	Aqueous Ferric Chloride	Ferric chloride 10 gm, Hydrochloric acid 30 c.c., Water 120 c.c.

It is observed that profile of interface wave approximates a sine wave for similar metal combination (Fig. 6.7) and the wave shape is distorted for dissimilar metal combinations (Fig. 6.8). Vortices are noticed ahead of the wave crest and trough in the direction of stream for the case of similar metal combination (Fig. 6.7).

A close look at the photographs in Fig. (6.7) and (6.8) shows that the average size of waves is smaller for dissimilar metal combination.

Average value of amplitude to wavelength ratio for dissimilar metal combination is found to be less than the average value h/λ for similar metal combination (Table 6.4).

Average value of distortion for dissimilar metal combination is higher than that for similar metal combination (Table 6.4).

In certain cases, depending upon the welding conditions, the welded interface is straight (Fig. 6.9).

Weldability window for two materials, copper and steel are drawn (Figs. (6.10) and (6.11)) using equations (5.30), (5.28) and (5.20) for β_L, β_W and β_E and using the velocity condition 200 m/s $<$ V_p $<$ 800 m/s. Experimental results are also plotted in Figs. (6.10) and (6.11).

It is seen that welding is possible if the welding conditions fall within the permissible range. This demonstrates the applicability of the selection procedure of explosive welding parameters outlined in the previous chapter. In Figs. (6.10) and (6.11) results of variable angle experiments (see article 6.3.2) are also shown by bars.

Average values of wave amplitude to wavelength ratio and distortion η for some metal combinations are given in Table 6.4.

TABLE 6.4

Amplitude to Wavelength Ratio and distortion

Metal Combination	Density Ratio	Average Value of Amplitude to Wavelength Ratio h/λ	Average Value of Degree of distortion η
Copper-Copper	1.0	0.38	0.03
Stainless steel-Stainless steel	1.0	0.43	0.01
Brass-Stainless steel	0.93	0.31	0.06
Stainless steel-Bronze	0.90	0.29	0.25
Stainless steel-Cast Iron	0.98	0.24	0.07
Stainless steel-Mild steel	0.99	0.38	0.05
Stainless steel-Copper	0.89	0.31	0.11
Copper-Stainless steel	0.89	0.22	0.40

6.3.2 Variable Obliquity Angle Experiments

Two methods are tried for variable obliquity angle experiments using (i) curved parent block (Fig. 6.12-a) and (ii) curved flyer plate (Fig. 6.12-d). In the first case a flat flyer plate is hung by strings and a curved parent block is kept at the anvil, whereas, in the second case a curved flyer plate is hung and a flat parent plate is kept at the anvil. Suitable stand off is provided by adjusting the screws. In variable angle experiments, the obliquity angle $\beta = \alpha + \emptyset$ varies along the periphery due to variation in inclination angle α. Details and results of variable angle experiments are given in Tables (6.5) and (6.6).

Results of variable angle experiments are also shown in Figs. (6.10) and (6.11). It is seen that the wave starts after a certain angle β_L and wave remains upto an angle β_W whereas welding continues to take place upto an angle β_E. These angles depend upon the plate velocity and also on material properties. The flyer plate in certain cases sheared off at the end. Variation of wave size with obliquity angle are shown in Table (6.6) plotted in Figs. 6.13 and 6.14.

The results (Figs. 6.13 and 6.14) of curved flyer plate experiments and curved parent block experiments show that the nature of the experimental variation of h versus β

TABLE 6.5

Details of Variable Angle Experiments

Sl. No.	Metal Combination	Arrangement	Radius cm	Explosive	e/m	V_p m/s
V-1	Stainless steel-En-8 steel	Cylindrical parent block	13	Cordtex	0.220	394
V-2	"	"	"	"	0.441	718
V-3	Copper-En-8 steel	"	"	"	0.256	452
V-4	"	"	"	"	0.385	642
V-5	Copper-Copper	Curved flyer plate	"	"	0.192	349
V-6	Aluminium-Aluminium	"	"	"	0.323	553
V-7	Brass-Aluminium	"	"	"	0.378	632

TABLE 6.6.a

Curved Parent Block Experiments

Variation of Amplitude (h), Wavelength (λ) with Inclination Angle (α)

EXPERIMENT NO. V-1

α deg	h mm	λ mm	Remarks
0	-	-	
2	-	-	
4	0.00	-	
5	0.02	0.28	Wave starts
6	0.06	0.35	Maximum Amplitude
7	0.03	0.17	
8	0.00	-	Wave vanishes
9	-	-	No welding

EXPERIMENT No. V-2

α deg	h mm	λ mm	Remarks
0	-	-	
4	0.00	-	
6	0.02	-	Wave starts
8	0.06	0.30	
10	0.22	0.37	
12	0.24	0.80	
14	0.30	1.00	
16	0.37	1.30	Maximum Amplitude
18	0.32	1.32	
20	0.15	1.95	Flyer plate sheared off
22	0.10	1.50	Wave still persists
24	0.05	1.20	
26	0.02	0.90	

Contd..

TABLE 6.6.a

Curved Parent Block Experiments

Variation of Amplitude (h), Wavelength (λ) with Inclination Angle (α)

EXPERIMENT NO. V-3

α deg	h mm	λ mm	Remarks
0	-	-	
2	0.08	-	Wave starts
4	0.10	0.50	
8	0.22	0.50	
10	0.23	0.80	
12	0.26	0.83	
13	0.33	0.90	Maximum Amplitude
14	0.27	0.75	
16	0.20	0.87	
18	0.08	1.00	
20	0.01	1.00	
21	0.00	-	Wave-No-Wave Boundary
25	-	-	End of Weld
30	-	-	Flyer plate sheared off

EXPERIMENT NO. V-4

α deg	h mm	λ mm	Remarks
0	-	-	
5	0.00	0.00	
6	0.07	0.30	Wave starts
8	0.10	0.42	
10	0.23	0.63	
12	0.42	1.05	
14	0.42	1.15	
16	0.46	1.46	Maximum Amplitude
18	0.38	2.00	
20	-	-	
21	0.00	-	Wave-No-Wave Boundary
22	0.00	-	Flyer plate sheared off

TABLE 6.6.b

Curved Flyer Plate Experiments

Variation of Amplitude (h), Wavelength (λ) with Inclination Angle (α)

EXPERIMENT NO. V-5

α deg	h mm	λ mm	Remarks
0	-	-	
2	0.01	0.10	Wave starts
4	0.04	0.14	
6	0.09	0.25	
8	0.10	0.30	
10	0.12	0.38	
12	0.16	0.57	Maximum Amplitude
14	0.05	-	
16	0.00	-	Wave vanished

EXPERIMENT NO. V-6

α deg	h mm	λ mm	Remarks
0	-	-	
1	0.00	-	
2	0.03	0.14	Wave starts
4	0.04	0.25	
6	0.08	0.30	
8	0.08	0.50	
10	0.12	0.90	Maximum Amplitude
12	0.06	0.80	
14	0.07	0.90	
16	0.05	0.38	
17	-	-	Flyer plate sheared off

EXPERIMENT NO. V-7

α deg	h mm	λ mm	Remarks
0	-	-	
2	0.03	0.10	Wave starts
4	0.04	0.12	
6	0.06	0.30	
8	0.06	0.25	
10	0.10	0.52	
12	0.12	0.74	
14	0.14	0.80	
15	-	-	Crack developed in the flyer plate
16	0.17	2.0	Maximum Amplitude
18	0.07		
20	0.00	-	Wave vanished

is similar to the one shows in Fig. 5.1. However, it is easy to make the curved flyer plate rather than to make curved parent block, hence, the curved flyer plate experiment as an alternative method for variable angle experiments may also be used.

6.3.3 Tube to Tube-Plate Welding

In tube to tube-plate welding experiment, the tube is considered as flyer plate and tube-plate as parent plate. Thus the same selection procedure for parameters of explosive welding is also used for tube to tube-plate experiments. Both the parallel and taper arrangements (Fig. 6.15) are employed. Suitable explosive packs are used depending upon the requirement. The details of the tests conducted are shown in Table 6.8.a. Table 6.8.b gives the results of these tests.

The following conclusions are drawn from a perusal of the above results for tube to tube-plate welding.

(1) In order to keep the obliquity angle β within the permissible range, high detonation velocity explosive could be used with taper arrangement (Expts. No. 7 and 10). Parallel arrangement is suitable with low detonation velocity explosive (Expts. No. 1, 2, 3, 5, 6 and 8).

TABLE 6.8.a

EXPLOSIVE WELDING OF TUBE TO TUBE PLATE

	Tube Plate						Tube			Buffer	Explosive Pack		
Test No.	Material	W Cm	L Cm	D_c Cm	D_t Cm	α deg	Material	l Cm	t Cm	t_b Cm	Explosive	D_e Cm	d_e Cm	l_e Cm
1.	M.S.	9.0	7.0	2.92	2.52	0	S.S.	18.0	0.175	0.175	NG	1.77	0	6.5
2.	M.S.	9.8	6.5	4.00	3.80	0	S.S.	17.5	0.165	0.250	NG	2.95	0	4.5
3.	M.S.	7.0	5.0	4.85	4.70	0	M.S.	11.0	0.270	0.175	NG	3.80	0	5.0
4.	M.S.	10.0	5.0	3.42	2.55	5	Al	17.5	0.100	0.237	NG	1.77	0	7.5
5.	M.S.	11.7	8.0	5.00	4.70	0	M.S.	18.0	0.250	0.175	NG	3.80	2	4.3
6.	M.S.	8.6	6.5	3.50	3.20	0	Cu	17.2	0.300	0.175	NG	2.15	0	4.8
7.	M.S.	9.3	7.0	4.80	3.80	5	S.S.	18.0	0.165	0.175	Cord-tex	3.00	0.6	2.5
8.	M.S.	8.6	6.5	3.15	2.85	0	Brass	16.0	0.175	0.100	NG	2.40	0	4.5
9.	M.S.	12.3	8.5	5.10	4.70	0	M.S.	18.0	0.170	0.175	Cord-tex	3.80	0	6.5
10.	M.S.	9.1	5.0	4.65	3.80	5	S.S.	16.5	0.175	0.175	PEK-I	1.77	0	3.0
11.	M.S.	7.0	4.5	3.16	2.52	5	S.S.	16.0	0.175	0.175	Cord-tex	1.77	0	1.5

TABLE 6.8.b

RESULT OF TUBE TO TUBE PLATE WELDING

Test No.	Tube to Tube Plate	Arrangement	Detonation End	e/m	V_P m/s	Results
1.	Stainless steel - Mild steel	Parallel	A	0.278	187	Welded with little bulge of tube outside tube plate.
2.	Stainless steel - Mild steel	Parallel	B	0.380	245	Welded with bulging of tube at end A.
3.	Mild steel-Mild steel	Parallel	B	0.494	303	M.S. tube burst at the seam.
4.	Aluminium-Mild steel	Taper	A	0.876	466	Thin Aluminium tube fractured at the extreme tapered end.
5.	Mild steel-Mild steel	Parallel	B	0.330	216	Satisfactory welding
6.	Copper-Mild steel	Parallel	B	0.190	132	Welding done.
7.	Stainless steel - Mild steel	Taper	A	0.145	269	Welding satisfactory without bulge.
8.	Brass - Mild steel	Parallel	B	0.270	182	Welding satisfactory without bulge
9.	Mild steel-Mild steel	Parallel	B	0.219	392	M.S. tube burst at the seam, Tube plate developed cracks.
10.	Stainless steel-Mild steel	Taper	A	0.227	405	Bulging of tube and cracks in tube plate.
11.	Stainless steel-Mild steel	Taper	A	-	-	No welding due to insufficient explosive length.

(2) Taper arrangement is found to be unsuitable for tubes of low thickness and soft material such as Aluminium, as the tube burst at the outer end due to the strain exceeding limiting strain for the material (Expt. No. 4).

(3) Tubes with seam are not suitable for explosive welding with tube plates (Expt. No. 3).

(4) Bulge occurs due to excessive charge length (Expts. No. 2 and 10). Hence, the charge length should be chosen carefully to avoid bulge. Tube plate develops cracks (Expts. No. 9 and 10) due to excessive charge.

(5) In parallel arrangement, detonation from the end A (Fig. 6.15) may be preferable as it leaves the space for re-entrant jet to escape out (Expt. No. 1).

Some welded samples of tube to tube-plate are shown in Fig. 6.16. A half cut specimen is also shown in Fig. 6.16.

6.3.4 Half-Length-Explosive Experiments

Half-length-explosive welding experiments (Table 6.9) are carried out to study the configuration of the plate during the process of explosive welding (Fig. 6.17-a). Resulting configuration after welding (Fig. 6.17-b) is found to be similar to the configuration shown in Fig.1.1-b.

TABLE 6.9

Half-Length-Explosive Experiment

S.No.	Metal Combination	Explosive	e/m	V_P m/s	α degrees	β degrees (Calculated)
1.	Aluminium-Aluminium	Cordtex	0.323	552	5	9.87
2.	Copper-Copper	Cordtex	0.256	452	10	14.00
3.	Copper-Copper	PEK-I	0.342	580	10	15.10
4.	Aluminium-Copper	Cordtex	0.323	552	5	9.87

After macro-etching, the welded piece shows the re-entrant jet (Fig. 6.17-c).

The measured obliquity angle from the welded pieces is found to be much higher than the calculated obliquity angle given in the Table 6.9. This may be due to the fact that the dynamic configuration may not be 'frozen' because, in half-length-explosive experiments, even after the complete explosion the pressure on the remaining part of the plate still persists for some time. Hence the obliquity angle from the above test does not represent the correct condition. Nevertheless the half-length-explosive experiment is suitable to demonstrate the configuration of the welding process and presence of the re-entrant jet.

6.4 MECHANICAL TESTING AND BOND STRENGTH

The strength of the welded specimen is tested by using the following tests.

(1) Tensile Test

(2) Shear Test

(3) Shear Test as recommended by ASTM.

Before testing the cladded specimen, the tensile stress and hardness of individual plates are found and are listed in Table 6.10.

6.4.1 Tensile Test

Circular specimens are made with a central hole as shown in Fig. 6.18. Loading the specimen on universal testing machine by a punch through the hole introduces tensile stress in welded joint. The dimensions of the specimen are designed so that the punch does not pierce the plate instead. The test results are given in Table 6.11.

6.4.2 Shear Test

Figure 6.19 shows the test specimen used for shear test of the weld. The specimen is subjected to shear on INSTRON testing machine. The welded specimen sheares off at the interface at certain stress. Results of the tests are given in Table 6.12.

6.4.3 Shear Test as recommended by ASTM

In the shear test described in section 6.4.2, tensile force creates shearing on a small welded area. However, the shear test as recommended by ASTM is more close to the shearing of interface (Fig. 6.20). The specimen is loaded on universal testing machine producing shear stress at the interface. Results of the tests are given in Table 6.13.

TABLE 6.10

Tensile Strength and Hardness of Metal Plates

S.No.	Metal	Density	Tensile Strength		Hardness
		gm/cm^3	kgf/cm^2	N/m^2	VHN
1.	Copper	8.9	2455	2408×10^6	85
2.	Stainless steel	7.8	6215	6097×10^6	256
3.	Mild steel	7.8	5295	5194×10^6	176
4.	Aluminium	2.6	1350	1324×10^6	45

TABLE 6.11

Tensile Strength of the Welded Specimen

Specimen No.	Metal Combination	Tensile Strength kgf/cm^2
A-1	Stainless steel-Stainless steel	2850
A-4	Stainless steel-Stainless steel	6108
A-5	Stainless steel-Stainless steel	9706
A-6	Stainless steel-Stainless steel	2468
A-7	Stainless steel-Stainless steel	4020
A-8	Stainless steel-Stainless steel	2033
A-10	Stainless steel-Stainless steel	2552
S-1	Stainless steel-Stainless steel	4842
S-2	Stainless steel-Stainless steel	8768
A-12	Copper - Copper	714
A-13	Copper - Copper	372
A-15	Copper - Copper	658
A-18	Copper - Copper	598
A-20	Copper - Copper	306
A-21	Stainless steel-Stainless steel	2103
A-22	Stainless steel-Stainless steel	4590
A-23	Stainless steel-Mild Steel	3333

Contd...

Contd. Table 6.11

Specimen No.	Metal Combination	Tensile Strength kgf/cm^2
A-24	Stainless steel- Mild steel	2906
A-25	Stainless steel - Bronze	596
A-27	Aluminium - Aluminium	656
S-3	Aluminium - Aluminium	1403
A-28	Aluminium - Copper	554
A-29	Aluminium - Stainless steel	643
A-34	Copper - Stainless steel	2117
A-35	Copper - Mild steel	464

TABLE 6.12

Shear Strength of the Welded Specimen

Specimen No.	Metal Combination	Shear Strength kgf/cm^2
A-1	Stainless steel-Stainless steel	1667
A-5	Stainless steel-Stainless steel	1721
A-7	Stainless steel-Stainless steel	2451
A-9	Stainless steel-Stainless steel	1702
A-10	Stainless steel-Stainless steel	2124
A-13	Copper - Copper	750
A-18	Copper - Copper	1469
A-20	Copper - Copper	1501
A-24	Stainless steel-Mild steel	1267
A-35	Copper - Mild steel	166

TABLE 6.13

Shear Test as Recommended by ASTM

Specimen No.	Metal Combination	Shear Strength . kgf/cm^2
A-1	Stainless steel-Stainless steel	2110
A-5	Stainless steel-Stainless steel	3597
A-7	Stainless steel-Stainless steel	2351
A-8	Stainless steel-Stainless steel	1947
A-9	Stainless steel-Stainless steel	2053
A-10	Stainless steel-Stainless steel	1916
S-2	Stainless steel-Stainless steel	4604
A-12	Copper - Copper	562
A-13	Copper - Copper	1319
A-14	Copper - Copper	1005
A-15	Copper - Copper	825
A-17	Copper - Copper	1616
A-18	Copper - Copper	454
A-20	Copper - Copper	770
A-21	Stainless steel - Copper	1435
A-22	Stainless steel - Copper	1518
A-24	Stainless steel - Mild steel	2541
A-25	Stainless steel - Bronze	1892
A-27	Aluminium - Aluminium	668
A-28	Aluminium - Copper	166
A-29	Aluminium - Stainless steel	558
A-34	Copper - Stainless steel	2158

6.4.4 Discussion on Results of Bond Strength

A study of the results of the tensile test (Table 6.11) on stainless steel - stainless steel welds shows a large variation in the strength of the bond (0.3 to 1.6 times the tensile strength of the original sheet). The strength of copper-copper bond is very low (0.12 to 0.25 of the original strength).

Shear strength results obtained by tensile loading (Table 6.12) are found to be much lower than the values obtained by shear test as recommended by ASTM (Table 6.13). This may be due to the fact that the shear test specimen under tensile loading are associated with bending at the interface under shear (Fig. 6.19). As such shear test recommended by ASTM is found to give better results. The results of the shear strength (Table 6.13) also show a large variation in strength 0.6 to 1.5 of the original shear strength for stainless steel-stainless steel welds, and 0.4 to 1.3 of the original shear strength for copper-copper welds.

The results of other research workers also show a large variation in weld strength [168].

The results of welding test with dissimilar metals show that the strength of the bond is generally greater than the weaker of the two metals.

(i) The Half-Length-Explosive experiments show that the conventional configuration of explosive welding is justified. Presence of the re-entrant jet is also confirmed.

(ii) The plate cladding experiments demonstrate the applicability of the weldability window and selection procedure for explosive welding parameters described in the previous chapter V.

(iii) The selection procedure for explosive welding could also be extended for tube to tube-plate welding provided tube plate velocity is accurately estimated, and a suitable explosive charge length is decided upon.

(iv) The variable angle experiments further confirm the existance of β_L, β_W and β_E.

(v) Metallographic examination showed wavy interface in majority of the cases. Despite the variation in strength of the bond due to various factors, the shear strength of the bond is satisfactory specially in the case of dissimilar metal combinations.

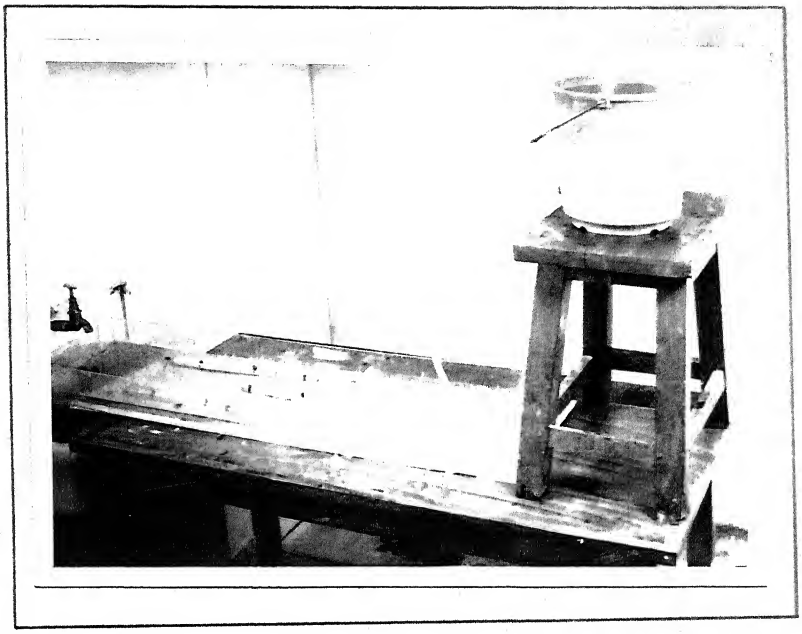

(a) FLOW ANALOGUE EXPERIMENTAL SET-UP

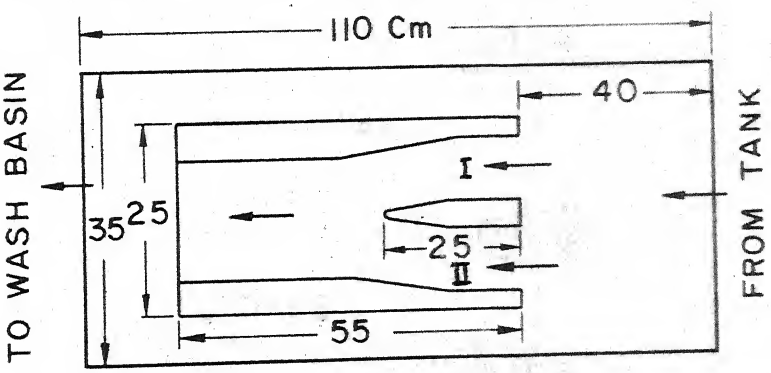

(b) SCHEMATIC DIAGRAM OF PERSPEX MODEL

FIG. 6.1 PERSPEX MODEL REPRESENTING HYDRODYNAMIC EXPLOSIVE WELDING

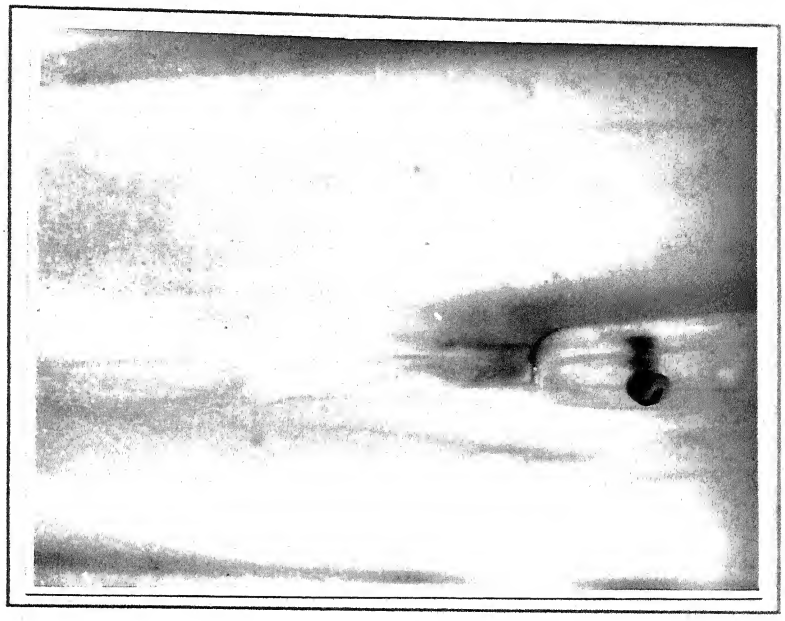

(a)

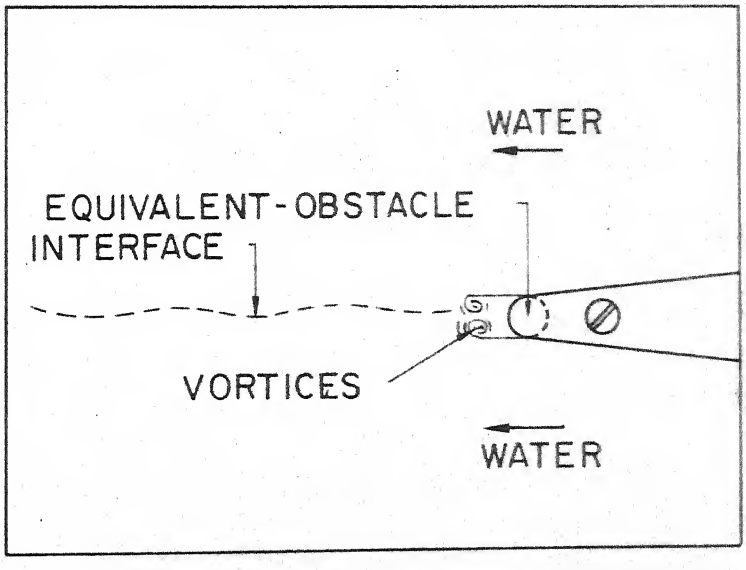

(b)

FIG. 6.2 VORTEX SHEDDING FOR THE CASE OF SIMILAR FLUIDS

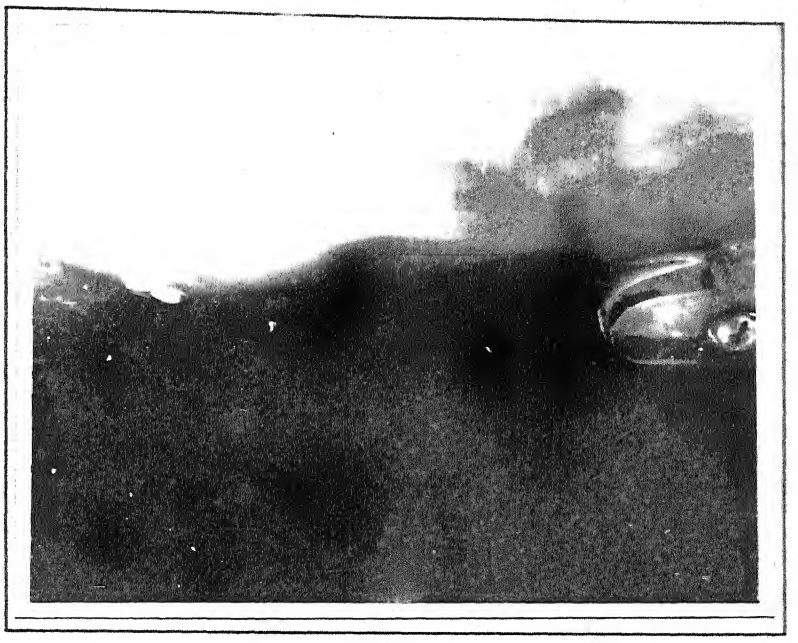

(a)

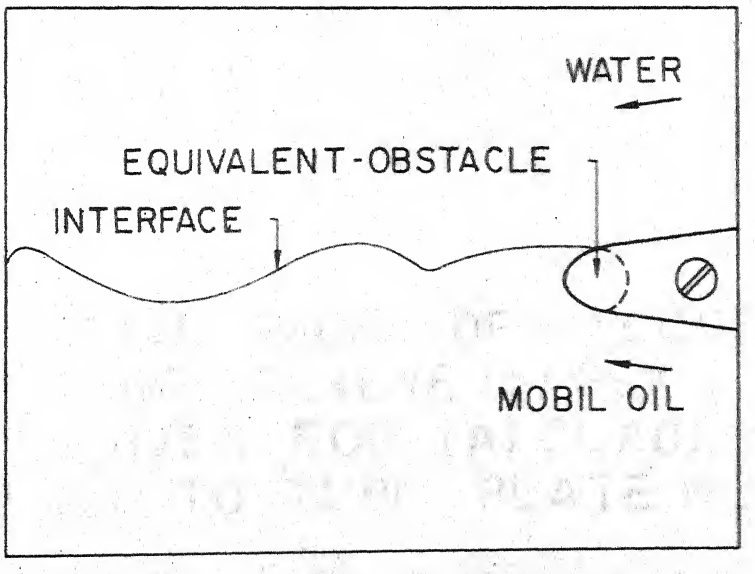

(b)

FIG. 6.3 DISTORTED INTERFACE FOR THE CASE OF DISSIMILAR FLUIDS

EXPLOSIVE

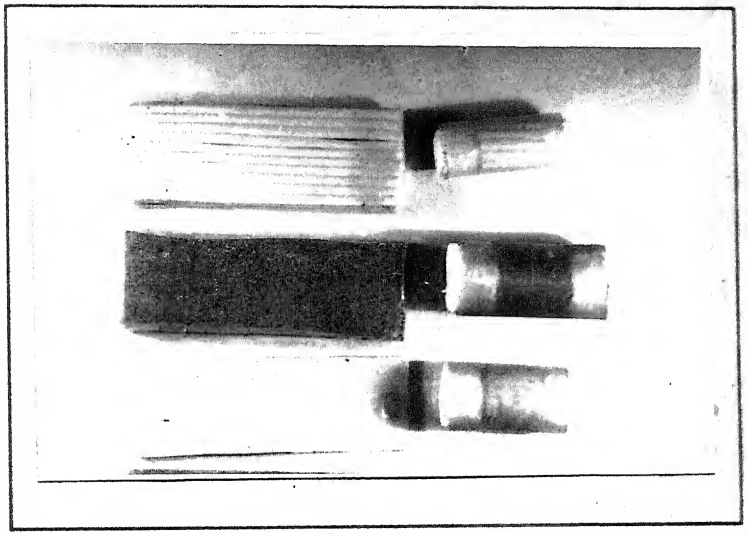

(a) CORDTEX

(b) NITROGLYCERENE

(c) PEK - I

PROCESS	(A) CLADDING	(B) TUBE TO TUBE - PLATE WELDING

FIG. 6.4 EXPLOSIVE PACKS OF (a) CORDTEX (b) NITROGLYCERENE (c) PEK-I EXPLOSIVES FOR (A) CLADDING (B) TUBE TO TUBE - PLATE WELDING

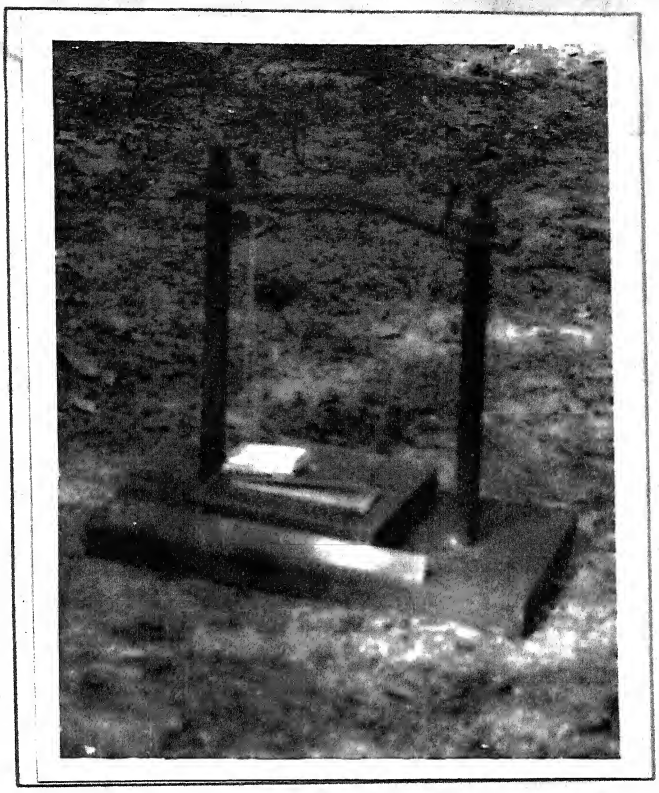

(a) SET-UP FOR EXPLOSIVE WELDING

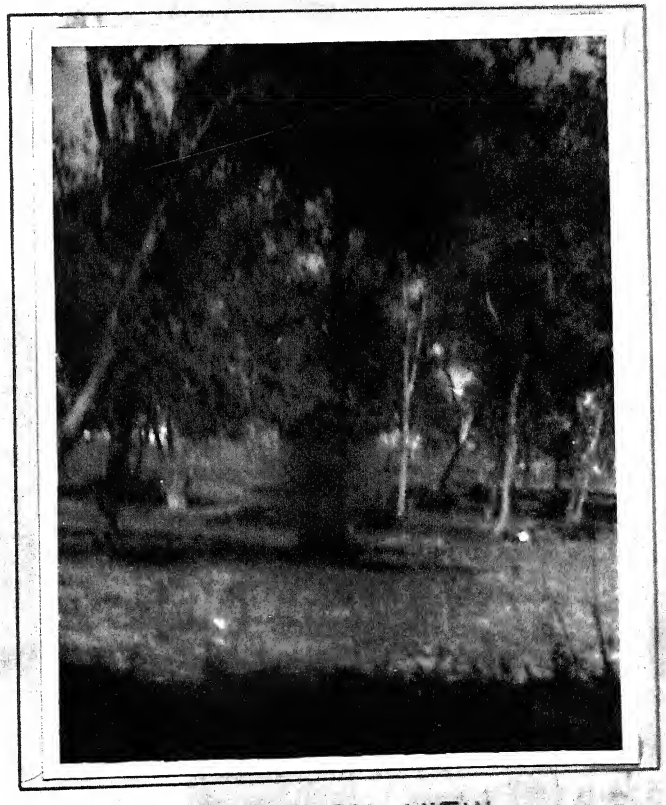

(b) EXPLOSION VIEW

FIG. 6.5 EXPLOSIVE WELDING SET-UP AND VIEW AFTER DETONATION

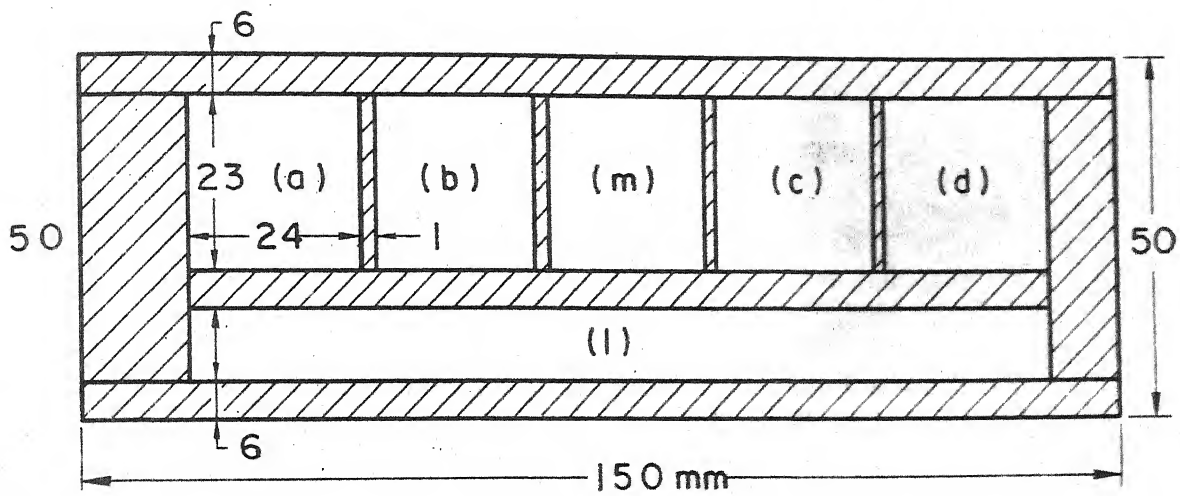

▨ MATERIAL REMOVED BY MACHINING

PIECES (b),(d) FOR MAKING SPECIMEN FOR TENSILE TEST (FIG.6.18)

PIECES (a),(c) FOR MAKING SPECIMEN FOR SHEAR TEST AS RECOMMEND BY ASTM (FIG. 6.20)

PIECE (l) FOR MAKING SPECIMEN FOR SHEAR TEST BY TENSILE LOAD (FIG. 6.19)

PIECE (m) FOR METALLOGRAPHIC EXAMINATION (FIG. 6.7 - 6.9)

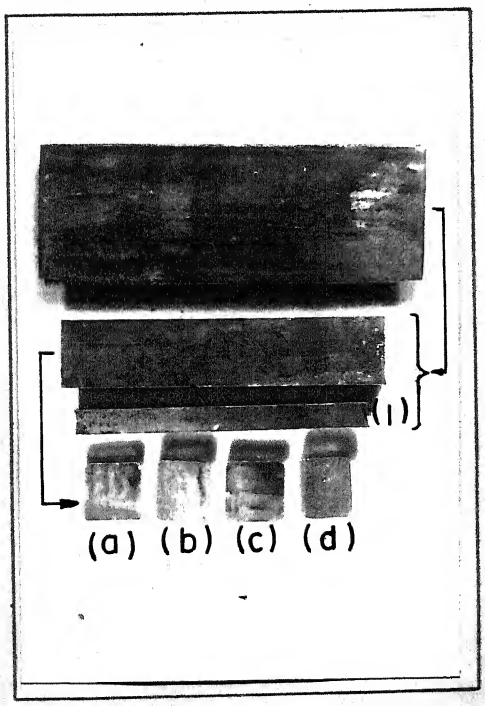

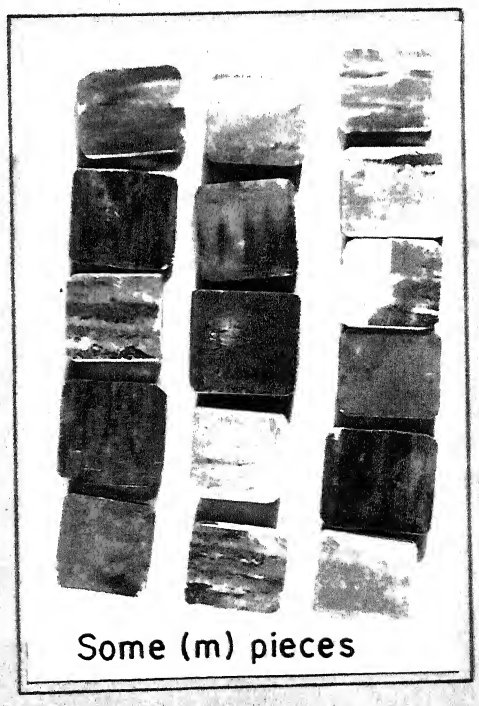

FIG.6.6 SCHEME FOR CUTTING OF CLLADDED PLATES

A-15

V_P = 227 m/s β = 7.0 deg.

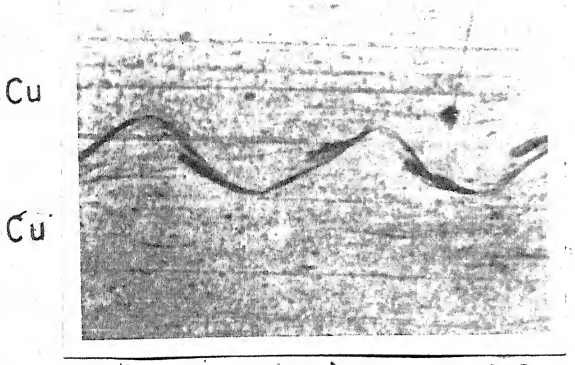

(a) X100

A-12

V_P = 300 m/s β = 11.9 deg.

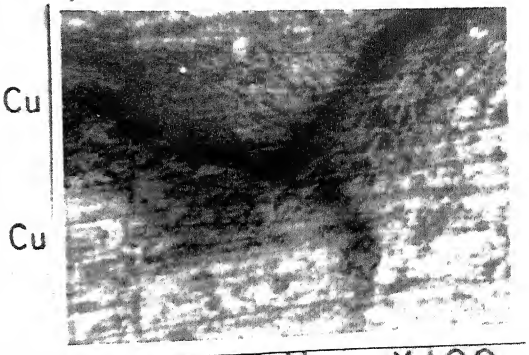

(d) X100

A-18

V_P = 240 m/s β = 42

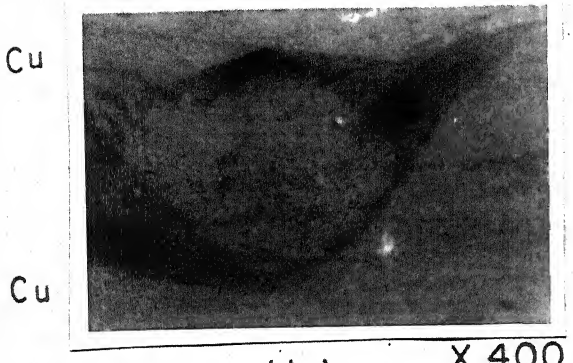

(b) X 400

A-20

V_P = 331 m/s β = 12.9

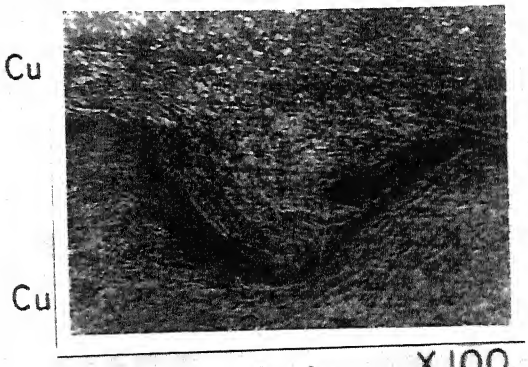

(e) X100

A-13

V_P = 291 β = 7.6 deg.

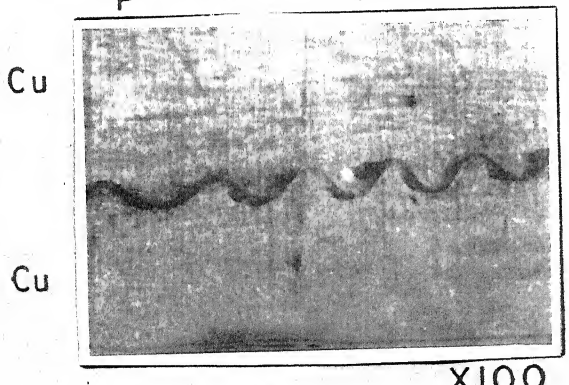

(c) X100

A-10

V_P = 334 m/s β 8.0 deg.

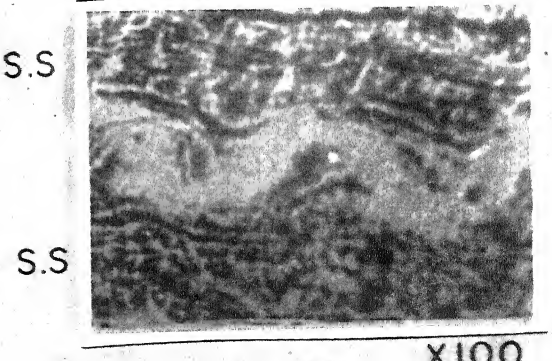

(f) X100

FIG. 6.7 WELD-INTERFACE-WAVE FOR SIMILAR METAL COMBINATION

A - 30

V_p = 284 m/s β = 6.5

(a) X 400

A - 24

V_p = 394 m/s β = 13.9 deg

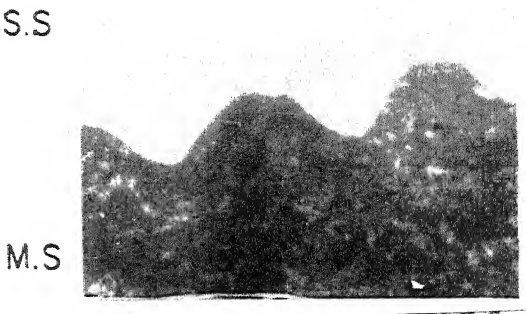

(d) X 100

A - 25

V_p = 394 m/s β = 11.5 deg.

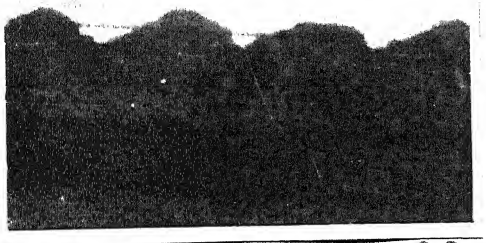

X 100

(b)

A - 22

V_p = 447 m/s β = 10.2 deg.

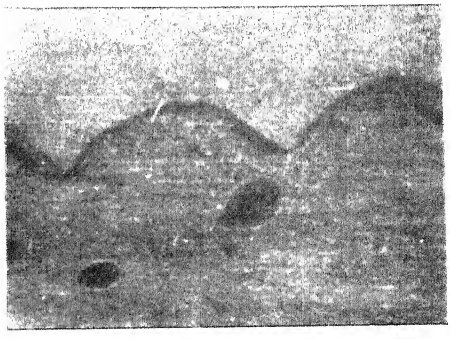

X 100

(e)

A - 26

V_p = 394 m/s β = 9.5 deg.

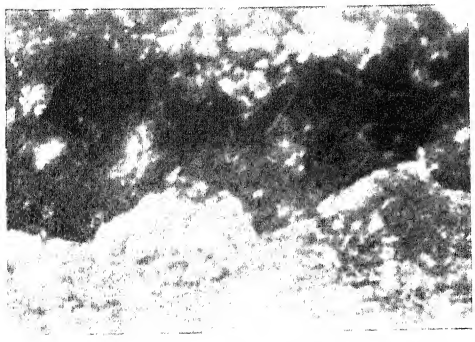

X 100

(c)

A - 34

V_p = 452 m/s β = 14.0 deg.

X100

(f)

FIG. 6.8 WELD-INTERFACE FOR DISSIMILAR METALS COMBINATION

A-28

V_P = 278 m/s β = 6.5 deg.

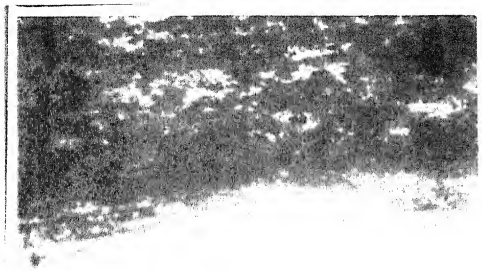

X 100

(a)

A-27

V_P = 278 m/s β = 6.5 deg.

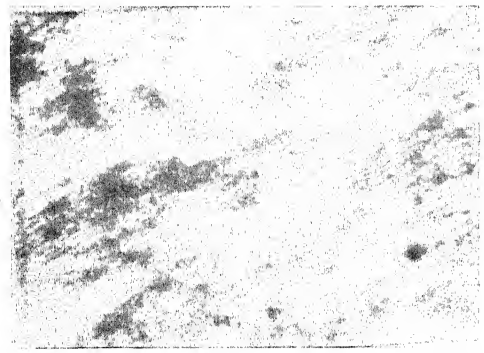

X 100

(b)

A-29

V_P = 278 m/s β = 7.0 deg.

X 100

(c)

A-31

V_P = 344 m/s β = [illegible] deg

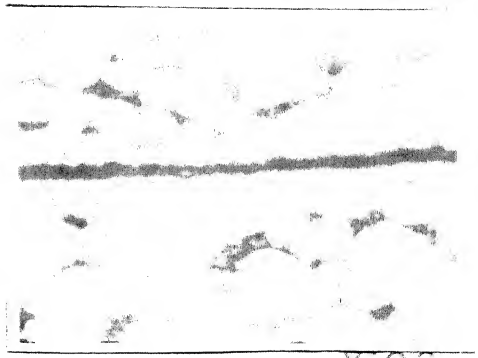

X 100

(d)

A-32

V_P = 343 m/s β = 13.6 deg.

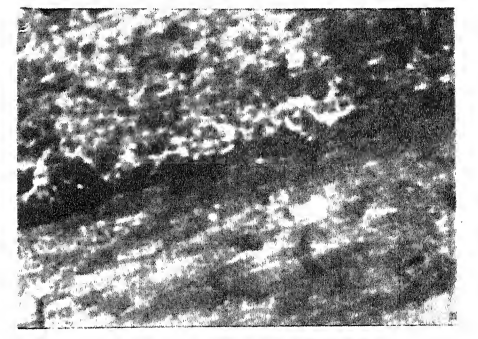

X 100

(e)

A-16

V_P = 431 m/s β = 29.9 deg

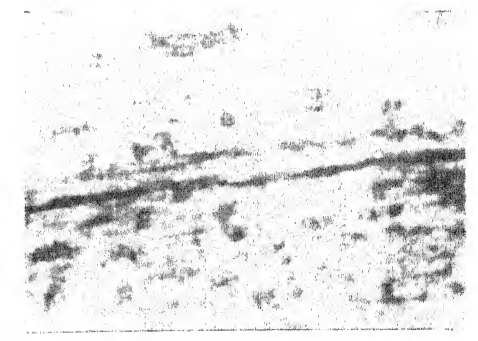

X 100

(f)

FIG. 6.9 STRAIGHT INTERFACE

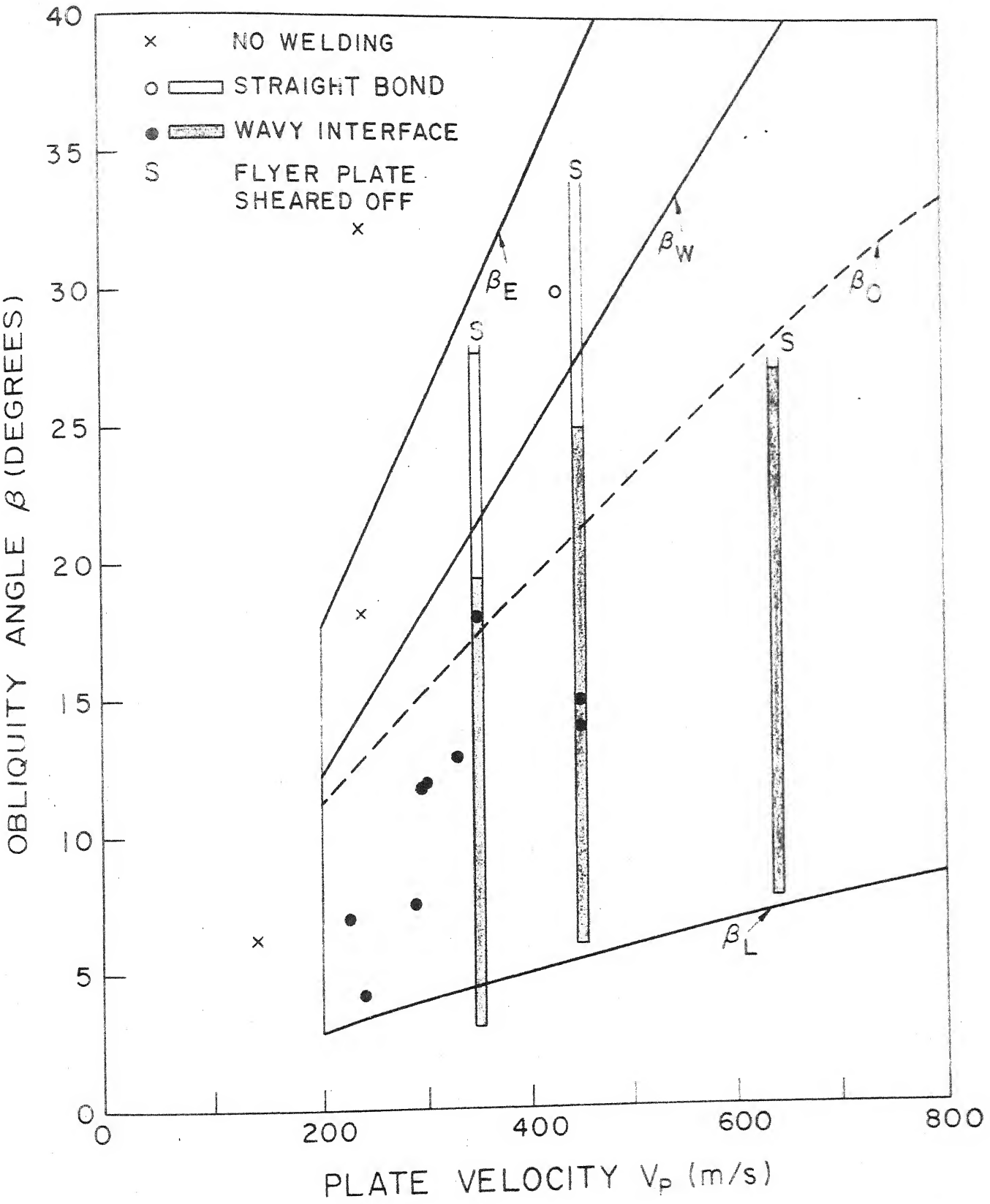

FIG. 6.10 WELDABILITY WINDOW FOR COPPER WITH EXPERIMENTAL DATA

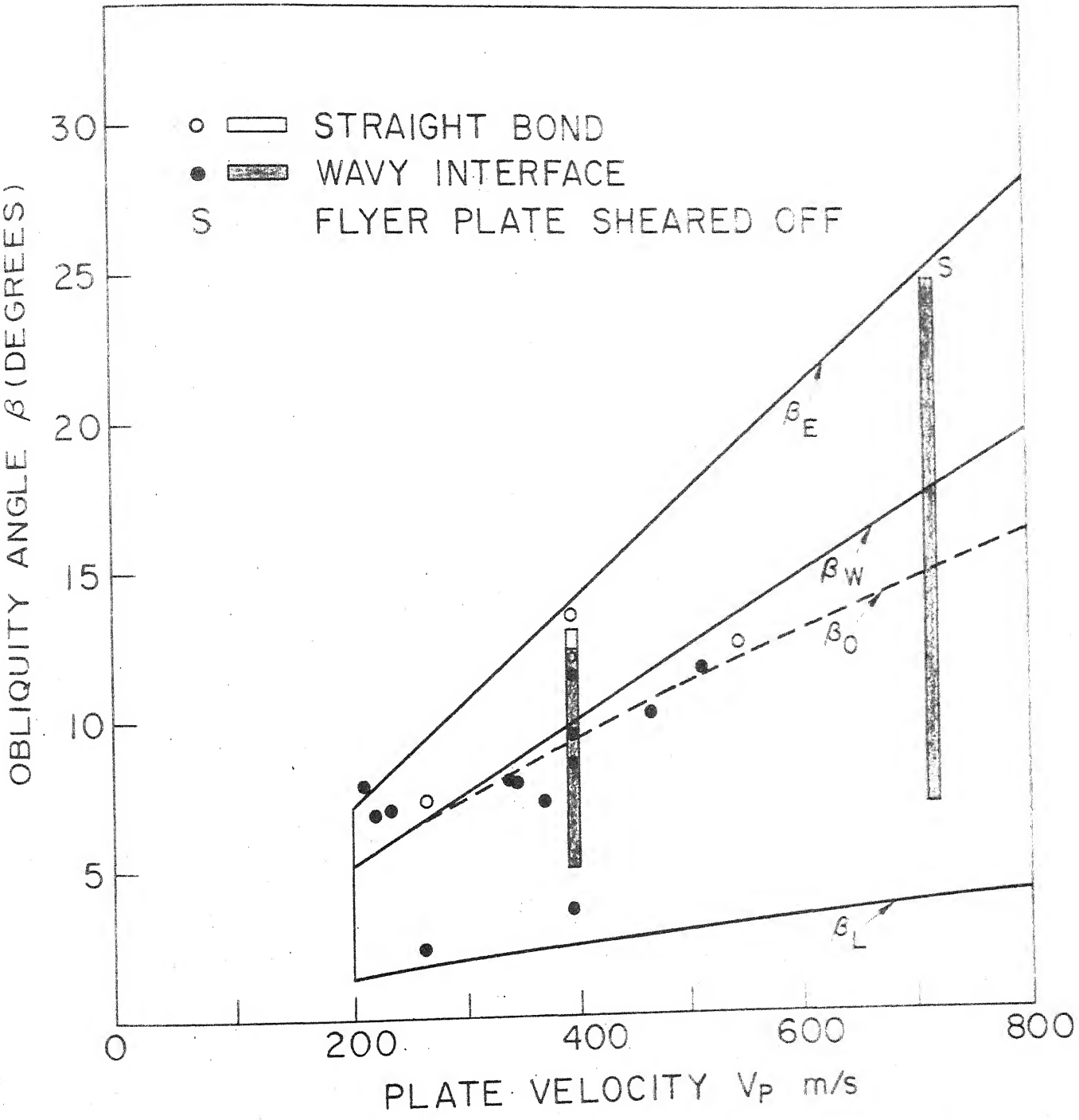

FIG. 6.11 WELDABILITY WINDOW FOR STEEL WITH EXPERIMENTAL DATA

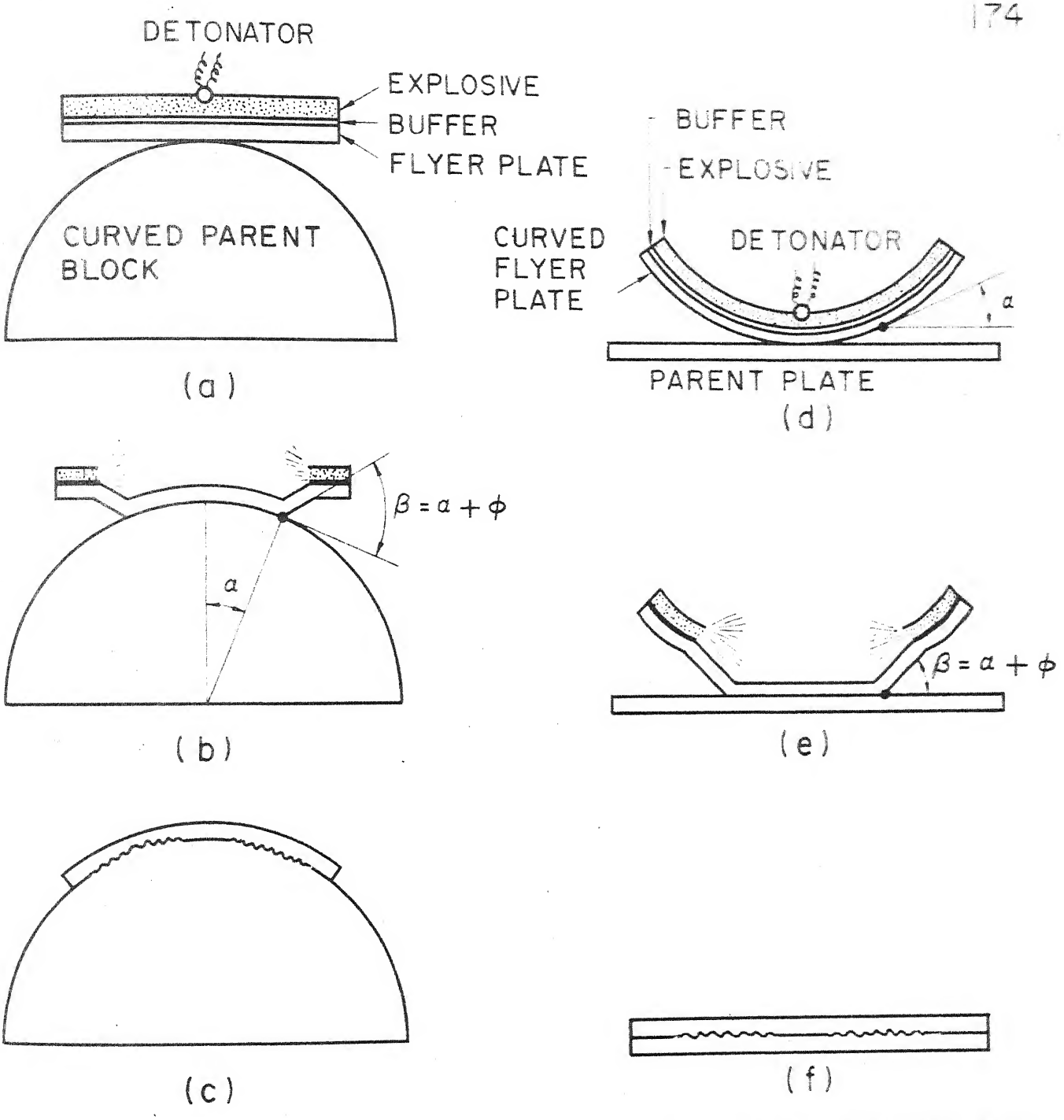

(i) CURVED PARENT BLOCK EXPERIMENT

(ii) CURVED FLYER PLATE EXPERIMENT

(a), (d) BEFORE DETONATION
(b), (e), DURING DETONATION
(c), (f), AFTER DETONATION

FIG. 6.12 VARIABLE ANGLE EXPERIMENTS

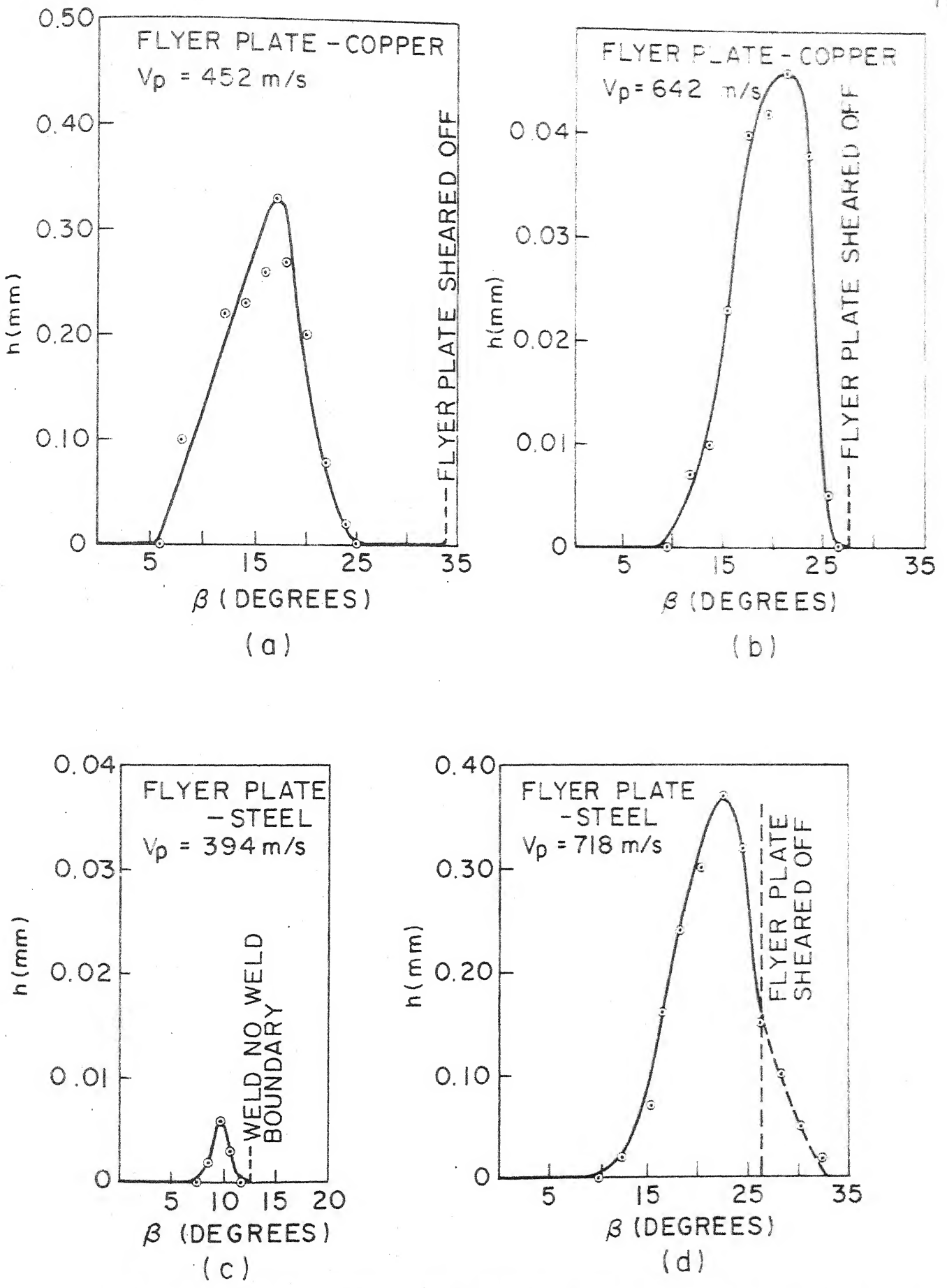

FIG. 6.13 VARIATION OF WAVE SIZE WITH OBLIQUITY ANGLE (CURVED PARENT BLOCK EXPERIMENTS)

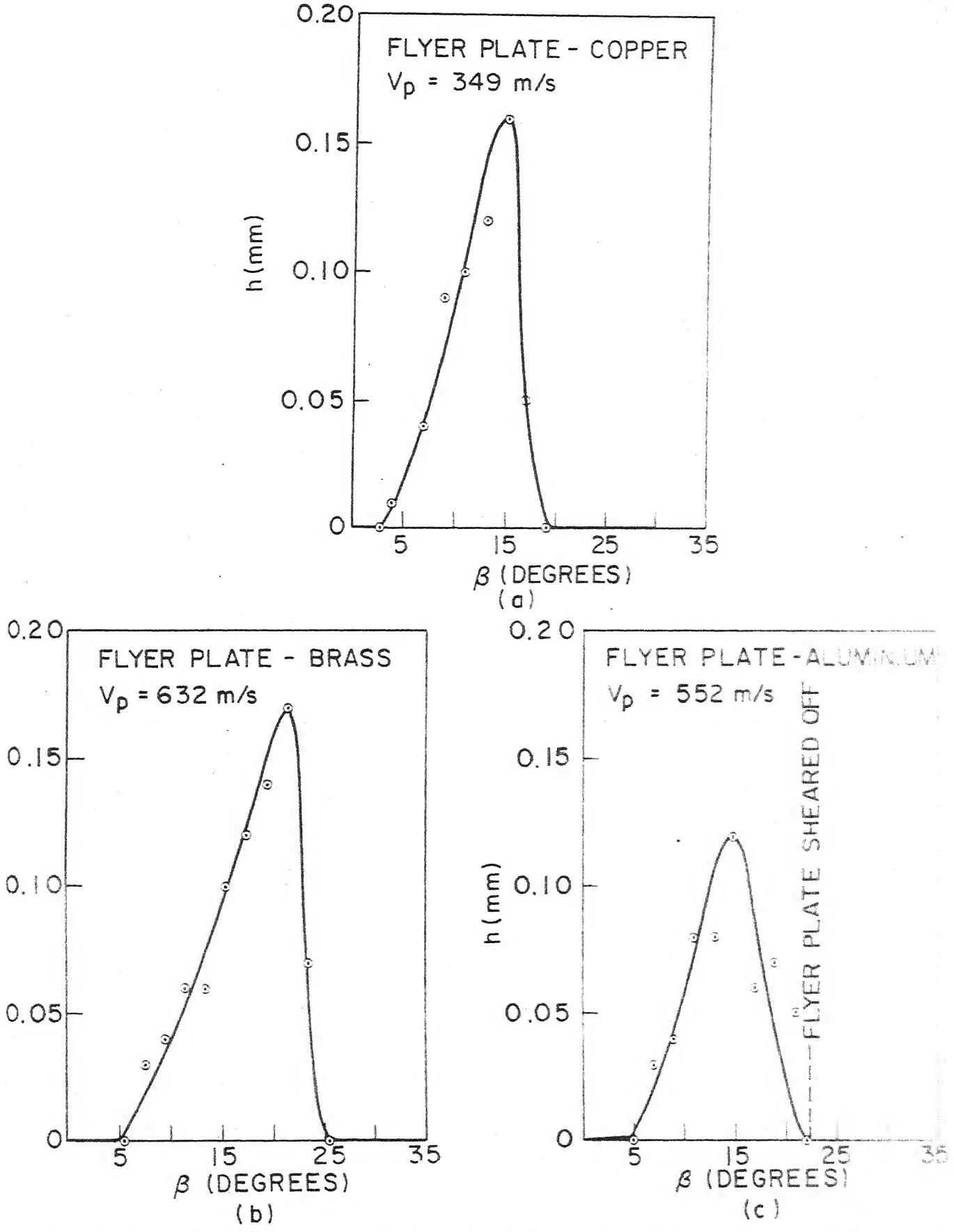

FIG. 6.14 VARIATION OF WAVE SIZE WITH OBLIQUITY ANGLE (CURVED FLYER PLATE EXPERIMENTS

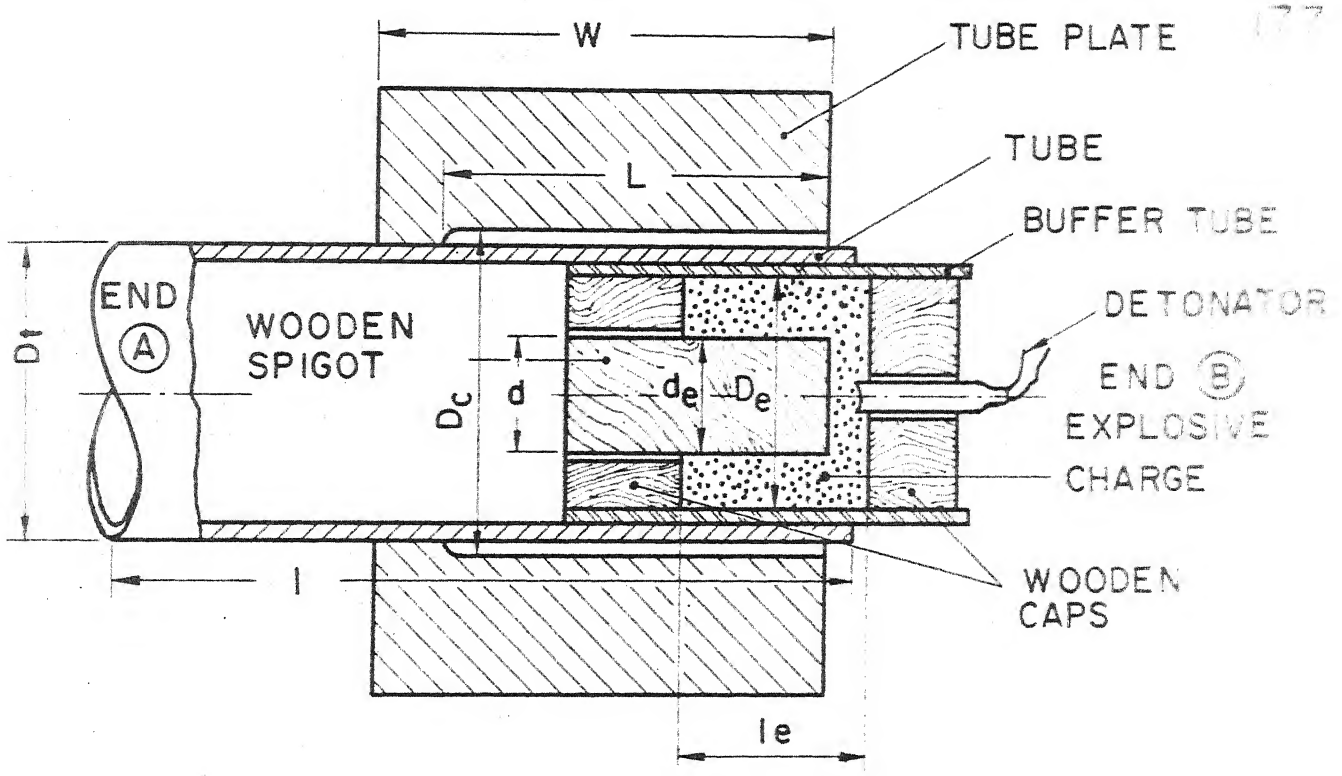

(a) PARALLEL ARRANGEMENT

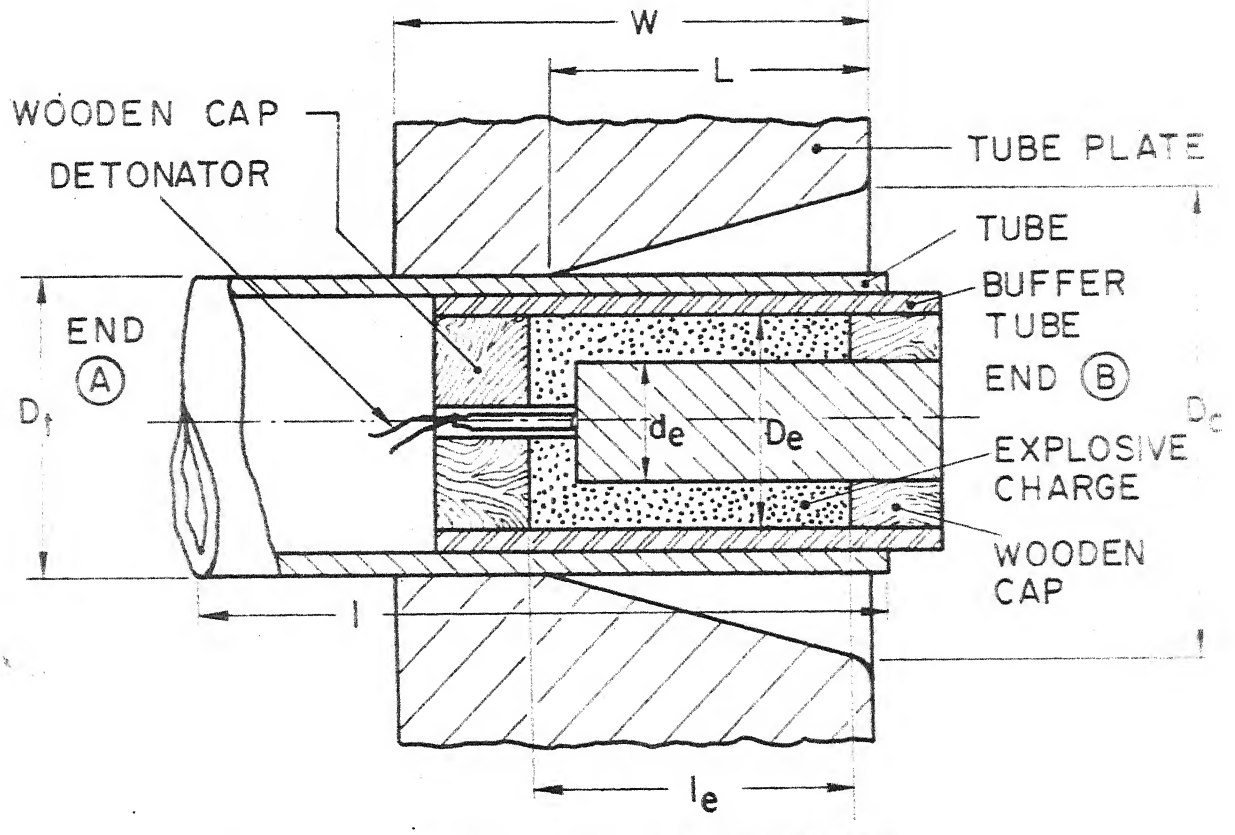

(b) INCLINED ARRANGEMENT

FIG. 6.15 TUBE TO TUBE-PLATE WELDING

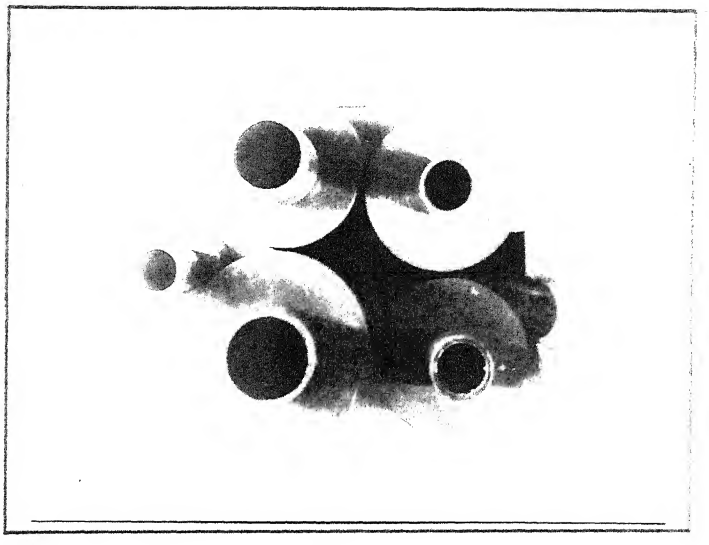

(a)

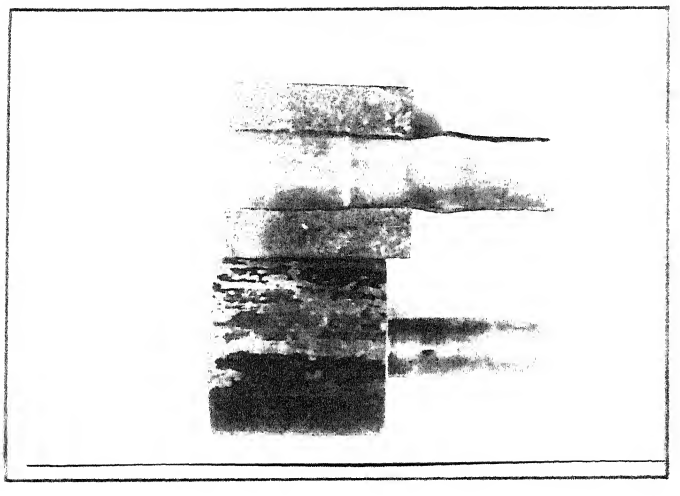

(b)

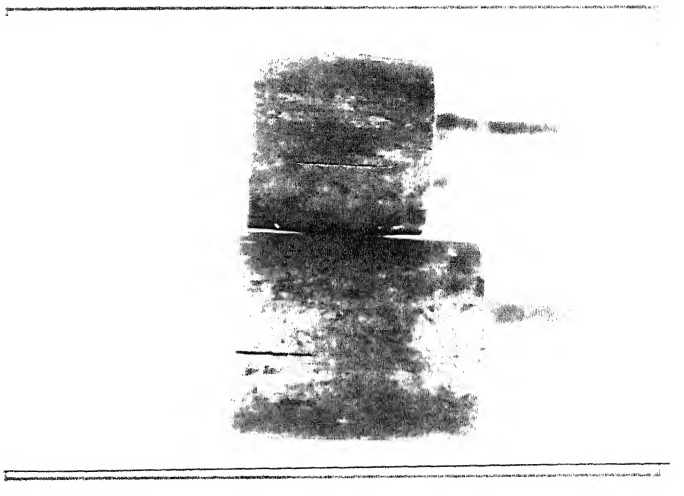

(c)

FIG. 6.16 SOME TUBE TO TUBE-PLATE WELDED PIECES

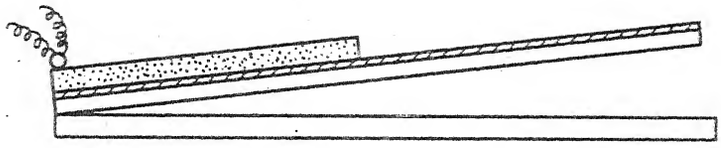

(a) SCHEMATIC DIAGRAM OF HALF-LENGTH -EXPLOSIVE EXPERIMENT (BEFORE DETONATION

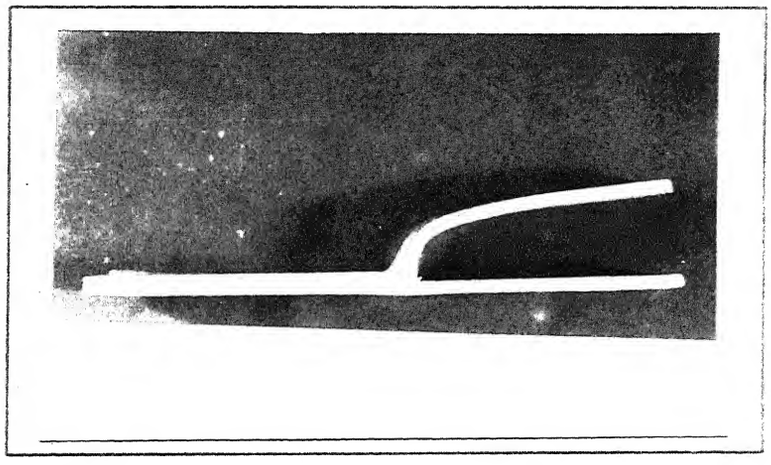

(b) WELDED PIECE (AFTER DETONATION)

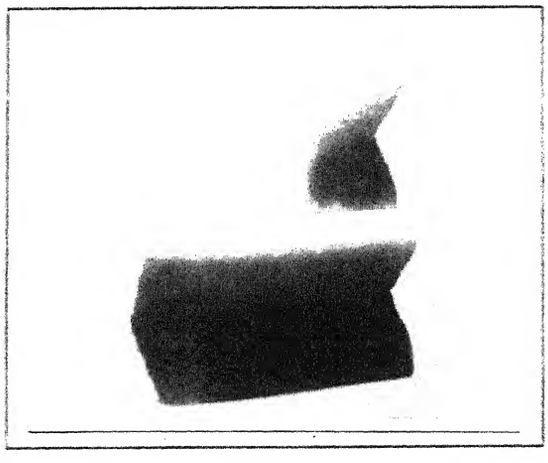

(c) PRESENCE OF RE-ENTRANT JET

FIG. 6.17 WELDED PIECE OF HALF LENGTH EXPLOSIVE EXPERIMENT SHOWING THE RE-ENTRANT JET

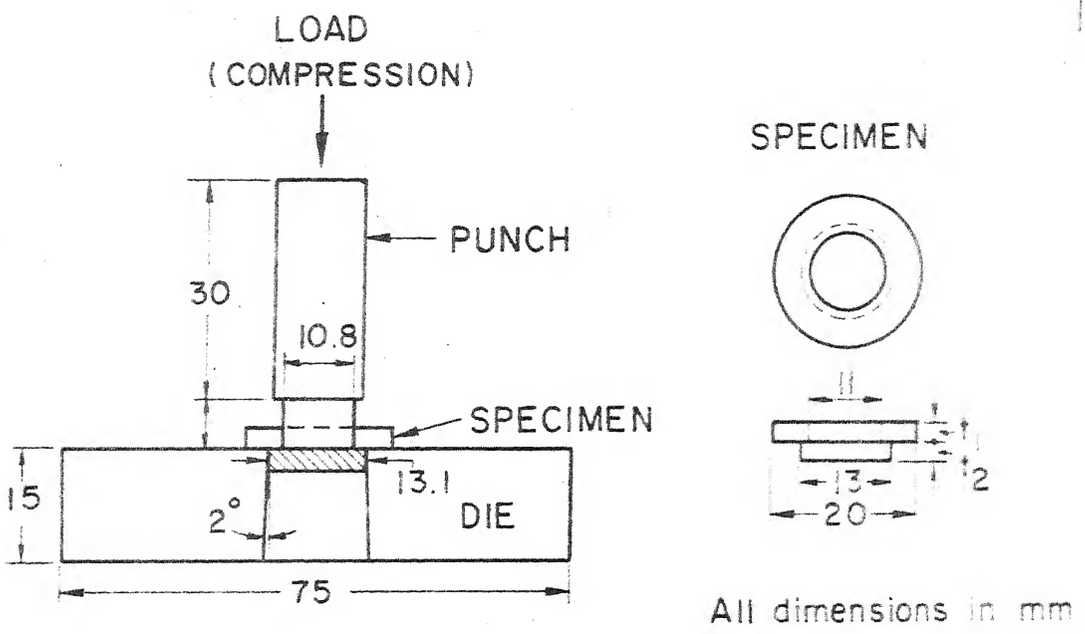

(a) SCHEMATIC DIAGRAM SHOWING TENSILE SPECIMEN AND FIXTURE

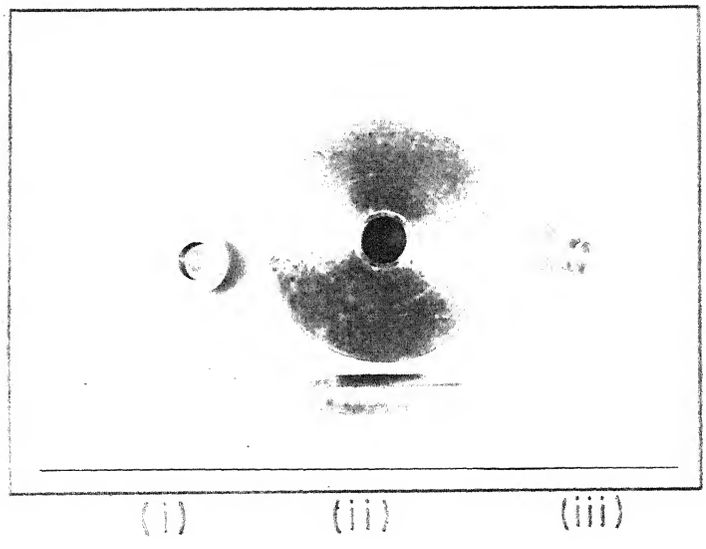

(b) PHOTOGRAPH SHOWING (i) TENSILE SPECIMEN (ii) FIXTURE (iii) SEPARATED SPECIMEN

FIG. 6.18 TENSILE TEST SPECIMEN AND FIXTURE

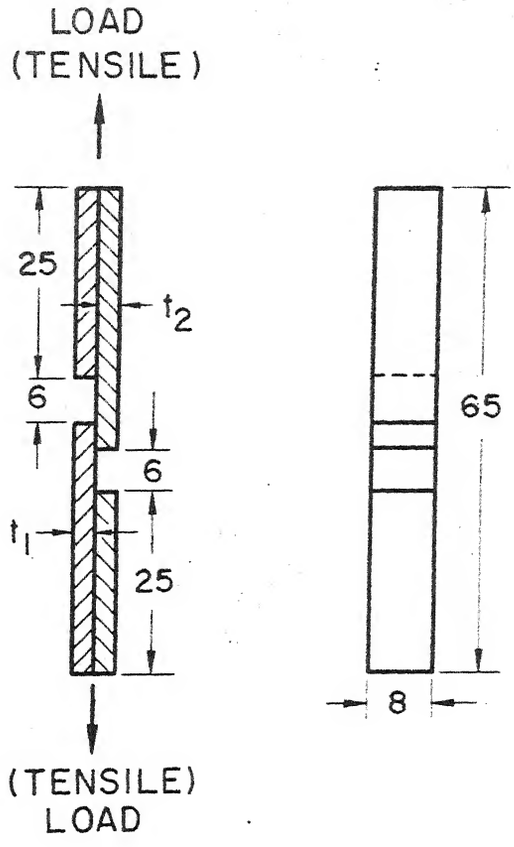

(a) SHEAR SPECIMEN

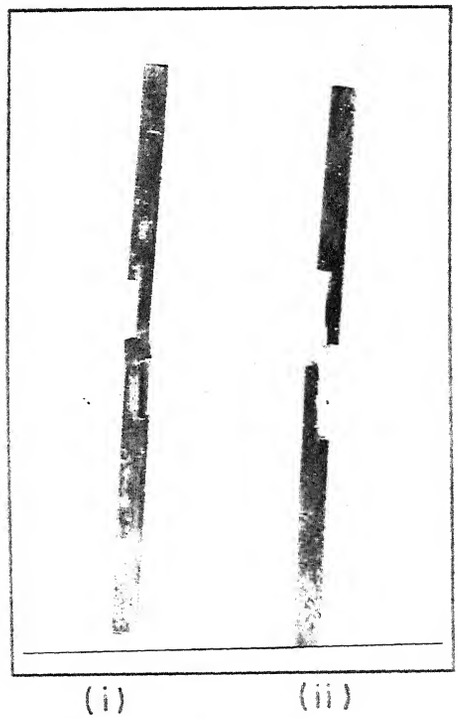

(b) PHOTOGRAPH SHOWING
(i) SHEAR SPECIMEN
(ii) SEPERATED SPECIMEN

FIG. 6.19 SHEAR TEST SPECIMEN BY TENSILE LOAD

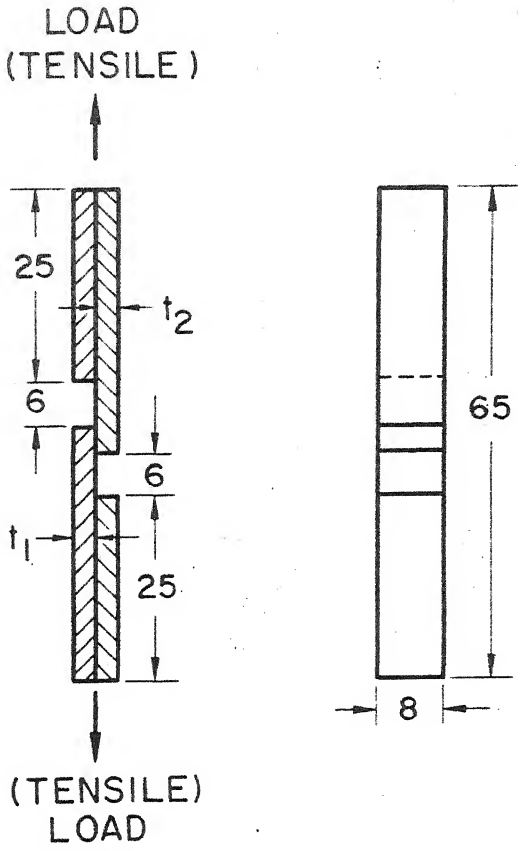

(a) SHEAR SPECIMEN

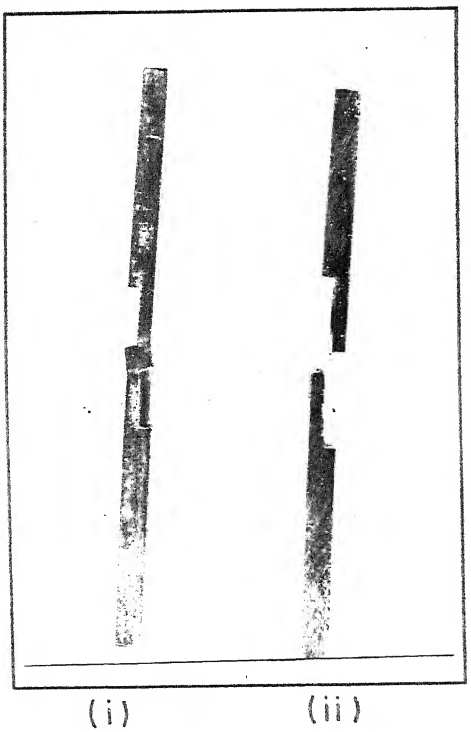

(b) PHOTOGRAPH SHOWING
(i) SHEAR SPECIMEN
(ii) SEPERATED SPECIMEN

FIG. 6.19 SHEAR TEST SPECIMEN BY TENSILE LOAD

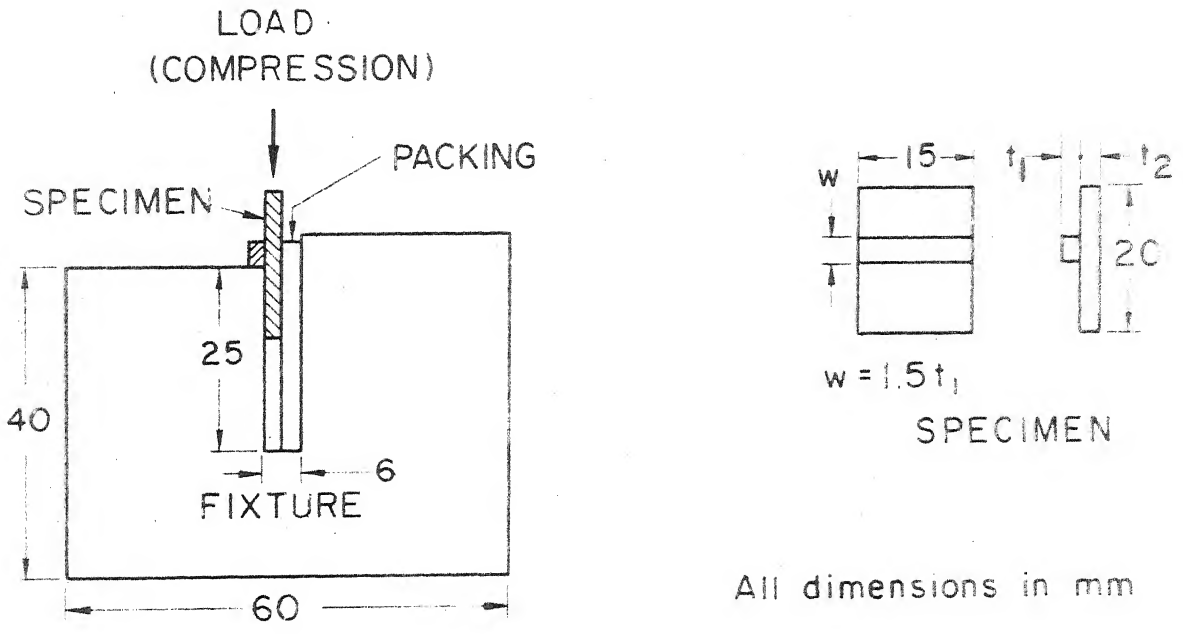

(a) SCHEMATIC DIAGRAM SHOWING SHEAR SPECIMEN AND FIXTURE

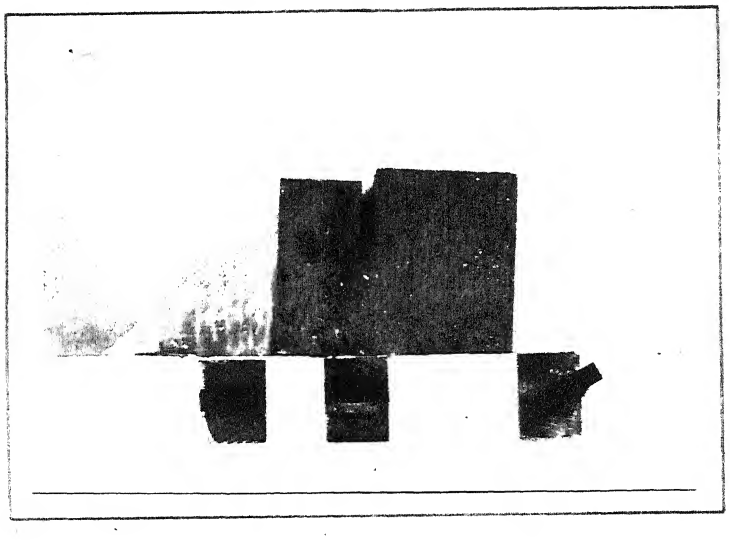

(b) PHOTOGRAPH SHOWING (i) SHEAR SPECIMENS AND FIXTURE

FIG. 6.20 SHEAR TEST SPECIMEN AND FIXTURE AS RECOMMEND BY ASTM

CHAPTER VII

CONCLUSIONS AND SUGGESTIONS FOR FURTHER WORK

7.1 CONCLUSIONS

The following conclusions are drawn on the basis of work presented in this thesis.

1. Various types of asymmetries arising from variation in plate material and explosive are classified. Even if the materials of the two plates are different in geometrically symmetric situation the re-entrant jet (collision direction) does not necessarily bisect the set-up angle and the interface wave may not be sinusoidal. Thus for general case, two plate-jets are inclined at obliquity angles β_1 and β_2 with respect to the collision direction.

2. 'Swinging Wake Mechanism' proposed in the present work considers an obstacle bounded by two stagnation streamlines and that the interface wave is generated by swinging of the wake in the fluidized plates. The force acting on the wake governs the interface wave characteristics and it is a function of the densities (ρ_1, ρ_2) of the two plates and the obliquity angles (β_1, β_2).

3. The 'Swinging Wake Mechanism' adequately explains the generation and distortion of wavy weld interface.

4. The theory predicts that lower the value of density ratio (ρ_1/ρ_2) the larger is the deviation of the wavy interface from a sine wave. This is in agreement with the experimental results of Onzawa and Ishii [90] and the results of present investigation. The distortion is only marginally affected by obliquity angle ratio β_2/β_1. It is the 'metal plate density asymmetry' which causes a significant distorition of interface wave and all other types of asymmetries leading to the condition $\beta_2 < \beta_1$ do not produce any significant wave distortion.

5. The theory predicts that the average value of amplitude to wavelength ratio of interface wave for dissimilar metal combination is expected to be lower than that for similar metal combination. This agrees with the experimental results of Onzawa and Ishii [90].and the results of the present investigation.

6. The obstacle size in general arrangement of explosive welding is a function of obliquity angles (β_1, β_2) thicknesses (t_1, t_2) and densities (ρ_1, ρ_2) of the plates. Predicted diameter of obstacle is smaller in asymmetric situation than that in symmetric situation.

7. Smaller size of waves will be produced (a) in asymmetric welding as compared to symmetric welding situation and (b) for dissimilar metal combination as compared to waves in similar metal combination.

8. Experimental variation of wave amplitude with obliquity angle in explosive welding shows that wavy interface is formed above a certain angle β_L and below an angle β_W. Furthermore there is a maxima in wavy amplitude corresponding to an obliquity angle β_O. A straight bond is formed when obliquity angle is increased from β_W to β_E and no welding takes place beyond β_E. These angles depend upon the material properties of flyer plate and its velocity V_P.

9. In explosive welding, the extent of fluid zone, within which fluidlike behaviour occurs, is usually limited. Furthermore there is some energy loss during the collision in explosive welding. Considering the limited extent of fluid zone and energy loss in collision, the expressions for β_L, β_O, β_W and β_E are developed. For welding to take place, the generated obliquity angle β should be such that $\beta_L < \beta < \beta_E$. The lower obliquity angle β_L and the upper obliquity angle β_E represent the jet-no-jet boundaries (weld-no-weld boundaries).

10. Wave-no-wave condition, corresponding to a critical Reynolds number, represents the boundary of wavy-interface and straight bond. A wavy interface is formed if $\beta_L < \beta < \beta_W$ and a straight interface is formed if $\beta_W < \beta < \beta_E$.

11. Besides the set-up angle α and explosive loading e/m, specific pressure (Euler's number) $p_s = \frac{p}{\frac{1}{2}\rho V_P^2}$ and explosive welding number $E_W = \frac{p}{\frac{1}{2}\rho V_D^2}$ are important parameters and govern the explosive welding process.

12. For parallel arrangement, use of low detonation velocity explosive is recommended whereas for inclined arrangement high detonation velocity explosive may also be used.

13. From the expression developed for limiting obliquity angles, theoretical weldability window (β versus V_P) for explosive welding for a given material can be constructed to find permissible range of parameters for explosive welding. Thus, suitable values of explosive loading e/m and set-up angle α can be selected as to keep the obliquity angle β and plate velocity V_P within the permissible region.

14. The consideration of energy loss in the collision of two plate-jets shows that there is a reduction

in the velocity of the jet after collision and that the mass of the jet is less than that without energy loss. The energy loss consideration explains the dependence of the jet mass on plate velocity and obliquity angle β as found experimentally by Meyer [91].

15. The following conclusions are drawn from the explosive welding experiments carried out.

(i) The plate cladding experiments demonstrate the validity of the proposed weldability window and selection procedure for explosive welding parameters.

(ii) The selection procedure for explosive welding parameters may also be extended for tube to tube-plate welding provided the tube velocity is correctly estimated.

(iii) The variable angle experiments further confirm the existence of β_L, β_W and β_E.

7.2 SUGGESTIONS FOR FURTHER WORK

1. While deriving the expression for diameter of obstacle in chapter IV the thicknesses of two jets of different densities are normalised, because the relationship between z and ν as given in equation (4.5) is not available for jets of different densities.

An attempt to derive such an equation for jets of different densities may lead to a more realistic expression for obstacle size. In explosive-welding configuration, the direction of the re-entrant jet is taken to be the same as the collision direction e.g., in asymmetric situation the re-entrant jet is usually considered parallel to the parent plate. However, experiments show that in the case of asymmetric welding, the re-entrant jet comes out at an angle to the parent plate. The problem of collision of jets in such a case is indeterminate. Attempts may be made to solve the problem.

2. Various limiting obliquity angles have been suggested for asymmetric explosive welding. Variable angle experiments reveal that the flyer plate shears off if the obliquity angle is too high (say for $\beta > \beta_s$). The angle β_s is found to be lower for higher plate velocity and is dependent upon material properties of the flyer plate. An attempt be made to develop a theoretical expression for β_s which may be used as another limiting condition in β versus V_p weldability window.

3. The amplitude and wavelength of interface wave and the obliquity angle at which the wave size is maximum can be predicted theoretically. But it appears that the conditions for maximum strength of weld do not

coincide with the conditions for maximum wave size. It seems that although the interface wave does provide mechanical interlocking but too big a wave size introduces stress concentration. A theoretical and experimental investigation is needed, to study the effect of wave-size on bond-strength and to find out the condition for maximum strength of the bond.

4. It may be useful to carryout the fluid analogue experiment as suggested in chapter VI in greater detail to see the effect of various parameters such as obliquity angles β_1, β_2, densities ρ_1, ρ_2 and flow velocity on the process of wave formation.

REFERENCES

1. T.Z. Blazynski, " Industrial Application of Explosive Welding ", J. Eng. Production, Vol. 2, No. 2, pp.93-110.

2. O.R. Bergmann, " Explosive Bonding of Metals - Application and Mechanism ", Metal Eng. Quart., 6, No. 2, 1966, p. 60.

3. J.M. Stone, Select Conf. on Explosive Welding, Pub. Inst. Welding (London), 1968, p. 21.

4. B. Crossland, J.D. Williams and V. Shribman, "Explosive Cladding of Large Plates", Proc. Select Conf. on Explosive Welding, Pub. Inst. Welding (London), 1968, p. 15.

5. H.K. Wylie and B. Crossland, "Explosive Cladding of Thick Flyer Plates of Large Area", Proc. Int. Conf. on the Use of High Energy Rate Methods for Forming, Welding and Compaction, Leeds, 1973, p. 1.

6. B. Crossland, J.A. Cave, S.K. Banerjee and H.K. Wylie, "Explosive Cladding of Large and Relatively Thick Flyer Plates", Proc. 5th Int. Conf. on High Energy Rate Fabrication, Denver, 1975, pp. 4.10.1 - 4.10.23.

7. A.H. Holtzman and C.G. Rudershausen, "Recent Advances in Metal working with Explosives", Sheet Metal Ind., 39, 1962, p. 399.

8. B. Crossland, A.S. Bahrani, J.D. Williams and V. Shribman, "Explosive Welding of Tubes to Tube-Plates", Welding and Metal Fabrication, Vol. 35, No. 3, 1967, pp. 88-94.

9. J.H. Cairns and R. Hardwick, "Explosive Welding of Tubes into Tube-Plates Using Angular Geometry", Select Conf. on Explosive Welding, Pub. Inst. Welding (London), 1968, p. 17.

10. J.H. Cairns, R. Hardwick and D.G. Telford, "Explosive Welding of Titanium Tubes to Tube-Plates Yimpact Process", Proc. 3rd Int. Conf. of the Centre for High Energy Forming, Denver, 1971, pp. 2.3.1 - 2.3.17.

11. R. Hardwick, "The Application of Explosive Welding to Industrial Heat Exchangers", Proc. Int. Conf. - The Use of High Energy Rate Methods for Forming, Welding and Compaction, Univ. of Leeds, 1973, paper 20.

12. K. Thyboe Christensen, N. Seest Egly and L. Alting, "Explosive Welding of Tubes to Tube-Plates", 4th Int. Conf. of the Centre for High Energy Forming, Denver, 1973, pp. 4.3.1 - 4.3.37.

13. P.E.G. Williams, "Explosive Welding of Tube to Tube-Plates", Ph.D. Thesis, Queen's Univ. of Belfast, 1972.

14. M.D. Chadwick, D. Howd, G. Wildsmith and J.H. Cairns, "Explosive Welding of Tubes and Tube-Plates", British Welding Journal, 15, 1968, pp. 480-492.

15. B. Crossland and P.E.G. Williams, "An Experimental Investigation of the Permissible Ligament Thickness in Explosive Tube to Tube-Plate Welding", Proc. Int. Conf. on the Use of High Energy Rate Methods for Forming, Welding and Compaction, Leeds, 1973, p.13.

16. P.E.G. Williams and B. Crossland, 'Explosive Welding of Tubes to Tube-Plates", Proc. 2nd Int. Conf. on Pressure Vessel Technology, San Autonio, 1973, pp. 1131-1149.

17. P.E.G. Williams and B. Crossland, "Deformation of Tube-Plates in which Tubes are Explosively Welded", Proc. Int. Conf. on Advances in Welding Process, 1974, pp. 249-262.

18. R. Hardwick, "Methods for Fabricating and Plugging of Tubes to Tube Sheet Joints by Explosive Welding", Welding Journal, April 1975.

19. A.S. Bahrani, R.F. Halliburton and B. Crossland, "The Explosive Plugging of Heat Exchangers", Proc. of the Int. Conf. on Welding Research Related to Power Plant, Southampton, 1972, paper 17.

20. B. Crossland, R.F. Halliburton and A.S. Bahrani, "Explosive Plugging of Heat Exchangers", Proc. 4th Int. Conf. of the Centre for High Energy Forming, 1973,pp. 4.4.1 - 4.4.34.

21. A.S. Bahrani, R.F. Halliburton and B. Crossland, "A parallel Technique of Tube to Tube-Plate Welding Applied to Plugging of Heat Exchangers'', Int. J. of Pressure Vessel and Piping, Vol. 1, 1973, pp. 17-35.

22. B. Crossland and A.S. Bahrani, ''Further Experiments on Explosive Plugging of Heat Exchangers'', Proc. Int. Conf. - The Use of High Energy Rate Methods for Forming Welding and Compaction, 1973, paper 21.

23. B. Crossland, A.S. Bahrani and W.J. Townsley, ''Explosive Plugging of Nuclear Heat Exchangers'', Proc. III Symposium on Explosive Working of Metals, Czechoslovakia, 1976, p. 59.

24. W.J. Townsley and B. Crossland, ''The Explosive Plugging of Tubes of the Heat Exchangers of the Advanced Gas Cooled Reactor'', Proc. 6th Int. Conf. on High Energy Rate Fabrication, Essen, 1977.

25. W.R. Johnson, ''Explosive Welding Plugs into Heat Exchangers Tubes'', Welding Journal, Jan. 1971, pp. 22-32.

26. T.S. Sahansra, R.R. Noe and M.W. Costic, ''Report on Explosive Plugs in Feed Water Heater and Heat Exchangers'', Proc. Feed Water Heater Workshop, New Orleans, March 1979, pp. 191-226.

27. G. Stanko, ''Explosive Tube Plugging'', Pressure Vessel and Piping Conference, Aug. 1980, San Francisco, ASME Special Publication, Explosive Welding, Forming, Plugging and Compaction, pp. 13-24.

28. J. Willis and D.C. Murdie, ''Explosive Joining of Aluminium Alloy Pipes'', Sheet Metal Ind., 39, 1962, p. 811.

29. H.M. Copper and F.S. Chaplin, ''Development of a Propelled Actuated Pipe Joining System'', Proc. 3rd Int. Conf. of the Centre for High Energy Forming, 1971, pp. 8.2.1-8.2.23.

30. M.D. Chadwick and N.H. Evans, ''Explosive Techniques'', Metal Construction, 5, 1973, pp. 285-292.

31. M.D. Chadwick and N.H. Evans, ''Explosive Welding Techniques for Joining Steel Pipes'', Pipes and Pipelines International, 12, 1973, p. 23.

32. H.K. Wylie and B. Crossland, "Explosive Welding of Tubes to Collars", Proc. 4th Int. Conf. of Centre for High Energy Forming, Denver, 1973, pp. 4.2.1-4.2.24.

33. J.F. Rocha, W.G. Howell and H.E. Otto, "The Development of Explosive Metal Working in Brazil", Proc. 5th Int. Conf. on High Energy Rate Fabrication, Denver, 1975, pp. 4.15.1 - 4.15.16.

34. R.P. Grollo, "Explosive Joining of Dissimilar (Transition) Metal Tubes", Proc.3rd Int. Conf. of the Centre for High Energy Forming, Denver, 1971, paper 8.4.

35. H.E. Otto, "Explosive Welding of Pipes", Ist. Symp. on Pipe Joining Methods, Chicago, Jan. 1978, p. 83.

36. A.E. Doherty and L.H. Knop, Proc. 2nd Int. Conf. of the Centre for High Energy Forming, 1969, p. 2.4.2.

37. T.Z. Blazynski and A.R. Dara, " The Use of Explosives for Implosive Welding of Duplex Cylinders", Proc. 11th Int. MTDR Conf., 1971, p. 943.

38. T.Z. Blazynski and A.R. Dara, "A Comparison Between the Implosive and Explosive Systems for Welding of Duplex Cylinders", Proc. 3rd Int. Conf. of the Centre for High Energy Forming, 1971, pp. 8.3.1 - 8.3.26.

39. L.M. Schetky, "The Explosive Fabrication of Duplex Tube", J. Inst. Metals, 98, 1970, p. 364.

40. H.K. Wylie and B. Crossland, "A Feasibility Study of Explosive Fabrication of Triplex Tubing", Proc. 6th Int. Conf. on High Energy Rate Fabrication, Essen, 1977.

41. C.V. Jarvis and P.M.B. Slate, "Explosion Fabrication of Composite Materials," Nature, 220, 1968, pp.782-783.

42. O.Y. Recce, "Molybdenum Wire Reinforced Columbium Composites", Proc. 3rd Int. Conf. of the Centre for High Energy Forming, Denver, 1971, pp. 2.1.1 - 2.1.11.

43. H.K. Wylie, J.D. Williams and B. Crossland, "Explosive Fabrication of Fibre Reinforced Aluminium", Proc. 3rd Int. Conf. of the Centre for High Energy Forming, 1971, pp. 2.2.1 - 2.2.26.

44. H.K. Wylie, J.D. Williams and B. Crossland, "Fabrication of Metal/Metal Wire Composite Materials by the Use of Explosives", Welding and Metal Fabrication, 39, 1971, p. 214.

45. V. Shribman, A.S. Bahrani and B. Crossland, "The Techniques and Mechanism of Explosive Welding", Production Engineer, 48, 1968, p. 69.

46. Y. Bedroud, H. El-Sobky and T.Z. Blazynski, "Implosive Welding of Mono and Bimetallic Arrays of Rods", Metal Technology, Vo. 3, Part I, 1976, pp. 21-28.

47. H. El-Sobky and T.Z. Blazynski, "Implosive Welding of Composite Metal Foil Cylinders", Proc. 15th MTDR Conf., 1974, p. 399.

48. H. El-Sobky and T.Z. Blazynski, "Explosive Welding of Multilayer, Wire - Mesh Reinforced, Metal Foil Cylinder", Proc. 5th Int. Conf. on High Energy Rate Fabrication, Denver, 1975, p.4.6.1.

49. R. Velton, "Practical Applications of Explosive Welding", Proc. 4th Int. Conf. of the Centre for High Energy Forming, Denver, 1973, p.8.4.1.

50. P.I. Persson, "Explosive Clad Materials for the Electrochemical Industry and Off-Shore Oil Plateforms", Proc. III Symposium on Explosive Working of Metals, Czechoslovkia, 1976, p. 193.

51. D.K.C. Anderson, "Industrial Application of Explosively Clad Metals", Proc. Int. Conf. - The Use of High Energy Rate Methods for Forming, Welding and Compaction", Leeds 1973, paper 18.

52. H.E. Pattee and N.S. Lalwaney, "Commercialization of Explosive Welding - Present and Future", Proc. 6th Int. Conf. on High Energy Rate Fabrication, Essen, 1977.

53. L.R. Carl, "Brass Welds Made by Detonation Impulse", Metal Progress, 1944. 46, pp. 102-103.

54. A.A. Deribas, Explosive Welding (Siberian Branch of Acd. of Sci.), 1967.

55. V. Phillipchuk, "Explosive Welding Status - 1965", ASTME Creative Manufacturing Seminar, 1965, paper SP-65-100.

56. V. Phillipchuk and Le Roy Bois, 1960, US Patent No. 3024526.

57. J. Pearson, J. Metals, 1960, 12, pp. 673-681.

58. J. Pearson, "Explosive Welding", ASTME Advanced High Energy Rate Forming, Book 1, 1961, paper SP-60-159.

59. G. Birkhoff, D.P. Mac Dougall, E.M. Pugh and G.I. Taylor, "Explosive with Lined Cavities", J. of Appl. Phys., Vol. 19, 1948, pp. 563-583.

60. J.M. Walsh, R.G. Shreffler and F.J. Willing, "Limiting Conditions for Jet Formation in High Velocity Collisions", J. of Appl. Phys., Vol. 24, No. 3, 1953, pp. 349-358.

61. W.A. Allen, J.M. Mapes and W.G. Wilson, "An Effects Produced by Oblique Impact of a Cylinder on a Thin Target", J. App. Phys., 25, 1954, pp. 675-676.

62. D.E. Davenport and G.E. Duvall, "Explosive Welding", ASTME High Rate Energy Forming Seminar, 1961, paper SP-60-61.

63. D.E. Davenport, "Explosive Welding", ASTME Advanced High Energy Rate Forming, Book II, 1962, paper SP-62-77.

64. G.R. Cowan and A.H. Holtzman, "Flow Configuration in Colliding Plates : Explosive Bonding", J. of App. Phys., Vol. 34, 1963, pp. 928-939.

65. A.H. Holtzman and G.R. Cowan, "Bonding of Metals by Explosive", Weld Res. Coun. Bull. No. 104, April 1959.

66. H.P. Tardif, Metal Progress, 77, 1960, pp. 128-130.

67. P.J.M. Boes, "Some Aspects of Explosive Welding", Tech. Centre for Metal Working (T.N.O.), Delft, 1962, Publication 103.

68. A. Pocalyko and C.P. Williams, "Clad Plate Products by Explosive Bonding", Weld. J., Oct. 1964, 43, pp. 854-861.

69. H.G. Baron and E.L. Costello, "Explosive Forming", Metallurgical Reviews, 8, No. 2, 1963, p. 369.

70. J.S. Reinehart and J. Pearson, "Explosive Working of Metals", Pergamon Press, London, 1962.

71. A.S. Bahrani and B. Crossland, "Explosive Welding and Cladding : An Introductory Survey and Preliminary Result", Proc. Inst. Mech. Enginers., 1964, 179, p. 264.

72. H. Addison, W.E. Fogg, I.G. Betz and F.W. Hussey, "Explosive Welding of Aluminium Alloys", Weld. J., Vol. 42, No. 8, Res. Suppl., 1963, p. 359-S.

73. B. Crossland and A.S. Bahrani, "Review of Explosive Welding Research Carried out in Queen's Univ. of Belfast", Proc. First Int. Conf. of the Centre for High Energy Forming, Denver, 1967, pp. 1.1.1 - 1.1.50.

74. B. Crossland, J.D. Williams and V. Shribman, "Developments in Explosive Welding", Aircraft Engg., 1968, 40, 12, p. 11.

75. B. Crossland and A.S. Bahrani, "Fundamentals of Explosive Welding", Contemp. Physics, Vol. 9, No. 1, 1968, pp. 71-87.

76. B. Crossland and J.D. Williams, "Explosive Welding", Metallurgical Rev., 1970, p. 70.

77. B. Crossland, "The Development of Explosive Welding and its Application in Engineering", Metals and Materials, 5, 1971, pp. 401-413.

78. B. Crossland, "Review of the Present State-of-the art in Explosive Welding", Metal Technology, 1976, pp. 8-20.

79. D.M. Adamson, "Explosive Welding", Certif. Eng., Vol. 49, No. 3, March 1976, pp. 59-62.

80. B. Crossland, "The Present State of the Theory and Application of Explosive Welding", Inst. Phys. Conf. Ser. No. 47, Chapter 4, 1979, pp. 394-409.

81. T. Gurney and T.E. Sterne, Ballastic Research Lab., Report No. 405 and 648, Aberdeen Proving Ground, Maryland, 1947.

82. G.E. Duwall and J.W. Erkman, "Acceleration of Plates by High Explosives", Tech. Report No. 1, Stanford Research Institute Project GU-2426, 1958.

83. A.K. Aziz, "Energy Transfer to a Rigid Piston Under Detonation Loading", Third Symposium of Detonation, Princeton, Sept. 1960.

84. V. Shribman, "Some Further Work on Explosive Welding", Ph.D. Thesis, Queen's Univ. of Belfast, Nov. 1968.

85. V. Shribman and B. Crossland, "An Experimental Investigation of the Velocity of Flyer Plate in Explosive Welding", Proc. 2nd Int. Conf. of the Centre for High Energy Forming, Vol. 2, Denver, 1969, paper 7.3.1.

86. D.R. Hay, "Explosive Welding : Applications and Techniques", High Pressure Science and Technology, Plenum, New York, Vol. 2, 1979, pp. 781-804.

87. R.L. Robinson, ''The Mechanism of Wave Formation in Impact Welding'', Philosophical Magazine, Vol. 31, 1975, pp. 587-597.

88. S.R. Reid, ''A Discussion of the Mechanism of Interface Wave Generation in Explosive Welding'', Int. J. of Mech. Sciences, Vol. 16,1974, pp. 399-413.

89. O.R. Bergmann, G.R. Cowan and A.H. Holtzman, ''Experimental Evidence of Jet Formation During Explosion Cladding'', Trans. Metallurgical Soc. of AIME, Vol. 236, 1966, pp. 649-653.

90. T. Onzawa and Y. Ishii, ''Fundamental Studies on Explosive Welding : Observation of Metal Jet and Wavy Pattern'', Trans. Japan Welding Society, Vol. 6, No. 2, 1975, pp.18-24.

91. M.D. Meyer, ''Impact Welding Using Magnetically Driven Flyer Plates'', Proc. 4th Int. Conf. of the Centre for High Energy Forming, Denver, July 1973, pp. 5.3.1-5.3.23.

92. W.A. Allen, H.L. Morrison, D.B. Ray and J.W. Rogers, ''Fluid Mechanics of Copper'', The Physics of Fluids, Vol. 2, No. 3, 1959, pp. 329-333.

93. A.E. Bayce, Stanford Research Institute Report, SRI Project, 4441, April 1964.

94. A.S. Bahrani and B. Crossland, ''Further Experiments on Explosive Welding and Cladding with Particular Reference to the Strength of the Bond'', Applied Mechanics Convention, England, Vol. 80, 1966, pp. 1-16.

95. M.P.H. Wilson and J.H. Brunton, ''Wave Formation Between Impacting Liquids in Explosive Welding and Erosion'', Nature, Vol. 226, May 1970, pp. 538-541.

96. G.R. Abrahamson, ''Permanent Periodic Surface Deformations due to a Travelling Jet'', J. of Applied Mechanics, Trans. ASME, Dec. 1961, pp. 519-528.

97. A.S. Bahrani, T.J. Black and B. Crossland, ''The Mechanism of Wave Formation in Explosive Welding'', Proc. Royal Society of London, 1967 (A), pp. 123-136.

98. M. Watanable, Z. Murakami, I. Fukuyama, Y. Mukai, T. Makihata, and M. Matsushita, Proc. Conf. on Advances in Welding Processes, 1970, paper No. 23, p. 173.

111. J.F. Kowalick and D.R. Hay, ''A Flow Analogue for Explosive Bonding'', Proc. 3rd Int. Conf. of the Centre for High Energy Forming, 1971, pp.1.1.1-1.1.21.

112. M. Nishioka and H. Sato, ''Mechanism of Determination of the Shedding Frequency of Vortices Behind a Cylinder at Low Reynolds Number'', J. Fluid Mech., Vol. 89, Part 1, 1978, pp. 49-60.

113. T. Sarpkaya, ''Vortex-Induced Oscillations'', Trans. ASME, J. of App. Mech., Vol. 48, No. 2, 1979, pp. 241-258.

114. J.S. Son, ''Experimental and Computational Studies on Flow Around a Circular Cylinder'', Ph.D. Thesis, Univ. of Illinois, 1968.

115. G. Birkhoff and E.H. Zarantonello, ''Periodic Waves'', Jets Wakes and Cavities, , Academic, New York, 1948, pp. 290-292.

116. G. Birkhoff, ''Formation of Vortex Street'', J. of App. Phys., Vol. 24, No. 1, 1953, pp. 98-103.

117. R.C. Gupta and G.S. Kainth, ''Swinging Wake Mechanism for Interface Wave Generation in Explosive Welding of Metals'', Technical Note Included, in Discussion at Int. Conf. on New Directions in Welding Research and Development, Massachusetts, Oct. 1979.

118. K.K. Botros and T.K. Groves, ''Characteristics of Wavy Interface and the Mechanism of its Formation in High-Velocity Impact Welding'', J. App. Phys., Vol. 51, No.7, July 1980, pp. 3715-3721.

119. T. Onzawa and Y. Ishii, ''Wave Formation in Explosive Welding'', J. of Japan Welding Society, 41, 1972, p.446.

120. S.R. Reid and N.H.S. Sherif, ''Prediction of Wavelength of Interface Waves in Symmetric Explosive Welding'', J. of Mechanical Engineering Sciences, Vol. 18, No. 2, 1976, pp. 87-94.

121. S.R. Reid, ''Wake Instability Mechanism for Wave Formation in Explosive Welding'', Int. J. of Mech. Sci., Vol. 20, 1978, pp. 247-255.

122. H. El-Sobky and T.Z. Blazynski, ''Experimental Investigation of the Mechanisms of Explosive Welding by Means of a Liquid Analogue'', Proc. 5th Int. Conf. on High Energy Rate Fabrication, Denver, 1975, pp.4.5.1-4.5.21.

123. H. El-Sobky and T.Z. Blazynski, ''A Fundamental Approach to Interfacial Wave Formation in Explosive Welding'', Proc. 6th Int. Conf. on High Energy Rate Fabrication, Essen, 1977, pp. 1-14.

124. S.R. Reid and W. Johnson, ''Note on the Estimation of the Parameters Describing the Interface Wave Pattern in Explosive Welding'', Nature, Phy.Sci., 231, 1971, p. 203.

125. S.R. Reid and D.J. Langdale, ''Investigation of the Modulation of Interface Waves in Explosive Welding'', Proc. 15th Int. MTDR Conf., 1975, pp. 391-398.

126. D.J. Langdale, ''Measurement of Interface Wave Dimensions and Investigation of Flyer Plate Kinematics in Explosive Welding'', M.Sc. Dissertation, Univ. of Manchester, Inst. of Sci. and Tech., 1973.

127. N.H.S. Sherif, ''Investigation of Interfacial Wave Dimensions in Explosive Welding under Symmetric Conditions'', M.Sc. Dissertation, University of Manchester, Inst. of Sci. and Tech., 1974.

128. A.R. Rosenfield and G.T. Hahn, ''Numerical Description of the Ambient Low-Temperature, and High Strain Rate Flow and Fracture Behaviour of Plain Carbon Steel'', Trans. Am. Soc. of Metals, Vol. 59, 1966, pp. 962-980.

129. J.L. Robinson, ''Fluid Mechanics of Copper : Viscous Energy Dissipation in Impact Welding'', J. of App. Phys., Vol. 48, No. 6, 1977, pp. 2202-2207.

130. S.K. Godunov, A.A. Deribas and V.I. Mali, ''Influence of Material Viscosity on the Jet Formation Process during Collision of Metal Plates'', Fizika Goreniya i Vzryva, Vol. 11, No. 1, 1975, pp. 3-18.

131. V.S. Sedikh and M.P. Bondar, ''Basic Parameters of Explosive Welding and Strength Characteristics of Welded Joints'', Weld Production, 1963, 10, pp. 1-5.

132. S.H. Carpentar, R.H. Wittman and R.J. Carlson, ''The Relationship of Explosive Welding Parameters to Material Properties and Geometrical Factors'', Proc. Ist. Int. Conf. of the Centre for High Energy Forming, Denver, 1967, pp. 1.2.1 - 1.2.23.

133. S.H. Carpenter, R.H. Wittman and H.E. Otto, ''Explosion Welding Research at University of Denver'', Advances in Machining Tool Design and Research, 1970, Vol. 8, pp. 873-888.

134. J.F. Kowalick and D.R. Hay, ''Metallographic Measurements of Explosive Welding Parameters'', Proc. Select Conf. on Explosive Welding - Welding Institute (London), 1968, pp. 78-82.

135. J.F. Kowalick and D.R. Hay, ''Explosive Bonding, Dimensional Analysis'', Proc. 2nd Conf. of the Centre for High Energy Forming, 1969, pp. 7.2.1 - 7.2.18.

136. H.K. Wylie, P.E.G. Williams and B. Crossland, ''An Experimental Investigation of Explosive Welding Parameters'', Proc. of the Ist. Int. Symp. on Use of Explosive Energy in Manufacturing Metallic Materials of New Properties and Possibilities of Application thereof in Chemical Industry, Marianske Lazne, 1970, p. 45.

137. H.K. Wylie, P.E.G. Williams and B. Crossland, ''Further Experimental Investigation of Explosive Welding Parameters'', Proc. 3rd Int. Conf. of the Centre for High Energy Forming, Denver, 1971, pp. 1.3.1 - 1.3.43.

138. S.H. Carpenter and R.H. Wittman, Society of Manufacturing Engineers, 1974, paper MF-74-819, pp. 1-17.

139. A. Loyer, D.R. Hay and G. Gagnon, ''Weldability Windows and the Selection of Explosive Welding Process Parameters'', Proc. 5th Int. Conf. on High Energy Rate Fabrication, 1975, pp. 4.3.1 - 4.3.14.

140. A. Loyer, M. Talerman, D.R. Hay and G. Gagnon, ''Explosive Welding, the Weldability Window for Dissimilar Metals and Alloys'', Proc. 3rd Int. Symp. on Use of Explosive Energy in Manufacturing Metallic Materials, Czeckoslovakian Inst. of Ind. Chem., 1976, pp. 43-57.

141. A.A. Deribas, V.A. Simonov and I.D. Zakharenko, Proc. 5th Int. Conf. on High Energy Rate Fabrication, Denver, 1975, pp. 4.1.1 - 4.1.24.

142. V.V. Babul, ''Conditions for Explosive Welding of Metals'', 2nd Int. Symp. on the Use of Explosion Energy to Produce Metallic Materials with New Properties'', Oct. 1973, Marianske Lazne (Czechoslovakia).

143. A.A. Deribas and I.D. Zakharenko, ''Determination of Limiting Collision Condition Ensuring the Welding of Metal by Explosion'', Fizika Goreniya i Vzryva, Vol. 11, No. 1, 1975, pp. 151-153.

144. A.A. Deribas, ''The Classification of Flows Arising from Oblique Impacts of Metal Plates'', 2nd Int. Symp. on the Use of Explosion Energy to Produce Metallic Materials with New Properties, Oct. 1973, Marianske Lazne (Czechoslovakia).

145. A.A. Deribas and I.D. Zakharenko, ''Surface Effects with Oblique Collision between Metallic Plates'', Fizika Goreniya i Vzryva, Vol. 10, No. 3, 1974, pp. 409-421.

146. S.W. Stivers and R.H. Wittman, ''Computer Selection of the Optimum Explosive Loading and Weld Geometry'', Proc. 5th Int. Conf. on High Rate Energy Fabrication, Denver, 1975, pp. 4.2.1 - 4.2.16.

147. F.A. Mckee and B. Crossland, Proc. 5th Int. Conf. on High Energy Rate Fabrication, 1975, pp. 4.11.1 - 4.11.25.

148. R.H. Wittman, Proc. 2nd Symp. on Use of Explosive Energy in Manufacturing Metallic Materials, Marianske Lanze, Oct. 1973.

149. Y. Takizawa and T. Izuma, Proc. 3rd Int. Symp. on Use of Explosive Energy in Manufacturing Metallic Materials, Czechoslovakian Inst. of Ind. Chem., 1976, pp. 15-32.

150. H.K. Balakrishna and V.C. Venkatesh, ''Influence of Collision Parameters on the Morphology of Interface in Aluminium-Steel Welds'', 6th Int. Conf. on High Energy Rate Fabrication, Essen, 1977.

151. A.A. Popoff, ''Explosion Welding'', Mechanical Engineering, Vol. 100, No. 5, May 1978, pp. 28-35.

152. B. Crossland and J.D. Williams, ''Welding Parameters for Explosive Cladding'', Proc. Conf. Advances in Welding Process, Welding Inst., 1970, pp. 78-82.

153. K.K. Botros and T.K. Groves, ''Fundamental Impact Welding Parameters - An Experimental Investigation Using a 76 mm Power Cannon'', J. App. Phys., 57, 7, July 1980, pp. 3706-3714.

154. W. Lucas, J.D. Williams and B. Crossland, ''Some Metallurgical Observations on Explosive Welding'', Proc. of the 2nd Int. Conf. of the Centre for High Energy Forming, 1969, p. 8.1.1.

155. J.D. Williams, P. Dhir and B. Crossland, ''The Nature of Vortices in Explosive Welds'', Proc. of the 3rd Int. Conf. of the Centre for High Energy Forming, Denver, 1971, pp. 3.1.1 - 3.1.22.

156. Y. Dor-Ram, B.Z. Weiss and Y. Komen, ''Explosive Cladding of Cu/Cu Systems : An Electron Microscopy Study and a Thermomechanical Model'', Acta Metallurgia, Vol. 27, 1979, pp. 1417-1429.

157. M.D. Nagarkar and S.H. Carpenter, ''An Investigation of Atomic Diffusion at the Interface of Explosion Welded Cu-Ni Couples'', Mater. Sci. Eng., 1975, 20, p. 251.

158. H.K. Balakrishna, ''Investigation into Some Aspects of Explosive Welding of Aluminium to Steel'', Ph.D. Thesis, I.I.T. Madras, 1977.

159. R.V. Tamhankar and J. Ramesan, ''Metallography of Explosion Welds'', Mater. Sci. Eng., 1974, 13, 3, p.245.

160. Y. Ishii, T. Onzawa and T. Oinuma, ''A Study of Fusion Layer in Explosive Bonded Boundary'', Trans. Japan Welding Society, Vol. 1, No. 2, Sept. 1970, pp. 117-124.

161. A.A. Ezra, ''Principles and Practice of Explosive Metal Working'', Industrial Newspaper Ltd., 1973.

162. J. Ramesan, S.R. Sahay, P.C. Angelo and R.V. Tamhankar, ''A Metallurgical Study of the Weld Zones in Explosive Welded Samples'', Trans. Ind. Inst. Metals, 1971, 24, 2, p. 49.

163. D.C. Murdie and G. Blankenburgs, ''Examination of Two Explosively Welded Interfaces'', J. Inst. Metals, 1966, 94, 3, p. 119.

164. P.C. Angelo, J. Ramesan, S.R. Sahay and R.V. Tamhankar, ''Electron Microprobe Study of Explosive Welded Samples'', Trans. Ind. Inst. Metals, 1970, 23, 3, p. 68.

165. L.F. Trueb, ''An Electron Microscope Investigation of Explosion Bonded Metals'', Trans. Metall. Soc., AIME, 242, 1968, pp. 1057-1065.

166. H.K. Balakrishna, P.K. Phillip and V.C. Venkatesh, ''Influence of Collision Parameters on the Performance of Aluminium-Steel Explosion Welds'', Proc. 9th All India MTDR Conf., IIT-Kanpur, Dec. 1980, pp. 369-373.

167. R.A. Pruemmer, ''Metallurgical Microradiographic and X-ray Residual Stress Investigation of Explosively Welded Aluminium-Steel'', Proc. 3rd Int. Conf. of Centre for High Energy Forming, Denver, July 1971.

168. Maj. S.K. Salwan, S. Prasad and A.S. Deshpande, ''Explosive Welding Parameters'', Indian Welding Journal, Vol. 11, No. 1, Jan. 1979, pp. 1-8.

169. H.K. Balakrishna and P.K. Phillip, ''Explosive Welding of Metal Combination'', Inst. of Engineers (India), Vol. 57, July 1976, pp. 36-40.

170. H.K. Balakrishna and P.K. Phillip, ''Nature of Bond Interface in Explosively Welded Metal Systems'', Inst. of Engineers (India), Vol. 57, Sept. 1976, pp. 96-101.

171. H.K. Balakrishna, V.C. Venkatesh and P.K. Phillip, ''Influence of Surface Integrity on the Quality of Explosive Welds'', Proc. Int. Conf. on Prod. Engg., New Delhi.

172. H.K. Balakrishna, V.C. Venkatesh and P.K. Phillip, ''On Ultrasonic Testing of Aluminium Steel Explosion Welds'', Proc. Indo-British Conf. on Eng. Prod., Dec. 1976, p. 67.

173. P.K. Phillip, H.K. Balakrishna and V.C. Venkatesh, "Explosive Welding of Aluminium to Steel", Proc. 7th All India MTDR Conf., Coimbatore, June 1976, pp. 325-328.

174. H.K. Balakrishna and V.C. Venkatesh, ''Influence of Collision Parameters on the Performance of Aluminium-Steel Explosion Welds'', 6th Int. Conf. on High Energy Rate Fabrication, Essen, 1977.

175. J. Singh, ''Explosive Welding of Aluminium, Copper, Brass, Mild Steel and Stainless Steel Combination'', M.Sc. Thesis, I.I.T., Madras, 1980.

176. Von. K. Keller, ''Beitragezum Explosiveplattieven : Eigenschaften der Sprengschweifungen'', Z-Metallkunde, 59, 1968, pp. 503-513.

177. R. Pruemmer,''Bond Strength, Microstructure and Residual Stress State of Explosive Welded Steel to Aluminium'', 5th Int. Conf. on High Energy Rate Forming, Denver, 1975, pp. 4.13.1 - 4.13.14.

178. R.H. Wittman, ''The Influence of Collision Parameters on the Strength and Microstructure of an Explosion Welded Aluminium Alloy'', 2nd Int. Symp. on Use of Explosive Energy in Manufacturing Metallic Materials, Marianske Lazne, Czech., Oct. 1973.

179. T. Nilsson, T. Hagwall and U. Stahlberg, ''Reduction of Residual Stresses in Explosive Welded Plates by Cold Forging'', Scandinavian Journal of Metallurgy, 9, 1980, pp. 31-33.

180. W. Kaufman, ''The Airfoil'', Fluid Mechanics, McGraw-Hill Company, Inc., 2nd Ed., Translated by E.C.Chilton, 1969, pp. 311-315.

181. S.A. Thorpe, ''Experiments on the Instability of Strattified Shear Flows: Immisible Fluids'', Journal of Fluid Mechanics, Vol. 39, 1969, pp. 25-48.

182. L.M. Milne-Thomson, ''Jets and Currents'', Theoretical Hydrodynamics, 4th Ed., Macmillan, New York, 1960, pp. 287-290.

183. A.S. Bahrani, ''An Experimental Investigation into Some Aspects of Explosive Welding and Cladding'', Ph.D. Thesis, Part Two, Queen's Univ., Belfast, May 1965.

184. G.E. Kuzmin, V.A. Simonov, I.V. Yakovlev, ''The Parameters in Explosive Welding and Coatings-Plate Acceleration'', Fizika Goreniya i Vzryva, Vol. 12, No. 3, 1975, pp. 411-413.

185. G.I. Taylor, ''Oblique Impact of Jet on a Plane Surface'', Phil. Trans. Royal Society (London), Series A, 260, 1966, pp. 96-100.

186. A. Kelly, Strong Solids, Oxford University Press, 1966, p. 19.

187. W. Bettridge, ''Nickel and Its Alloys'', MacDonald and Evan, 1977, pp. 3 and 31.

188. S. Abkowitz, J.J. Burke and R.H. Hiltz, ''Titanium in Industry'', D. Van Nostrand Company, 1955, p. 25.

List of publications from the thesis

1. R.C. Gupta and G.S. Kainth, ''Application of Hydrodynamics to Explosive Welding'', Proc. 8th National Conf. on Fluid Mechanics and Fluid Power, Coimbatore, 1978, pp. 43-47.

2. G.S. Kainth and R.C. Gupta, ''Prediction of Force on Swinging Wake in Explosive Welding of Dissimilar Metals'', Proc. 9th National Conf. on Fluid Mechanics and Fluid Power, Surat, Dec. 1979, pp. 137-141.

3. G.S. Kainth and R.C. Gupta, ''Swinging Wake Mechanism for Interface Wave Generation in Explosive Welding of Metals'', Technical Note Included in Discussion at Int. Conf. on New Directions in Welding Research and Development, Massachusetts, Oct. 1979.

4. R.C. Gupta and G.S. Kainth, ''Asymmetries in Explosive Welding'', Proc. 3rd ISME Conf. on Mechanical Engineering, I.I.T. Delhi, Feb. 1980, pp. 167-170.

5. R.C. Gupta and G.S. Kainth, ''Permissible Range of Parameters for Interface Wave Formation'', Proc. Pressure Vessel Piping Technology, San Francisco, Aug. 1980, ASME special publication, pp. 99-119.

6. R.C. Gupta and G.S. Kainth, ''Obstacle Size in Hydrodynamic Model of Explosive Welding of Metals'', Silver Jubili Congress of Indian Society of Theoretical and Applied Mechanics, Kharagpur, Dec. 1980.

7. R.C. Gupta and G.S. Kainth, ''Weldability Window for Explosive Welding'', National Welding Seminar, I.I.T. Madras, 1981, pp. 103-109.

8. R.C. Gupta and G.S. Kainth, ''A Hydrodynamic Model of Explosive Welding Considering Kinetic Energy Loss'', Proc. 9th AIMTDR Conf. I.I.T. Kanpur, Dec. 1980, pp. 374-378.